Short-Ranged Central and Tensor Correlations in Nuclear Many-Body Systems

Towards ab initio Calculations using Realistic Interactions within the Unitary Correlation Operator Method

---

Vom Fachbereich Physik
der Technischen Universität Darmstadt

zur Erlangung des Grades
eines Doktors der Naturwissenschaften
(Dr. rer. nat.)

genehmigte Dissertation von

Dipl.-Phys. Thomas Neff
aus Bensheim

Darmstadt 2002
D 17

Referent:	Prof. Dr. W. Nörenberg
Koreferent:	Prof. Dr. J. Wambach
Tag der Einreichung:	7. Dezember 2001
Tag der Prüfung:	29. Mai 2002

Things should be made as simple as possible, but not any simpler.

Albert Einstein

Contents

Introduction and Summary

Quantum Chromo Dynamics (QCD) is the fundamental theory of the strong interaction and the nucleons represent bound systems of quark and gluon degrees of freedom. Nuclear physics in the low energy regime is considered as an effective theory where the nucleons are the essential degrees of freedom, whose interaction can be described by a nucleon-nucleon force. In the QCD picture the force between the color neutral nucleons is a residual interaction like the van-der-Waals force between electrically neutral atoms. Therefore it is expected that the nuclear interaction is not a simple local potential but has a rich operator structure in spin and isospin and in many-body systems may also include genuine three- and higher-body forces.

There are attempts to derive the nucleon-nucleon force using Chiral Perturbation Theory [EM01]. However this promising approach cannot compete yet with the so-called realistic interactions that reproduce the nucleon-nucleon scattering data and the deuteron properties. The realistic nucleon-nucleon forces are essentially phenomenological. The Bonn interactions [Mac89, Mac01] are based on meson-exchange that is treated in a relativistic nonlocal fashion. The Argonne interactions [WSA84, WSS95] on the other hand describe the pion exchange in a local approximation and use a purely phenomenological parameterization of the nuclear interaction at short and medium range.

It is a central challenge of nuclear physics to describe the properties of nuclear many-body systems in terms of such realistic nuclear interactions. However in mean-field and shell model approaches, typically employed to describe the properties of finite nuclei, realistic interactions cannot be used directly.

Mean-field calculations are successful in describing the ground state energies and mass and charge distributions for all nuclei in the nuclear chart but the lightest ones. There are both relativistic and nonrelativistic Hartree-Fock models. As the short-range central and tensor correlations induced by realistic forces cannot be represented by the Slater determinants of the Hartree-Fock method, direct parameterizations of the energy-density or an effective finite range force are used instead.

In shell model calculations with configuration mixing a two-body Hamiltonian is used in the vector space spanned by the many-body states that represent particle-hole configurations in selected shell model states. The solution of the energy eigenvalue problem in the high-dimensional many-body space yields detailed information on the spectra of nuclei, the transitions between the states, electromagnetic moments, charge and mass distributions, β-decay etc. However one has to use an effective interaction in the two-body Hamiltonian. Although one often starts with a G-matrix derived from realistic interactions the two-body matrix elements of the Hamiltonian have to be modified and adjusted to a large set of ground state and excitation energies for an accurate description of the data. This has to be done separately for each region of the nuclear chart.

Only recently it became possible to perform *ab initio* calculations of the nuclear many-body problem with realistic interactions. In Green's Function Monte Carlo (GFMC) calculations [PW01] the exact ground state wave function is calculated by approximating the many-body Green's functions in a Monte Carlo approach. The GFMC calculations of light nuclei up to

$A = 8 - 10$ with the Argonne interaction demonstrate the necessity of additional three-body forces. With three-body forces adjusted accordingly the experimental nuclear binding energies and radii as well as the spectra can be reproduced.

Another *ab initio* approach for nuclei up to $A = 12$ is the large-basis no core shell model [NVB00]. All nucleons are treated as active in a large shell model basis. Despite the large basis it is necessary to treat the short range correlations separately. An effective interaction for the model space is derived in a G-Matrix procedure in two-body approximation.

Ab inito calculations for the doubly magic nuclei ^{16}O and ^{40}Ca are performed with the Correlated Basis Function (CBF) method [FdSCF98, FdSC00]. Here a perturbation expansion on a complete set of correlated basis functions is performed. The evaluation of expectation values is done in the Fermi Hypernetted Chain (FHNC) method where the Single Operator Chain (SOC) approximation is used.

Aim

Our aim is to perform *ab initio* calculations of larger nuclei with realistic interactions in a mean-field or a shell model many-body approach. To make this possible we introduce a unitary correlation operator $\underset{\sim}{C}$ that takes care of the short-range and tensor correlations. The correlations are not expressed in a certain basis of a model space but are given analytically in terms of operators of relative distance, relative momentum and the spins and isospins of the nucleons. The correlated interaction

$$\hat{\underset{\sim}{H}} = \underset{\sim}{C}^{\dagger} \underset{\sim}{H} \underset{\sim}{C} \tag{1}$$

we obtain by applying the correlation operator to the realistic interaction is therefore not restricted to the model space of a certain many-body theory but can be used for example in a Hartree-Fock calculation as well as in shell model calculations with configuration mixing. The fact, that the correlations are not expressed for example in the harmonic oscillator basis of a model space but basis-free in coordinate space, makes it easier to understand the physics of the central and tensor correlations.

Furthermore the unitary correlation operator provides not only a correlated interaction, that can be considered as an effective interaction, but other operators can be correlated as well and the physical implications of the short-range correlations on other observables, for example on the nucleon momentum distributions or the spectroscopic factors, can be evaluated.

The correlated interaction is used successfully with simple shell model and Fermionic Molecular Dynamics Slater determinants. This allows us to perform calculations for all nuclei up to about $A = 50$. Although a single Slater determinant as many-body trial state is the most simple ansatz we obtain results very close to those of the quasi-exact methods.

Procedure

The repulsive core and the strong tensor force of the nuclear interaction induce strong short-range central and tensor correlations in the nuclear many-body system. These correlations cannot be represented with the simple many-body trial states of a Hartree-Fock or a shell model calculation that are Slater determinants of single-particle states

$$\left| \Psi \right\rangle = \mathcal{A} \left\{ \left| \psi_1 \right\rangle \otimes \ldots \otimes \left| \psi_A \right\rangle \right\} \ . \tag{2}$$

To illustrate the short-range central correlations in the nucleus the two-body density in the $S, T = 0, 1$ channel of the ^{4}He nucleus is shown in Fig. 1. The two-body density of the correlated trial state, plotted as a function of the distance r between two nucleons, is suppressed

in the region of the repulsive core of the interaction and shifted outwards. This correlation hole is completely absent in the two-body density of the uncorrelated trial state. The central correlations are discussed in section 1.6.

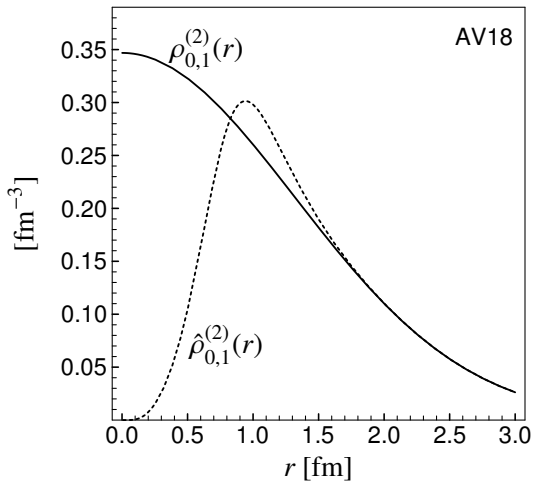

Figure 1: Two-body density $\rho^{(2)}_{S,T}(r)$ of an uncorrelated and two-body density $\hat{\rho}^{(2)}_{S,T}(r)$ of a correlated ^{4}He trial state in the $S, T = 0, 1$ channel. The correlation operator is determined for the Argonne V18 interaction.

The tensor force in the $S = 1$ channels of the nuclear interaction depends on the spins and the spatial orientation $\hat{\mathbf{r}}$ of the nucleons via the tensor operator

$$S_{12}(\hat{\mathbf{r}}, \hat{\mathbf{r}}) = 3(\boldsymbol{\sigma}_1 \cdot \hat{\mathbf{r}})(\boldsymbol{\sigma}_2 \cdot \hat{\mathbf{r}}) - (\boldsymbol{\sigma}_1 \cdot \boldsymbol{\sigma}_2) = 2(3(\mathbf{S} \cdot \hat{\mathbf{r}})^2 - \mathbf{S}^2) \,. \tag{3}$$

Therefore the induced tensor correlations also involve the spin degrees of freedom. An alignment of the nucleons with the total spin $\mathbf{S} = \frac{1}{2}(\boldsymbol{\sigma}_1 + \boldsymbol{\sigma}_2)$ is favored energetically. The correlation between spin orientation and density distribution induced by the tensor force is illustrated in Fig. 2. Here surfaces of constant two-body density in the deuteron are shown for the indicated orientation of the total spin $\langle\, \mathbf{S} \,\rangle$ as a function of the relative orientation $\mathbf{r}$ of the nucleons. The nucleon density is concentrated where the orientation $\hat{\mathbf{r}}$ is parallel or antiparallel to $\mathbf{S}$. This plot in addition visualizes the central correlation hole. The tensor correlations are discussed in detail in section 1.8. As with the central correlation hole, the alignment of spins and density in the two-body density of a many-body state cannot be represented by a Slater determinant.

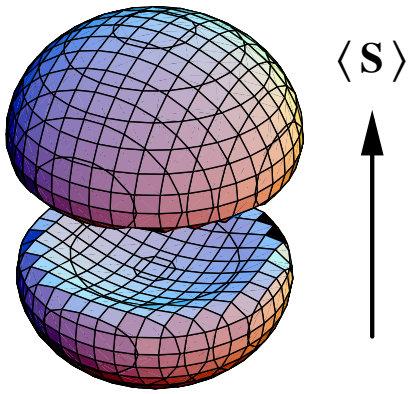

Figure 2: Surface of constant two-body density in the deuteron ($\rho^{(2)}_{1M_S,0}(\mathbf{r}) = 0.005\text{fm}^{-3}$) for $M_S = \pm 1$. The plot is done for the Argonne V18 interaction.

We describe the central and tensor correlations by a unitary correlation operator that is the product of a central correlator $\underset{\sim}{C}_r$ that only shifts radially and a tensor correlator $\underset{\sim}{C}_\Omega$ that only

performs shifts perpendicular to the relative orientation $\hat{\mathbf{r}}$

$$\underset{\sim}{C} = \underset{\sim}{C}_\Omega \underset{\sim}{C}_r \ . \tag{4}$$

To perform the radial shifts, that move probability out of the repulsive core (cf. Fig. 1), the generator of the central correlator $\underset{\sim}{C}_r$ uses the radial momentum operator $\underset{\sim}{p}_r$ together with a shift function $s(r)$ that depends on the distance of the two nucleons.

$$\underset{\sim}{C}_r = \exp\Big\{-i \sum_{i<j} \frac{1}{2}\Big(\underset{\sim}{p}_{rij} s(r_{ij}) + s(r_{ij}) \underset{\sim}{p}_{rij}\Big)\Big\} \tag{5}$$

The shift will be strong for short distances and will vanish at large distances.

The generator of the tensor correlator uses a tensor operator constructed with the orbital part of the momentum operator $\mathbf{p}_\Omega = \mathbf{p} - \mathbf{p}_r$. The r-dependent strength of the tensor correlations is controlled by $\vartheta(r)$.

$$\underset{\sim}{C}_\Omega = \exp\Big\{-i \sum_{i<j} \frac{1}{2}\Big(S_{12}(\mathbf{p}_{\Omega ij}, \mathbf{r}_{ij})\, \vartheta(r_{ij}) + \vartheta(r_{ij})\, S_{12}(\mathbf{r}_{ij}, \mathbf{p}_{\Omega ij})\Big)\Big\} \tag{6}$$

In section 1.8 it is demonstrated that the so constructed $\underset{\sim}{C}_\Omega$ moves probability from the "equator" to the "poles" such that a spherical distribution transforms into the one shown in Fig. 2. The tensor correlator is a scalar operator and does not change the total angular momentum of two nucleons but it transforms the spatial wave function of the relative motion in dependence on the spins of the nucleons. Its action is illustrated best in the angular momentum representation, where it mixes states $\big|\,(L = J \mp 1, S = 1)JM\,\big\rangle$ with states $\big|\,(L = J \pm 1, S = 1)JM\,\big\rangle$. The tensor correlator for example admixes the d-wave component of the deuteron wave function when starting from a trial state that has only an s-wave component.

We use central and tensor correlations that are of finite range so that

$$\underset{\sim}{C}(r \to \infty) = \underset{\sim}{1} \ . \tag{7}$$

This implies that the phase shifts of the correlated interaction $\underset{\sim}{\hat{H}} = \underset{\sim}{C}^\dagger \underset{\sim}{H} \underset{\sim}{C}$ are the same as for the uncorrelated interaction $\underset{\sim}{H}$.

As the nuclear interaction depends strongly on spin and isospin we use different correlators in the distinct spin-isospin channels. In each channel the correlator is determined for the lowest orbital angular momenta. For higher orbital angular momenta the centrifugal barrier shifts the nucleon density to larger distances and the effect of the short-range repulsion is smaller. Furthermore the lowest orbital angular momenta have the biggest weights in many-body calculations.

The correlated many-body trial state

$$\big|\,\hat{\Psi}\,\big\rangle = \underset{\sim}{C}\big|\,\Psi\,\big\rangle \tag{8}$$

consists of two parts, the correlator $\underset{\sim}{C}$ and the uncorrelated trial state $\big|\,\Psi\,\big\rangle$. In the sense of the Ritz variational principle both can be varied. The optimal correlator will however depend on the restrictions imposed on $\big|\,\Psi\,\big\rangle$. Or in other words: The more variational freedom is in $\big|\,\Psi\,\big\rangle$ the less remains for $\underset{\sim}{C}$. It is important to note that for trial states $\big|\,\Psi\,\big\rangle$ consisting of a superposition of few or many or even very many Slater determinants the corresponding correlators $\underset{\sim}{C}$ differ only in their long range behavior and are very similar at short distances.

The correlator is the exponential of a two-body operator and therefore the correlated Hamilton operator contains not only one- and two-body but in principle also higher-order contributions. If the correlators are of short-range and the densities are not too high, i.e. the mean distance of the nucleons is larger than the correlation length, the two-body approximation, where only the one- and two-body contributions are taken into account, is well justified. In this two-body approximation the central and the tensor correlations are evaluated analytically in the angular momentum representation without further approximations, see section 1.8.4.

Based on this we perform in section 1.10 *ab initio* calculations for the doubly magic nuclei ^{4}He, ^{16}O and ^{40}Ca where we use a single Slater determinant of harmonic oscillator shell model states. Despite this simple trial state the energy and radii compare very favorably with other much more expensive methods.

The correlations implemented with the correlators $\underset{\sim}{C}_r$ and $\underset{\sim}{C}_\Omega$ are extremely important. For example in ^{4}He calculated with the Argonne V18 interaction the inclusion of central repulsive correlations decreases the energy by 62 MeV and the tensor correlations result in a further decrease of 37 MeV to finally end up at a binding energy of $E = -25$ MeV. In addition we observe that, although the expectation values with the uncorrelated Argonne V18 and Bonn-A interaction differ greatly, the correlated interactions give almost identical results for the nuclei.

In section 1.12 we demonstrate that the correlated Bonn-A and Argonne V18 interactions not only give very similar results in the many-body calculations, they also agree extremely well in the momentum space representation. The correlated interactions in momentum space are compared with the V_{lowk} potential [BKS$^+$01] that is obtained by integrating out the high momentum modes. Although derived in a quite different scheme the V_{lowk} potential is very similar to our correlated potential.

We conclude from these observations that the unitary correlator extracts the common low-momentum behavior of the Bonn-A and the Argonne V18 interactions. With the unitary correlator we therefore have successfully performed a separation of scales. The high-momentum scale of the short-range correlations is covered by the unitary correlator, the low-momentum or long-range behavior is described by the uncorrelated many-body trial state

However the tensor correlations are longer in range than the central correlations and the separation in short-range or high-momentum components and long-range or low-momentum components as it is possible for the central correlations is not as clear cut for the tensor correlations. We can ensure the validity of the two-body approximation by using the unitary correlator only for the shorter part of the tensor correlations and use an improved many-body description for the long ranged part of the tensor correlations. Nevertheless a decent description is also possible with very simple many-body trial states and a long ranged tensor correlator when we tolerate larger uncertainties due to three-body contributions.

If the correlated interaction is not to be used in angular momentum eigenstates of closed shell nuclei but for example in Fermionic Molecular Dynamics we use a basis-free representation of the correlated interaction, as presented in section 1.11. With that we calculate in section 2.2 the ground state properties of about 140 nuclei up to $A = 48$. As in the GFMC calculations for light nuclei and the CBF calculations, that are numerically feasible only for ^{16}O and ^{40}Ca, the nuclei are not bound enough with realistic interactions.

The fact that the realistic two-body forces alone give not enough binding in the many-body system is unfortunate because it implies that additional genuine three-body forces have to be added. In principle Chiral Perturbation Theory should be able to provide a derivation of three-body forces that are consistent with the two-body forces. Because of the complexity of this approach a more phenomenological ansatz for three-body forces is used [PPWC01] whose parameters are adjusted to reproduce the many-body properties. The three-body contributions are

small compared to the two-body ones. Because of the large cancellations between kinetic and potential energy the three-body forces are nevertheless important for an accurate description of nuclei.

Summary

The unitary correlator provides a transparent and powerful method to use realistic nucleon-nucleon interactions in *ab initio* calculations for larger nuclei, but with comparatively little numerical effort. The big advantage of realistic interactions for nuclear structure calculations is that the spin and isospin dependence of the correlated two-body force is fixed. Different from effective interactions or mean-field parameterizations of the energy-density there are no free parameters in the two-body force. This is especially important for the predictions concerning exotic nuclei with large isospins and low density tails.

Our results show in agreement with GFMC calculations of light nuclei that the realistic two-body forces alone cannot successfully reproduce the experimental binding energies of the nuclei.

The *ab initio* calculations for about 140 nuclei up to $A = 48$ demonstrate that nevertheless a correlated realistic interaction is a very good starting point. The main problem, the short range repulsion and the short range part of the tensor correlations is successfully tackled by the unitary correlator. What remains to do is the inclusion of three-body forces and improvements in the uncorrelated trial state that take better account of the long range correlations.

Chapter 1

Short-Range Central and Tensor Correlations

1.1 Nucleon-Nucleon Interaction

Today it is common believe that the fundamental theory of nuclear physics is Quantum Chromo Dynamics (QCD). QCD is well tested at high energies where the asymptotic freedom allows to use perturbation theory. Unfortunately the situation is much more complicated in the low energy regime of nuclear structure physics. Due to the confinement property it is not possible to calculate properties of atomic nuclei starting from the QCD Lagrangian. A basic understanding of the masses of the baryons has been achieved by lattice calculations [Ric99], but investigations of nuclear structure using QCD is beyond hope.

It has been proposed by Weinberg [Wei90, Wei91] that in the low energy regime of nuclear physics ($\leq$ 1GeV) where the appropriate degrees of freedom are the nucleons and the pions one can describe those by an effective field theory based on broken chiral symmetry. In such a scheme the general structure of the nucleon-nucleon interaction can be derived. The parameters in this effective field theory are determined from the low-energy observables like scattering data. Work is under way to derive the nucleon-nucleon potential following these ideas [EM01]. Another encouraging aspect of this approach is that it allows to determine the structure of the three-body forces on the same footing – at least in principle. Up today this promising method cannot yet compete with the "established" nucleon-nucleon interactions in reproducing the well known scattering data.

Two prominent interactions of the 80's, that reproduce the nucleon-nucleon scattering data up to 300MeV and the deuteron properties, are the Bonn-A and the Argonne V14 interactions. With more precise and better analyzed scattering data improved versions of these interactions which include additional charge independence breaking and charge symmetry breaking components have been presented in the 90's, namely the Bonn-CD and the Argonne V18.

In the derivation of a nuclear force that is based on chiral symmetry one includes all terms up to a certain order that are compatible with the symmetries of the π-N-Lagrangian. In the Bonn approach the nuclear interaction is described in the meson-exchange picture. This includes also higher orders like the correlated two pion-exchange. In the end the interaction is parameterized by one-boson exchange in a relativistic treatment. The nonrelativistic variant of the Bonn interaction has nonlocal momentum dependent terms which appear as relativistic corrections. The nonrelativistic Argonne interaction on the other hand is rather phenomenological. The long range part of the interaction is given as in the Bonn potential by pion exchange,

the short-range part is modeled differently – where the Bonn interaction generates repulsion by momentum-dependent interaction terms the Argonne interaction has repulsive local contributions. Nevertheless they both describe the measured phase shifts equally well. The potentials are therefore identical on-shell but they differ in their off-shell behavior. In a bound nucleus only the total four-momentum of all nucleons is conserved. A single nucleon in the interacting many-body system as shown in Fig. 1.1 does not fulfill the dispersion relation for a free nucleon. The properties of a bound nucleus therefore depend on the off-shell behavior of the interaction.

Thus the nuclear force is not uniquely determined by the scattering data. Three-body forces that are added to reproduce the experimental binding energies and radii of light nuclei [PPC+97, WPCP00, PPWC01] are presently investigated and depend on the choice of the two-body force.

We want to remark that the Unitary Correlation Operator Method presented in this work allows the construction of a manifold of two-body interactions which are all phase shift equivalent.

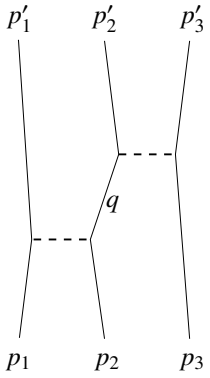

Figure 1.1: Three nucleons interacting via two-body forces. Only the total four-momentum of the three nucleons has to be conserved $p_1 + p_2 + p_3 = p'_1 + p'_2 + p'_3$. In this interacting system the momentum q of the intermediate state does not fulfill the on-shell dispersion relation $q^2 = m^2$ of a free nucleon.

Short-range Repulsion and Tensor Force

Common to all realistic interactions is that they cannot be used successfully in mean-field calculations. This is due to the strong repulsion at short distances and the strong tensor force. Both properties of the nuclear force create strong correlations in the nuclear many-body state. The short-range repulsion leads to a correlation hole in the two-body density and the tensor force to a correlation between the spins and the relative orientation of a pair of nucleons.

With a single Slater determinant it is not possible to describe these correlations. The two-body density of a Slater determinant has an exchange hole due to the Pauli principle but it cannot describe the much stronger depletion needed for the short-range correlations. The two-body density of a Slater determinant can also not represent the correlation between spin directions and the relative orientation of two nucleons as it is generated by the tensor force.

In the regime where they have been adjusted effective interactions without repulsive core and tensor reproduce the experimental nuclear data. But the connection to the underlying realistic two-body force is lost. Our aim is to explicitly incorporate the short-range central and the tensor correlations in the many-body state using the unitary correlation operator method. In this way we can use simple Slater determinants or a shell model approach with configuration mixing together with realistic interactions.

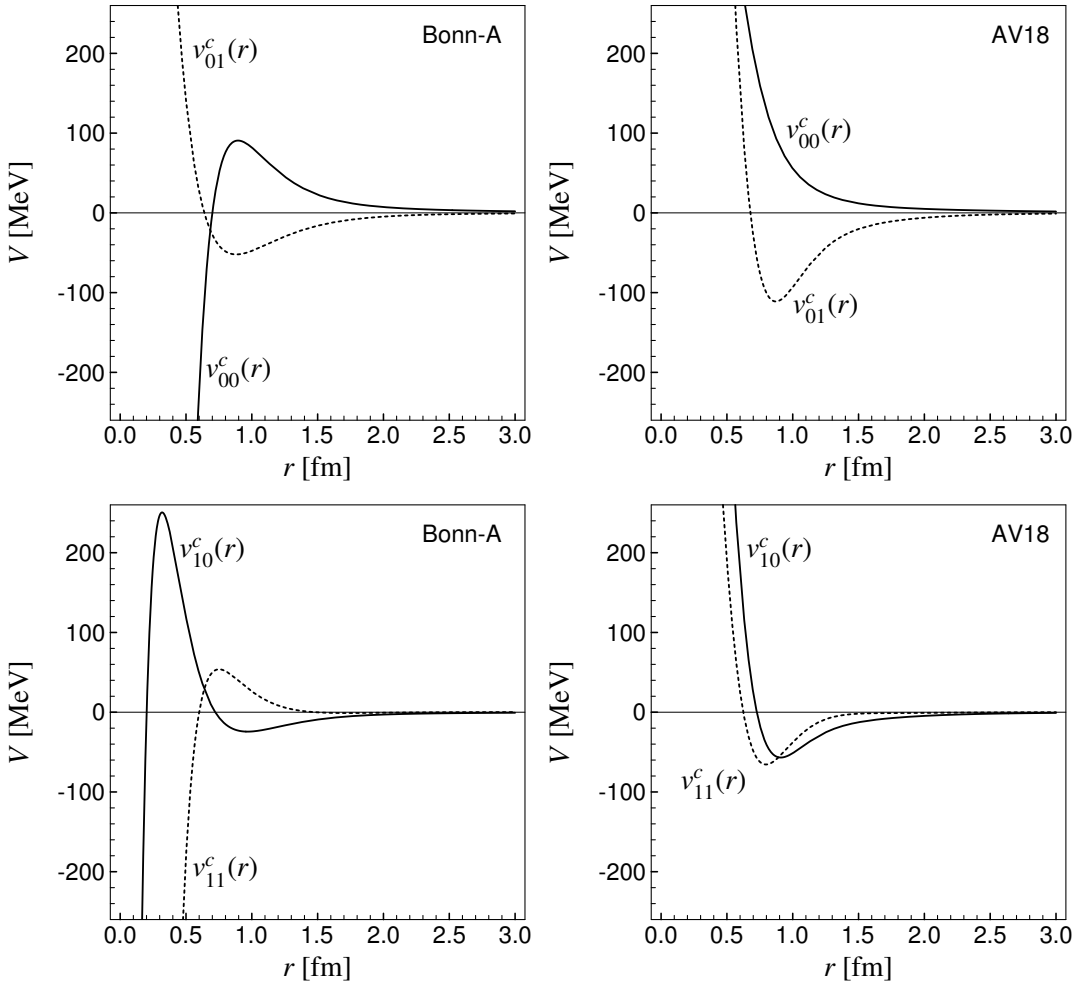

Figure 1.2: Central potential in the $S = 0$ and the $S = 1$ channels for the Bonn-A interaction Eq. (1.1) (left hand side) and the Argonne V18 interaction Eq. (1.2) (right hand side).

1.1.1 Bonn Potentials

Out of the family of the Bonn potentials we will use the (nonrelativistic) Bonn-A interaction [Mac89] which has strong nonlocal contributions and a relatively weak tensor force. Because of the technical problems arising with the nonlocal terms there are only a few many-body calculations using the Bonn-A potential in the literature.

We use a representation of the interaction where we project the potential on spin- and isospin-channels. This more convenient form is equivalent to the usual representation using the $\boldsymbol{\sigma}\cdot\boldsymbol{\sigma}$ and $\boldsymbol{\tau}\cdot\boldsymbol{\tau}$ or the exchange operators [1]

$$\begin{aligned} \underset{\sim}{v} \overset{\mathbf{r}}{\Rightarrow} & \sum_{S,T} v^c_{ST}(r)\,\Pi_{ST} + \sum_{T} v^t_{1T}(r)\, s_{12}(\hat{\mathbf{r}},\hat{\mathbf{r}})\,\Pi_{1T} + \sum_{T} v^b_{1T}(r)\,\mathbf{l}\cdot\mathbf{s}\,\Pi_{1T} \\ & + \sum_{S,T} \frac{1}{2}\left(\mathbf{p}^2 v^{p^2}_{ST}(r) + v^{p^2}_{ST}(r)\mathbf{p}^2\right)\Pi_{ST}\ . \end{aligned} \tag{1.1}$$

[1] The $\overset{\mathbf{r}}{\Rightarrow}$ symbol denotes the coordinate space representation of an Hilbert space operator. The operator Π_{ST} projects on the respective S, T channel. Further notational conventions are summarized in appendix A.

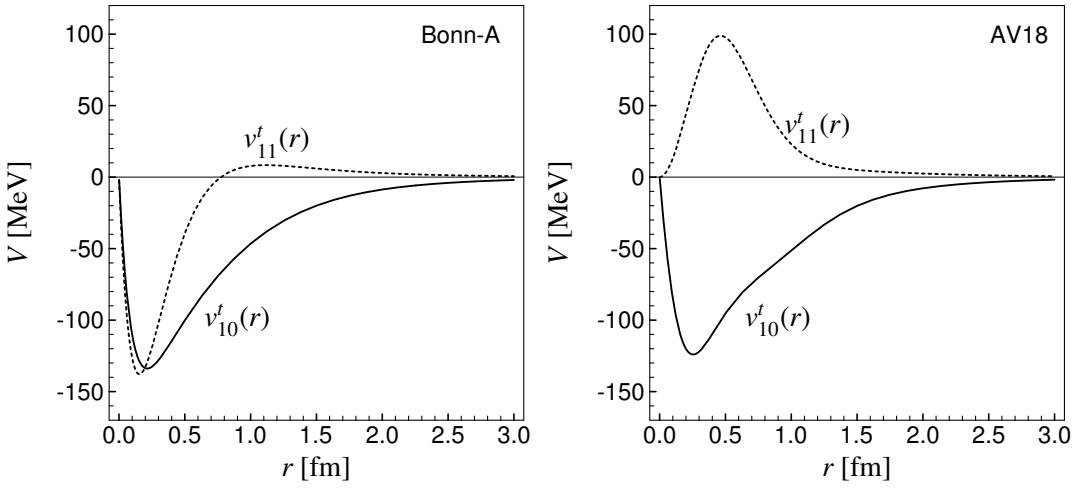

Figure 1.3: Tensor potential for the Bonn-A interaction Eq. (1.1) (left hand side) and the Argonne V18 interaction Eq. (1.2) (right hand side).

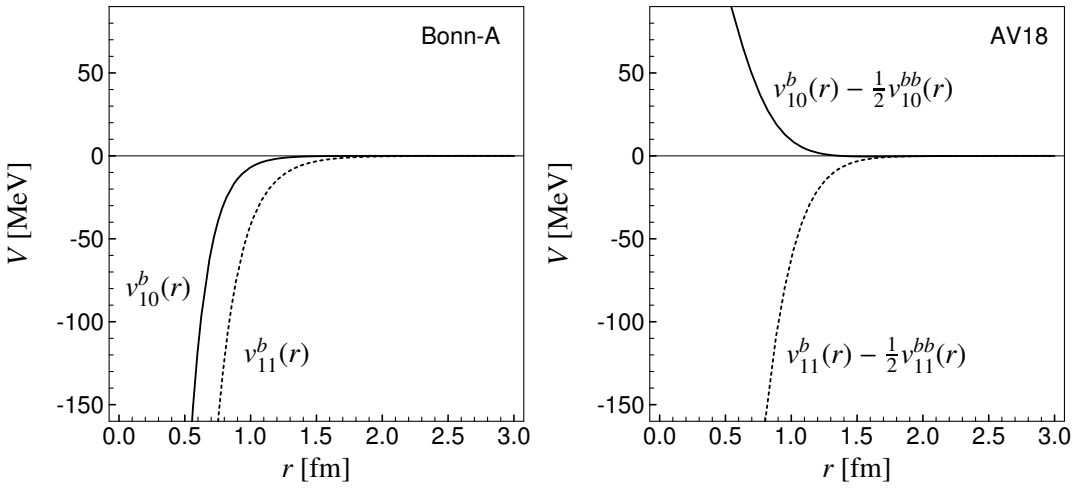

Figure 1.4: Spin-orbit potential for the Bonn-A interaction Eq. (1.1) (left hand side) and the Argonne V18 interaction Eq. (1.2) (right hand side). The spin-orbit part of the $(\mathbf{l}\cdot\mathbf{s})^2$ potential has been added for the Argonne V18 potential.

We can identify the nonlocal $\mathbf{p}^2$ dependent terms of the Bonn potential. The radial dependencies in this parameterization are plotted in Figs. 1.2-1.5 together with the plots for the Argonne V18 interaction.

The 90's version of the Bonn interaction has been refitted to the new set of scattering data and includes additional charge independence breaking and charge symmetry breaking parts. For this Bonn-CD interaction [Mac01] unfortunately no nonrelativistic parameterization is given. Therefore we shall use only the Bonn-A potential in our nonrelativistic approach.

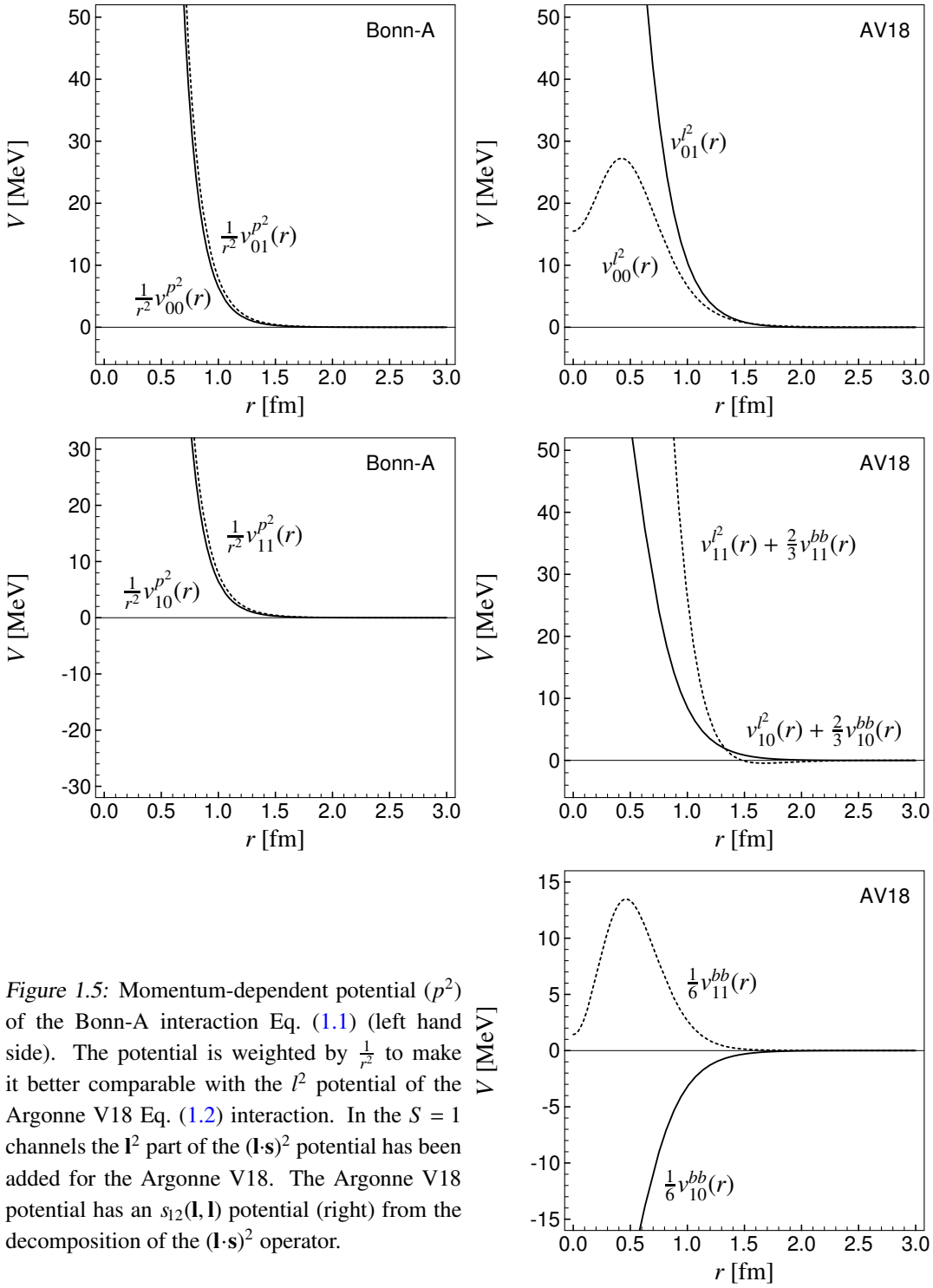

Figure 1.5: Momentum-dependent potential (p^2) of the Bonn-A interaction Eq. (1.1) (left hand side). The potential is weighted by $\frac{1}{r^2}$ to make it better comparable with the l^2 potential of the Argonne V18 Eq. (1.2) interaction. In the $S = 1$ channels the $\mathbf{l}^2$ part of the $(\mathbf{l}\cdot\mathbf{s})^2$ potential has been added for the Argonne V18. The Argonne V18 potential has an $s_{12}(\mathbf{l},\mathbf{l})$ potential (right) from the decomposition of the $(\mathbf{l}\cdot\mathbf{s})^2$ operator.

1.1.2 Argonne Potentials

Unlike the Bonn interaction the Argonne V14 interaction [WSA84] is designed using a phenomenological approach to be as *local* as possible. This is technically favorable in the GFMC calculations. However momentum dependence is needed to reproduce the phase-shifts. In the

Argonne potentials this is included via angular momentum dependence in form of $\mathbf{l}^2$ and $(\mathbf{l}\cdot\mathbf{s})^2$ terms in contrast to the $\mathbf{p}^2$ terms of the Bonn interaction.

The Argonne V14 potential can be written in the spin- and isospin channel representation as

$$\begin{aligned} \underset{\sim}{v} \overset{\mathbf{r}}{\Rightarrow} & \sum_{S,T} v^c_{ST}(r)\,\Pi_{ST} + \sum_{T} v^t_{1T}(r)\,s_{12}(\hat{\mathbf{r}},\hat{\mathbf{r}})\,\Pi_{1T} + \sum_{T} v^b_{1T}(r)\,\mathbf{l}\cdot\mathbf{s}\,\Pi_{1T} \\ & + \sum_{S,T} v^{l^2}_{ST}(r)\,\mathbf{l}^2\,\Pi_{ST} + \sum_{T} v^{bb}_{1T}(r)\,(\mathbf{l}\cdot\mathbf{s})^2\,\Pi_{1T}\ . \end{aligned} \tag{1.2}$$

We decompose the $(\mathbf{l}\cdot\mathbf{s})^2$ operator into irreducible tensor operators (see appendix B)

$$(\mathbf{l}\cdot\mathbf{s})^2 = \frac{2}{3}\mathbf{l}^2\,\Pi_{S=1} - \frac{1}{2}\mathbf{l}\cdot\mathbf{s} + \frac{1}{6}s_{12}(\mathbf{l},\mathbf{l})\ . \tag{1.3}$$

and add the $\mathbf{l}^2$ and $\mathbf{l}\cdot\mathbf{s}$ terms to the respective potential terms in the plots Figs. 1.2-1.5.

The improved Argonne V18 interaction [WSS95] fitted to the improved scattering data does include the electro-magnetic interaction beyond the static approximation and contains charge independence breaking and charge symmetry breaking terms. These additional terms give only minor corrections and we will use the Argonne V18 interactions without these additional terms.

Argonne V8'

A simplified version of the Argonne V18 is the Argonne V8' interaction [PPC+97]. In the Argonne V8' the $\mathbf{l}^2$ and $(\mathbf{l}\cdot\mathbf{s})^2$ parts of the full Argonne V18 interaction are projected onto the central, spin-orbit and tensor parts in such a way that the interaction is unchanged in the *s*- and *p*- waves and in the deuteron channel

$$\begin{aligned} v^c_{00}(r) &\longleftarrow v^c_{00}(r) + 2v^{l^2}_{00}(r) & v^c_{01}(r) &\longleftarrow v^c_{01}(r) \\ v^c_{10}(r) &\longleftarrow v^c_{10}(r) & v^c_{11}(r) &\longleftarrow v^c_{11}(r) + 2v^{l^2}_{11}(r) + \frac{4}{3}v^{bb}_{11}(r) \\ v^t_{10}(r) &\longleftarrow v^t_{10}(r) & v^t_{11}(r) &\longleftarrow v^t_{11}(r) - \frac{5}{12}v^{bb}_{11}(r) \\ v^b_{10}(r) &\longleftarrow v^b_{10}(r) - 2v^{l^2}_{10}(r) - 3v^{bb}_{10}(r) & v^b_{11}(r) &\longleftarrow v^b_{11}(r) - \frac{1}{2}v^{bb}_{11}(r)\ . \end{aligned} \tag{1.4a-h}$$

1.2 Unitary Correlation Operator

With the Unitary Correlation Operator Method (UCOM) we want to bring together realistic nuclear interactions and the simple many-body states of a mean field or shell model calculation. The short-range or high-momentum behavior of the many-body state is treated by the unitary correlator which is almost independent from the low energy scale of the long-range correlations that can be successfully described in a mean-field approach.

The correlated many-body states are constructed by applying the unitary correlation operator $\underset{\sim}{C}$ to the uncorrelated many-body state $\big|\,\Psi\,\rangle$ that may be a Slater determinant of harmonic oscillator states as used in shell model calculations or a Slater determinant of Gaussian wave packets as used in the Fermionic Molecular Dynamics (FMD) model

$$\big|\,\hat{\Psi}\,\rangle = \underset{\sim}{C}\big|\,\Psi\,\rangle\ . \tag{1.5}$$

Alternatively we can apply the correlations to the operators and define correlated operators

$$\hat{\underset{\sim}{A}} = \underset{\sim}{C}^{\dagger} \underset{\sim}{A} \underset{\sim}{C} \,. \tag{1.6}$$

Due to the unitarity of the correlation operator we can evaluate matrix elements either using uncorrelated operators and correlated states or using correlated operators and uncorrelated states:

$$\langle \Phi \left| \underset{\sim}{C}^{\dagger} \underset{\sim}{A} \underset{\sim}{C} \right| \Psi \rangle = \langle \hat{\Phi} \left| \underset{\sim}{A} \right| \hat{\Psi} \rangle = \langle \Phi \left| \hat{\underset{\sim}{A}} \right| \Psi \rangle \,. \tag{1.7}$$

As the correlation operator $\underset{\sim}{C}$ should be unitary and as it should describe two-body correlations we will construct it using a hermitian two-body generator $\underset{\sim}{G}$

$$\underset{\sim}{C} = \exp\{-i\underset{\sim}{G}\} \,. \tag{1.8}$$

The correlation operator $\underset{\sim}{C}$ itself is not a two-body operator, as the repetitive application of the generator generates operators of increasing order in particle number. If we want to describe genuine three-body correlations we would have to use a three-body generator $\underset{\sim}{G}$.

The correlated Hamilton operator should posses the same symmetries with respect to global transformations like translation, rotation, boost as the uncorrelated one. Therefore the generator can only depend on the relative coordinates and momenta of the two particles and it has to be a scalar operator with respect to rotations. Furthermore the correlations should fulfill the cluster decomposition property, that implies that observables of separated subsystems that are outside the range of the interaction are not affected by correlations between the subsystems. The correlations therefore have to be of finite range.

Before we look at the explicit form of the generators for central and tensor correlators we discuss the application of correlated operators in many-body systems, which is performed in the sense of the cluster expansion.

1.2.1 Cluster Expansion

As the correlation operator $\underset{\sim}{C}$ is the exponential of a two-body operator, the correlation operator itself and correlated operators have irreducible contributions of higher particle orders. The Fock space representation of the correlated operator $\hat{\underset{\sim}{A}}$ is given by the cluster expansion

$$\hat{\underset{\sim}{A}} = \underset{\sim}{C}^{\dagger} \underset{\sim}{A} \underset{\sim}{C} = \sum_{i=1} \hat{\underset{\sim}{A}}^{[i]} \,, \tag{1.9}$$

where i denotes the irreducible particle number.

Using an orthonormal one-body basis $\{\left| k \right\rangle = \underset{\sim}{a}_k^{\dagger} \left| 0 \right\rangle\}$ we get

$$\hat{\underset{\sim}{A}}^{[1]} = \sum_{k,k'} \langle k \left| \underset{\sim}{C}^{\dagger} \underset{\sim}{A} \underset{\sim}{C} \right| k' \rangle \, \underset{\sim}{a}_k^{\dagger} \underset{\sim}{a}_{k'} = \sum_{k,k'} \langle k \left| \underset{\sim}{A} \right| k' \rangle \, \underset{\sim}{a}_k^{\dagger} \underset{\sim}{a}_{k'} \tag{1.10}$$

$$\hat{\underset{\sim}{A}}^{[2]} = \frac{1}{4} \sum_{\substack{k_1,k_2 \\ k_1',k_2'}} {}_a\langle k_1, k_2 \left| \underset{\sim}{C}^{\dagger} \underset{\sim}{A} \underset{\sim}{C} - \hat{\underset{\sim}{A}}^{[1]} \right| k_1', k_2' \rangle_a \, \underset{\sim}{a}_{k_1}^{\dagger} \underset{\sim}{a}_{k_2}^{\dagger} \underset{\sim}{a}_{k_2'} \underset{\sim}{a}_{k_1'} \tag{1.11}$$

$$\vdots$$

$$\hat{\underset{\sim}{A}}^{[n]} = \frac{1}{(n!)^2} \sum_{\substack{k_1,\ldots,k_n \\ k_1',\ldots,k_n'}} {}_a\langle k_1, \ldots, k_n \left| \underset{\sim}{C}^{\dagger} \underset{\sim}{A} \underset{\sim}{C} - \sum_{i=1}^{n-1} \hat{\underset{\sim}{A}}^{[i]} \right| k_1', \ldots, k_n' \rangle_a \, \underset{\sim}{a}_{k_1}^{\dagger} \cdots \underset{\sim}{a}_{k_n}^{\dagger} \underset{\sim}{a}_{k_n'} \cdots \underset{\sim}{a}_{k_1'} \,, \tag{1.12}$$

where at each order of the cluster expansion the contributions of the lower particle orders have to be subtracted.

In practice we would like to restrict the calculations to the two-body level as the three-body contributions are already very involved. We should therefore use generators $\underset{\sim}{G}$ which cause only small three-body contributions. The importance of three-body contributions will increase with the range of the correlator and the density of the system.

We will use the notation

$$\left[\underset{\sim}{C}^{\dagger}\underset{\sim}{A}\underset{\sim}{C}\right]^{C2} = \underset{\sim}{\hat{A}}^{[1]} + \underset{\sim}{\hat{A}}^{[2]} \tag{1.13}$$

to indicate the two-body approximation.

1.3 Two-Body System

When we are calculating matrix elements of many-body states in two-body approximation we have to evaluate matrix elements of correlated operators in one- and two-body space only. In contrast to Fock space operators which are denoted by uppercase letters (e.g. $\underset{\sim}{C}$) we will use lowercase letters for operators in one- or two-body space (e.g. $\underset{\sim}{c}$ for the correlation operator in two-body space).

As the nuclear force does not connect states of different total spin and isospin the eigenstates of total spin and isospin provide the most convenient basis in these degrees of freedom. The transformation from the one-body variables with spin three-components χ_i and isospin three-components ξ_i into eigenstates of total spin and isospin is done with the help of Clebsch-Gordan coefficients

$$\left\langle \mathbf{x}_1\chi_1\xi_1;\mathbf{x}_2\chi_2\xi_2 \,\middle|\, \Phi \right\rangle = \sum_{S,M_S} \mathrm{C}\begin{pmatrix} \frac{1}{2} & \frac{1}{2} & \\ \chi_1 & \chi_2 & \end{pmatrix}\begin{matrix} S \\ M_S \end{matrix}\Bigg) \sum_{T,M_T} \mathrm{C}\begin{pmatrix} \frac{1}{2} & \frac{1}{2} & \\ \xi_1 & \xi_2 & \end{pmatrix}\begin{matrix} T \\ M_T \end{matrix}\Bigg) \left\langle \mathbf{r}\,\mathbf{x}_{\mathrm{cm}};S\,M_S\,T\,M_T \,\middle|\, \Phi \right\rangle . \tag{1.14}$$

The distance of the two nucleons $\mathbf{r}$ and the center of mass of the two nucleons $\mathbf{x}_{\mathrm{cm}}$ are given as

$$\mathbf{r} = \mathbf{x}_1 - \mathbf{x}_2 , \qquad \mathbf{x}_{\mathrm{cm}} = \frac{1}{2}(\mathbf{x}_1 + \mathbf{x}_2) . \tag{1.15a,b}$$

The correlator will only affect the relative and not the center of mass motion of two nucleons. Concerning the kinetic energy

$$\underset{\sim}{t} = \underset{\sim}{t}_{\mathrm{rel}} + \underset{\sim}{t}_{\mathrm{cm}} \tag{1.16}$$

we therefore only have to correlate the kinetic energy $\underset{\sim}{t}_{\mathrm{rel}}$ of the relative motion.

Using the relative momentum $\underset{\sim}{\mathbf{p}}$ and the total momentum $\underset{\sim}{\mathbf{p}}_{\mathrm{cm}}$

$$\underset{\sim}{\mathbf{p}} = \frac{1}{2}(\underset{\sim}{\mathbf{p}}_1 - \underset{\sim}{\mathbf{p}}_2) , \qquad \underset{\sim}{\mathbf{p}}_{\mathrm{cm}} = \underset{\sim}{\mathbf{p}}_1 + \underset{\sim}{\mathbf{p}}_2 \tag{1.17a,b}$$

the kinetic energy of relative and center of mass motion can be written as

$$\underset{\sim}{t}_{\mathrm{rel}} = \frac{1}{m}\underset{\sim}{\mathbf{p}}^2 , \qquad \underset{\sim}{t}_{\mathrm{cm}} = \frac{1}{4m}\underset{\sim}{\mathbf{p}}^2_{\mathrm{cm}} . \tag{1.18a,b}$$

The orbital angular momentum of the two-body system can also be decomposed into the orbital angular momentum of the center of mass motion and the orbital angular momentum of the relative motion

$$\underset{\sim}{\mathbf{l}}_1 + \underset{\sim}{\mathbf{l}}_2 = \underset{\sim}{\mathbf{l}}_{\mathrm{cm}} + \underset{\sim}{\mathbf{l}}_{\mathrm{rel}} \tag{1.19}$$

with

$$\underset{\sim}{\mathbf{l}}_{\mathrm{rel}} = \underset{\sim}{\mathbf{r}} \times \underset{\sim}{\mathbf{p}} , \qquad \underset{\sim}{\mathbf{l}}_{\mathrm{cm}} = \underset{\sim}{\mathbf{x}}_{\mathrm{cm}} \times \underset{\sim}{\mathbf{p}}_{\mathrm{cm}} . \tag{1.20a,b}$$

1.4 Correlated Densities

The short-range central and tensor correlations in the nucleus can be studied best by inspecting the one- and two-body density matrices. The density matrices of the many-body state $\left|\,\Phi\,\right\rangle$ in coordinate representation are defined as

$$\rho^{(1)}(\mathbf{x}_1\chi_1\xi_1;\mathbf{x}'_1\chi'_1\xi'_1) = \left\langle\,\Phi\,\middle|\,\underset{\sim}{\Psi}^\dagger_{\chi'_1\xi'_1}(\mathbf{x}'_1)\underset{\sim}{\Psi}_{\chi_1\xi_1}(\mathbf{x}_1)\,\middle|\,\Phi\,\right\rangle \tag{1.21}$$

and

$$\rho^{(2)}(\mathbf{x}_1\chi_1\xi_1,\mathbf{x}_2\chi_2\xi_2;\mathbf{x}'_1\chi'_1\xi'_1,\mathbf{x}'_2\chi'_2\xi'_2) = \left\langle\,\Phi\,\middle|\,\underset{\sim}{\Psi}^\dagger_{\chi'_1\xi'_1}(\mathbf{x}'_1)\underset{\sim}{\Psi}^\dagger_{\chi'_2\xi'_2}(\mathbf{x}'_2)\underset{\sim}{\Psi}_{\chi_2\xi_2}(\mathbf{x}_2)\underset{\sim}{\Psi}_{\chi_1\xi_1}(\mathbf{x}_1)\,\middle|\,\Phi\,\right\rangle . \tag{1.22}$$

The two-body correlations can be visualized best with the help of the two-body density matrix $\rho^{(2)}_{SM_S,TM_T}(\mathbf{r})$ which describes the probability density to find two nucleons at a distance $\mathbf{r}$ in the S,T channel with spin and isospin orientations M_S, M_T. The center of mass coordinate is integrated out.

$$\begin{aligned}\rho^{(2)}_{SM_S,TM_T}(\mathbf{r}) = &\sum_{\chi_1,\chi_2} \mathrm{C}\begin{pmatrix}\frac{1}{2} & \frac{1}{2} & S\\ \chi_1 & \chi_2 & M_S\end{pmatrix}\sum_{\xi_1,\xi_2}\mathrm{C}\begin{pmatrix}\frac{1}{2} & \frac{1}{2} & T\\ \xi_1 & \xi_2 & M_T\end{pmatrix}\\ &\times\int \mathrm{d}^3X\,\rho^{(2)}(\mathbf{X}+\tfrac{1}{2}\mathbf{r}\chi_1\xi_1,\mathbf{X}-\tfrac{1}{2}\mathbf{r}\chi_2\xi_2;\mathbf{X}+\tfrac{1}{2}\mathbf{r}\chi_1\xi_1,\mathbf{X}-\tfrac{1}{2}\mathbf{r}\chi_2\xi_2)\end{aligned} \tag{1.23}$$

The information about the short-range central correlations is contained in the radial dependence of this two-nucleon correlation function. The tensor correlations manifest themselves by the angular and the spin dependence.

If $\rho^{(2)}_{SM_S,TM_T}(\mathbf{r})$ does not depend on the three-components of spin and isospin we may use the abbreviation $\rho^{(2)}_{S,T}(\mathbf{r})$.

As with other operators the density matrices of correlated many-body states $\left|\,\hat\Phi\,\right\rangle = \underset{\sim}{C}\left|\,\Phi\,\right\rangle$ have to be calculated in the sense of the cluster expansion

$$\begin{aligned}\hat\rho^{(1)}(\mathbf{x}_1\chi_1\xi_1;\mathbf{x}'_1\chi'_1\xi'_1) &= \left\langle\,\Phi\,\middle|\,\underset{\sim}{C}^\dagger\underset{\sim}{\Psi}^\dagger_{\chi'_1\xi'_1}(\mathbf{x}'_1)\underset{\sim}{\Psi}_{\chi_1\xi_1}(\mathbf{x}_1)\underset{\sim}{C}\,\middle|\,\Phi\,\right\rangle\\ &= \sum_{n=1}^{A}\left\langle\,\Phi\,\middle|\,[\underset{\sim}{C}^\dagger\underset{\sim}{\Psi}^\dagger_{\chi'_1\xi'_1}(\mathbf{x}'_1)\underset{\sim}{\Psi}_{\chi_1\xi_1}(\mathbf{x}_1)\underset{\sim}{C}]^{[n]}\,\middle|\,\Phi\,\right\rangle ,\end{aligned} \tag{1.24}$$

$$\begin{aligned}\hat\rho^{(2)}(\mathbf{x}_1\chi_1\xi_1,\mathbf{x}_2\chi_2\xi_2;\mathbf{x}'_1\chi'_1\xi'_1,\mathbf{x}'_2\chi'_2\xi'_2) &=\\ &= \left\langle\,\Phi\,\middle|\,\underset{\sim}{C}^\dagger\underset{\sim}{\Psi}^\dagger_{\chi'_1\xi'_1}(\mathbf{x}'_1)\underset{\sim}{\Psi}^\dagger_{\chi'_2\xi'_2}(\mathbf{x}'_2)\underset{\sim}{\Psi}_{\chi_2\xi_2}(\mathbf{x}_2)\underset{\sim}{\Psi}_{\chi_1\xi_1}(\mathbf{x}_1)\underset{\sim}{C}\,\middle|\,\Phi\,\right\rangle\\ &= \sum_{n=2}^{A}\left\langle\,\Phi\,\middle|\,[\underset{\sim}{C}^\dagger\underset{\sim}{\Psi}^\dagger_{\chi'_1\xi'_1}(\mathbf{x}'_1)\underset{\sim}{\Psi}^\dagger_{\chi'_2\xi'_2}(\mathbf{x}'_2)\underset{\sim}{\Psi}_{\chi_2\xi_2}(\mathbf{x}_2)\underset{\sim}{\Psi}_{\chi_1\xi_1}(\mathbf{x}_1)\underset{\sim}{C}]^{[n]}\,\middle|\,\Phi\,\right\rangle .\end{aligned} \tag{1.25}$$

The expansions will be truncated in the two-body approximation after the second order. One should notice that density matrices calculated in a truncated cluster expansion fulfill the reduction property of the exact density matrices

$$\sum_{\chi_2,\xi_2}\int \mathrm{d}^3x_2\,\hat\rho^{(2)}(\mathbf{x}_1\chi_1\xi_1,\mathbf{x}_2\chi_2\xi_2;\mathbf{x}'_1\chi'_1\xi'_1,\mathbf{x}_2\chi_2\xi_2) = (A-1)\,\hat\rho^{(1)}(\mathbf{x}_1\chi_1\xi_1;\mathbf{x}'_1\chi'_1\xi'_1) \tag{1.26}$$

only approximately. If the truncation at second order is justified, Eq. (1.26) is well approximated.

1.4.1 Nucleon Density Distribution and Nucleon Momentum Distribution

The nucleon density distribution $\rho(\mathbf{x})$ is given by the diagonal part of the one-body density matrix which has been summed over spin and isospin indices

$$\rho^{(1)}(\mathbf{x}) = \sum_{\chi,\xi} \rho^{(1)}(\mathbf{x}\chi\xi;\mathbf{x}\chi\xi) \; . \tag{1.27}$$

The nucleon momentum distribution $n(\mathbf{p})$ is given by the Fourier transform of the off-diagonal matrix elements of the one-body density matrix

$$n(\mathbf{p}) = \int \mathrm{d}^3x_1 \int \mathrm{d}^3x_2 \sum_{\chi\xi} \rho^{(1)}(\mathbf{x}_1\chi\xi;\mathbf{x}_2\chi\xi)\, e^{i\mathbf{p}\cdot(\mathbf{x}_1-\mathbf{x}_2)} \; . \tag{1.28}$$

1.5 Spin-Isospin dependent Correlators

As the nuclear force depends strongly on spin and isospin also the correlations will be distinct in the different spin and isospin channels. In two-body space we use the ansatz

$$\underset{\sim}{g} = \sum_{ST} \underset{\sim}{g}_{ST}\, \underset{\sim}{\Pi}_{ST} \tag{1.29}$$

for a spin-isospin dependent generator with the projectors $\underset{\sim}{\Pi}_{ST}$ on the spin-isospin channels. Exploiting the projector properties we can rewrite the correlation operator

$$\underset{\sim}{c} = \exp\{-i\underset{\sim}{g}\} = \sum_{ST} \exp\{-i\underset{\sim}{g}_{ST}\}\, \underset{\sim}{\Pi}_{ST} \; , \tag{1.30}$$

and as the nuclear interaction does not connect the different spin and isospin channels[2] we obtain the correlated potential in two-body space as

$$\underset{\sim}{\hat{v}} = \underset{\sim}{c}^{\dagger}\underset{\sim}{v}\underset{\sim}{c} = \sum_{ST} \exp\{i\underset{\sim}{g}_{ST}\}\, \underset{\sim}{v}_{ST}\, \exp\{-i\underset{\sim}{g}_{ST}\}\, \underset{\sim}{\Pi}_{ST} \; . \tag{1.31}$$

We have thus the important result that the correlations in the different spin-isospin channels decouple and the correlation operators can be determined for each spin-isospin channel independently.

1.6 Central Correlations

Central correlations within the UCOM framework have already been studied in detail [FNRS98, Rot00]. In this section we shall only provide a short summary of the ideas and techniques. For the illustrations we use the Argonne V18 potential (which is identical to the Argonne V8' potential in the $L = 0$ channel) in the $S, T = 0, 1$ channel where we do not have to deal with additional complications from tensor correlations.

As with all realistic nuclear forces the Argonne V18 potential has a strong repulsive core at short distances between the nucleons. The probability density of nucleons in the range of the core of another nucleon is therefore strongly suppressed and we can observe a correlation

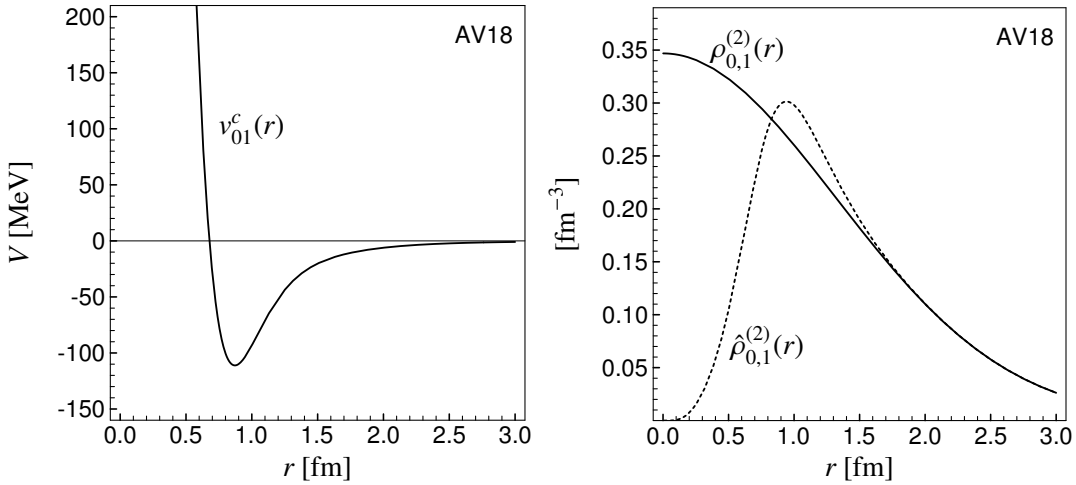

Figure 1.6: Correlation hole in the ^{4}He two-body density. The Argonne V18 potential in the $S, T = 0, 1$ channel is plotted on the left hand side. It is strongly repulsive at short distances. On the right hand side the effect of the repulsion is clearly visible in the correlated two-body density $\hat{\rho}^{(2)}_{0,1}$, that has to be compared with the uncorrelated two-body density $\rho^{(2)}_{0,1}$ of the trial state. The ^{4}He trial state has been chosen to reproduce the experimental radius of the ^{4}He nucleus.

hole in the two-body density as can be seen in Fig. 1.6 where we already show the correlated two-body density obtained with the UCOM method.

To describe these short-range correlations we need an operator that shifts the nucleons out of the range of the repulsive core. As the shift should be radial we use a generator $\underset{\sim}{g}_r$ built with the radial momentum operator $\underset{\sim}{p}_r$. The strength of the shift has to depend on the distance of the nucleons. If they find themselves in the range of the core the shift has to be strong and if they are far away from each other there should be no shift at all. This radial dependence is given by the shift function $s(r)$. As the generator has to be hermitian we make the ansatz

$$\underset{\sim}{g}_r \overset{\mathbf{r}}{\Rightarrow} \frac{1}{2}\Big\{p_r s(r) + s(r)p_r\Big\} \,. \tag{1.32}$$

See appendix B.1 for the properties of the radial momentum operator $\underset{\sim}{p}_r \overset{\mathbf{r}}{\Rightarrow} \frac{1}{i}\frac{1}{r}\frac{\partial}{\partial r}r$.

The correlator has to be of finite range for the application in the many-body system in order not to destroy the cluster decomposition property. The task of the unitary correlation operator is to introduce the short-range correlations induced by the repulsive core of the interaction in the many-body state. Possible long range correlations will have to be described by the many-body trial state and not by the correlation operator. If analyzed in momentum space the correlator describes the high momentum components of the state while the low momentum part is taken care of by the model space.

[2]This is not the case for terms that break charge symmetry and charge independence in the Argonne V18 and Bonn CD interactions. However we do not consider these terms, which give only minor corrections, in this work.

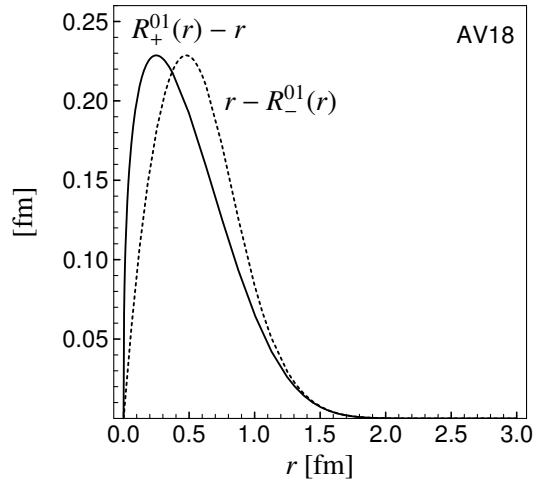

Figure 1.7: The correlation function $R_+^{01}(r)$ and the inverse correlation function $R_-^{01}(r)$ for the Argonne V18 potential in the $S, T = 0, 1$ channel.

Correlation Function $R_\pm(r)$

For technical reasons it is advantageous to use the correlation functions $R_+(r)$ or $R_-(r)$ instead of the shift function $s(r)$. They are related to the shift function by

$$\pm 1 = \int_r^{R_\pm(r)} \frac{d\xi}{s(\xi)} \,. \tag{1.33}$$

For small shifts we have approximately

$$R_\pm(r) \approx r \pm s(r) \,. \tag{1.34}$$

The correlation functions $R_+(r)$ or $R_-(r)$ for the $S, T = 0, 1$ channel of the Argonne V18 potential are displayed in Fig. 1.7. The correlations are strongest in the range up to about 0.5 fm and extend to about 1.5 fm.

The correlation functions are mutually inverse to each other

$$R_\pm(R_\mp(r)) = r \,, \tag{1.35}$$

this reflects the unitarity of the correlation operator.

1.6.1 Correlated Wave Function

Using the correlation functions we can give explicit formulas for the wave function of a correlated two-body system $\left|\, \hat{\Phi} \,\right\rangle = \underset{\sim}{c}_r \left|\, \Phi \,\right\rangle$

$$\left\langle\, \mathbf{X}, \mathbf{r} \,\middle|\, \underset{\sim}{c}_r \,\middle|\, \Phi \,\right\rangle = \mathcal{R}_-(r) \left\langle\, \mathbf{X}, R_-(r)\hat{\mathbf{r}} \,\middle|\, \Phi \,\right\rangle \tag{1.36}$$

$$\left\langle\, \mathbf{X}, \mathbf{r} \,\middle|\, \underset{\sim}{c}_r^\dagger \,\middle|\, \Phi \,\right\rangle = \mathcal{R}_+(r) \left\langle\, \mathbf{X}, R_+(r)\hat{\mathbf{r}} \,\middle|\, \Phi \,\right\rangle \,. \tag{1.37}$$

The metric factor

$$\mathcal{R}_\pm(r) = \frac{R_\pm(r)}{r} \sqrt{R'_\pm(r)} \,, \tag{1.38}$$

ensures the conservation of the norm. A correlated Gaussian wave function and a correlated constant wave function are displayed in Fig. 1.8. The correlated wave functions are almost identical in the range of the repulsive core of the interaction. As the correlations conserve the norm of the wave function the hole created at short distances has to be compensated by an enhancement of the wave function further out.

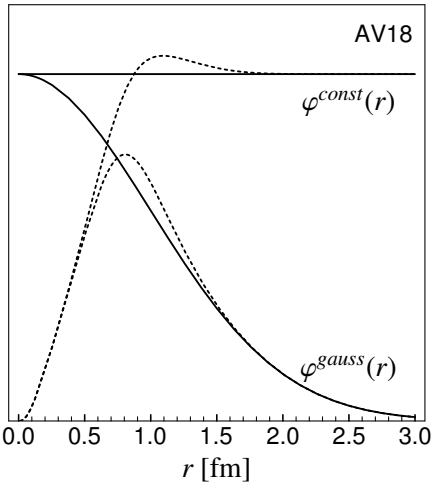

Figure 1.8: Correlated (dotted) and uncorrelated (solid) constant wave function and correlated (dotted) and uncorrelated (solid) Gaussian wave function. The norm of the wave functions is not changed by the correlation.

1.6.2 Correlated Operators

The calculation of the correlated kinetic energy in two-body approximation results in a one- and a two-body contribution to the correlated Hamilton operator. The one-body contribution is again the kinetic energy because the generator $\underset{\sim}{g}_r$ is a two-body operator and thus the correlator $\underset{\sim}{c} = \exp\{-i\underset{\sim}{g}\}$ contains besides the unit operator only two-body or higher terms.

$$\hat{\underset{\sim}{t}}^{[1]} = \underset{\sim}{c}^{\dagger}\underset{\sim}{t}^{[1]}\underset{\sim}{c} = \underset{\sim}{t}^{[1]} \tag{1.39}$$

For the calculation of the two-body contribution of the correlated kinetic energy we use the relative and center of mass variables introduced in section 1.3. The kinetic energy in the two-body system is the sum of the center of mass kinetic energy $t_{\rm cm}$ that is not influenced by the correlator and the kinetic energy of the relative motion that can be decomposed further in a radial and an angular part

$$\underset{\sim}{t}_{\rm rel} = \underset{\sim}{t}_r + \underset{\sim}{t}_\Omega \overset{\mathbf{r}}{\Rightarrow} \frac{1}{m}p_r^2 + \frac{1}{m}\frac{\mathbf{l}^2}{r^2}\,. \tag{1.40}$$

The correlated radial part of the kinetic energy leads to a momentum dependent potential

$$\hat{\underset{\sim}{t}}_r^{[2]} = \underset{\sim}{c}_r^{\dagger}\underset{\sim}{t}_r\underset{\sim}{c}_r - \underset{\sim}{t}_r \overset{\mathbf{r}}{\Rightarrow} \frac{1}{2}\left[p_r^2\frac{1}{2\hat{\mu}_r(r)} + \frac{1}{2\hat{\mu}_r(r)}p_r^2\right] + \hat{u}(r) \tag{1.41}$$

similar to the kinetic energy but with a correlated "radial mass"

$$\frac{1}{2\hat{\mu}_r(r)} = \frac{1}{m}\left(\frac{1}{R'_+(r)^2} - 1\right) \tag{1.42}$$

and an additional local potential[3]

$$\hat{u}(r) = \frac{1}{m}\left(\frac{7R''_+(r)^2}{4R'_+(r)^4} - \frac{R'''_+(r)}{2R'_+(r)^3}\right). \tag{1.43}$$

The angular part of the correlated kinetic energy

$$\hat{\underset{\sim}{t}}_\Omega^{[2]} = \underset{\sim}{c}_r^{\dagger}\underset{\sim}{t}_\Omega\underset{\sim}{c}_r - \underset{\sim}{t}_\Omega \overset{\mathbf{r}}{\Rightarrow} \frac{1}{2\hat{\mu}_\Omega(r)}\frac{\mathbf{l}^2}{r^2} \tag{1.44}$$

[3] We use a different representation of the momentum dependent part compared to [FNRS98]. The transformation rules between different parameterizations are given in appendix B.1.

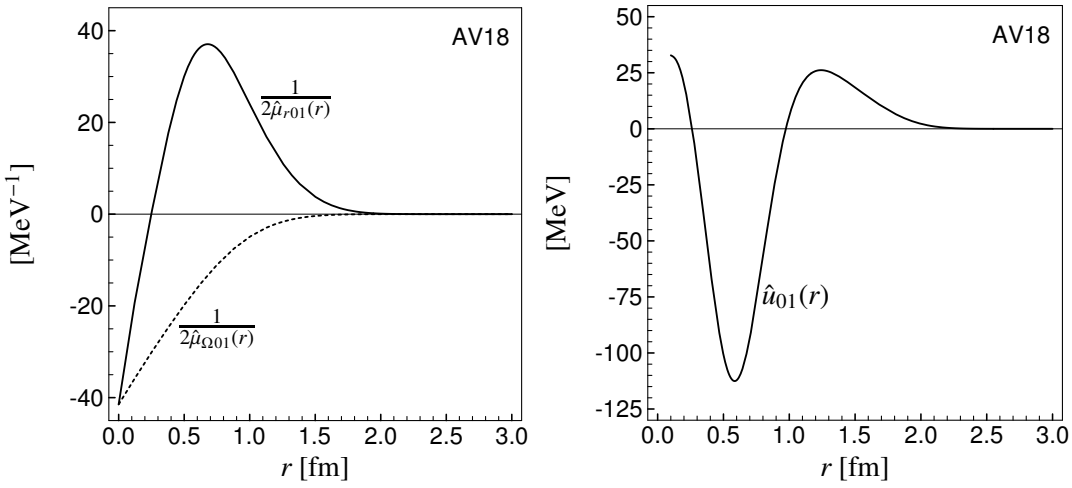

Figure 1.9: Radial and angular mass of the correlated kinetic energy on the left, potential part of the correlated kinetic energy on the right for the Argonne V18 potential in the $S, T = 0, 1$ channel.

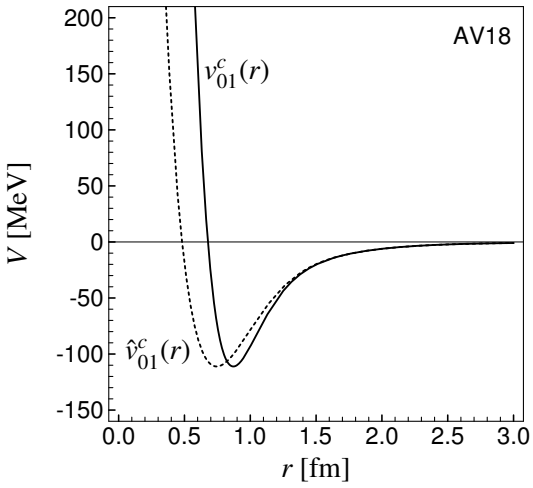

Figure 1.10: The correlated central potential of the Argonne V18 in the $S, T = 0, 1$ channel. The central correlator weakens the core of the interaction.

has a correlated "angular mass"

$$\frac{1}{2\hat{\mu}_\Omega(r)} = \frac{1}{m}\left(\frac{r^2}{R_+(r)^2} - 1\right). \tag{1.45}$$

The correlated kinetic energy has interaction components that we also find in the uncorrelated Bonn-A interaction, but there "radial mass" and "angular mass" are the same, and the Argonne V18 interaction (that only has the $\mathbf{l}^2$ terms). In Fig. 1.9 the contributions to the correlated kinetic energy of the Argonne V18 interaction are shown.

The correlated central potential $\hat{\underset{\sim}{v}}^c \overset{\mathbf{r}}{\Rightarrow} \hat{v}^c(r)$ plotted in Fig. 1.10 is expressed easily as the uncorrelated potential with a transformed radial dependence

$$\hat{\underset{\sim}{v}}^c = \underset{\sim}{c}^\dagger_r \underset{\sim}{v}^c \underset{\sim}{c}_r \overset{\mathbf{r}}{\Rightarrow} v^c(R_+(r)) \,. \tag{1.46}$$

Like for the central interaction, the central correlation of spin-orbit $\underset{\sim}{v}^b \overset{\mathbf{r}}{\Rightarrow} v^b(r)\,\mathbf{l}\cdot\mathbf{s}$ and tensor

potentials $\underset{\sim}{v}^t \overset{\mathbf{r}}{\Rightarrow} v^t(r)\, s_{12}(\hat{\mathbf{r}}, \hat{\mathbf{r}})$ leads only to a transformed radial dependence ($\underset{\sim}{p}_r$ commutes with the operators $\mathbf{l}\cdot\mathbf{s}$ and $s_{12}(\hat{\mathbf{r}}, \hat{\mathbf{r}})$)

$$\underset{\sim}{\hat{v}}^b = \underset{\sim}{c}_r^\dagger \underset{\sim}{v}^b \underset{\sim}{c}_r \overset{\mathbf{r}}{\Rightarrow} v^b(R_+(r))\, \mathbf{l}\cdot\mathbf{s}\ , \tag{1.47}$$

$$\underset{\sim}{\hat{v}}^t = \underset{\sim}{c}_r^\dagger \underset{\sim}{v}^t \underset{\sim}{c}_r \overset{\mathbf{r}}{\Rightarrow} v^t(R_+(r))\, s_{12}(\hat{\mathbf{r}}, \hat{\mathbf{r}})\ . \tag{1.48}$$

This holds also in case of the spin-orbit squared and orbital angular momentum squared potentials

$$\underset{\sim}{\hat{v}}^{l^2} = \underset{\sim}{c}_r^\dagger \underset{\sim}{v}^{l^2} \underset{\sim}{c}_r \overset{\mathbf{r}}{\Rightarrow} v^{l^2}(R_+(r))\, \mathbf{l}^2\ , \tag{1.49}$$

$$\underset{\sim}{\hat{v}}^{bb} = \underset{\sim}{c}_r^\dagger \underset{\sim}{v}^{bb} \underset{\sim}{c}_r \overset{\mathbf{r}}{\Rightarrow} v^{bb}(R_+(r))\, (\mathbf{l}\cdot\mathbf{s})^2\ . \tag{1.50}$$

The momentum-dependent potential $\underset{\sim}{v}^{p^2}$ occuring in the Bonn potential can be decomposed into a radial and an angular part

$$\underset{\sim}{v}^{p^2} \overset{\mathbf{r}}{\Rightarrow} \frac{1}{2}\Big[\mathbf{p}^2\, v^{p^2}(r) + v^{p^2}(r)\, \mathbf{p}^2\Big] = \frac{1}{2}\Big[p_r^2\, v^{p^2}(r) + v^{p^2}(r)\, p_r^2\Big] + \frac{v^{p^2}(r)}{r^2}\, \mathbf{l}^2\ . \tag{1.51}$$

The correlated momentum-dependent potential is similar in structure to the correlated kinetic energy but has an additional term because of the radial dependence of $v^{p^2}(r)$

$$\begin{aligned}\underset{\sim}{\hat{v}}^{p^2} = \underset{\sim}{c}_r^\dagger \underset{\sim}{v}^{p^2} \underset{\sim}{c}_r \overset{\mathbf{r}}{\Rightarrow}\ & \frac{1}{2}\Big[p_r^2\, \frac{v^{p^2}(R_+(r))}{R_+'(r)^2} + \frac{v^{p^2}(R_+(r))}{R_+'(r)^2}\, p_r^2\Big] \\ & + v^{p^2}(R_+(r))\Big(\frac{7R_+''(r)^2}{4R_+'(r)^4} - \frac{R_+'''(r)}{2R_+'(r)^3}\Big) - v^{p^2\prime}(R_+(r))\frac{R_+''(r)}{R_+'(r)^2} \\ & + \frac{v^{p^2}(R_+(r))}{R_+(r)^2}\, \mathbf{l}^2\ .\end{aligned} \tag{1.52}$$

1.6.3 Choice of Correlator

Up to now we have discussed the technical aspects of the central correlations but we have not yet addressed the question of how to determine the correlation operator $\underset{\sim}{c}$ or the equivalent correlation function $R_+(r)$.

In principle there are two ways to fix the correlator. The first idea defines the correlation operator as a mapping from a trial state to an exact solution in the two-body system. The second idea is to treat the correlation operator as an additional degree of freedom in the Ritz variational principle. This variation can be done in the two- or in the many-body system. In the following we will present these possibilities in detail.

Mapping to the Zero Energy Scattering Solution

In the two-body system we can define an "optimal" correlator that maps a chosen trial state $\big|\,\varphi\,\big\rangle$ onto an exact solution of the Hamiltonian $\underset{\sim}{H}\big|\,\psi\,\big\rangle = E\big|\,\psi\,\big\rangle$

$$\big|\,\psi\,\big\rangle = \underset{\sim}{c}\big|\,\varphi\,\big\rangle\ . \tag{1.53}$$

The exact state $\big|\,\psi\,\big\rangle$ can be a bound state or scattering state. Our choice is the zero energy scattering state because the correlator will be applied in nuclear structure calculations where

typical relative momenta are in the range of the Fermi momentum $k_F = 1.4\,\mathrm{fm}^{-1}$ which corresponds to a wave length much larger than the typical core radius. Therefore the trial state does not contain the high momenta that correspond to the momentum transfers of the repulsive core. These high momentum components should be induced by the correlation operator. In other words: the correlator describes the short range behavior of the relative wave function while the low momentum or long range part has to be described by the trial state.

If we have repulsive and attractive components of the interaction in the respective channel we get a natural separation of scales. The probability density of the uncorrelated state has to be shifted from the repulsive region of the potential to the attractive domain of the potential. The balance of repulsion and attraction allows us to find a separation point λ where the conditions

$$R_-(\lambda) = \lambda \quad \text{and} \quad R'_-(\lambda) = 1 \; . \tag{1.54a,b}$$

are fulfilled. This implies that at the distance $r = \lambda$ the correlation function $R_+(r)$ can be continued smoothly with $R_+(r) = r$ without correlations beyond the separation point λ.

As trial functions we can use a constant function

$$\varphi_{const}(r) = \sqrt{N} \tag{1.55}$$

where the normalization constant N is varied to fulfill the separation condition Eq. (1.54a,b) or a Gaussian trial function that is matched at a point ρ with the asymptotic solution of the zero-energy scattering problem (with the scattering length a). The Gaussian parameters α and κ are fixed by matching $\varphi_{gauss}(r)$ and its derivative at ρ

$$\varphi_{gauss}(r) = \begin{cases} \alpha \exp\left\{-\frac{r^2}{2\kappa}\right\} & r < \rho \\ \frac{1}{r}(r-a) & r > \rho \; . \end{cases} \tag{1.56}$$

Here ρ is varied to fulfill the separation condition Eq. (1.54a,b).

The result of this procedure is displayed on the left hand side of Fig. 1.11. The correlation functions are defined by mapping the constant wave function $\varphi_{const}(r)$ and the Gaussian wave function $\varphi_{gauss}(r)$ onto the scattering solution $\psi_{zero}(r)$. The norm of the wave function of the exact solution and the uncorrelated constant or Gaussian wave functions are identical up to the respective separation points λ.

We obtain the correlation functions $R_-(r)$ and $R_+(r)$ by solving the Eqs. (1.36-1.37). Using radial wave functions we get the differential equations

$$\sqrt{R'_+(r)}\, \psi_{zero}(R_+(r)) = \varphi(r) \; , \tag{1.57}$$

$$\sqrt{R'_-(r)}\, \varphi(R_-(r)) = \psi_{zero}(r) \; . \tag{1.58}$$

Because of the separation condition Eq. (1.54a,b) we can safely define the correlation functions for $r > \lambda$ as

$$R_+(r) = R_-(r) \equiv r \; , \tag{1.59}$$

so that the trial function is unchanged beyond the separation point. The two correlation functions $R_+(r)$ resulting from the constant and the Gaussian trial wave function are shown in Fig. 1.11. They are very similar at short distances or high momenta where $\psi_{zero}(r)$ varies rapidly. The trial wave functions $\varphi_{const}(r)$ and $\varphi_{gauss}(r)$ differ only slightly in this region.

In purely repulsive interaction channels we cannot define a unique separation point as described above. We can obtain a correlator by using a trial function which has the correct

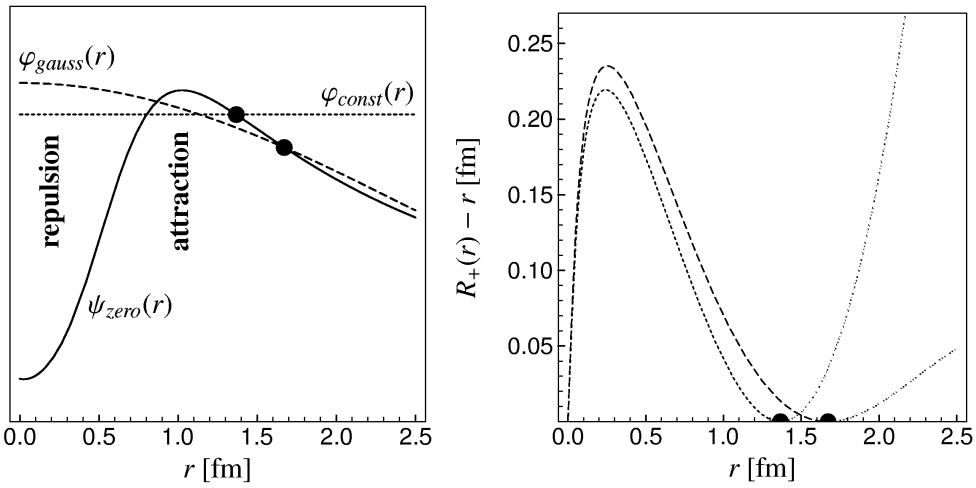

Figure 1.11: Determination of the central correlator for the $S, T = 1, 0$ channel of the Argonne V18 interaction by mapping a constant $\varphi_{const}(r)$ and a Gaussian trial function $\varphi_{gauss}(r)$ onto the zero-energy scattering solution $\psi_{zero}(r)$. The respective separation points λ are indicated by dots. The resulting correlation function are shown on the right. Beyond the separation points λ the correlation function will be continued as $R_+(r) = r$.

asymptotic behavior of the scattering solution. This corresponds to the idea that the correlator should be responsible for short range but not for long range correlations. However this procedure does not define the matching point between the asymptotic and the short-range part of the trial wave function. By moving the matching point the correlation range is changed. After all the allowed correlation range has to be determined in the many-body system. We want the three- and higher-body contributions to be small and therefore prefer correlators of shorter range.

Minimizing the Energy in the Two-Body System

Another possibility to determine the correlator is to minimize the energy in the two-body system. If one regards $\underset{\sim}{c}\big|\,\varphi\,\rangle$ as a variational ansatz for the ground state, both $\big|\,\varphi\,\rangle$ and the shape of the correlator $\underset{\sim}{c}$ can be varied. Again we demand that the correlator $\underset{\sim}{c}$ is responsible for the short range part while $\big|\,\varphi\,\rangle$ should represent the long range part. The choice of $\big|\,\varphi\,\rangle$ depends of course on the system under study.

If we assume that in the even channels the two-body density is almost constant in the range of the core or quadratic in the odd channels, trial functions

$$\varphi_{even}(r) = const \tag{1.60}$$

in the even and because of orbital angular momentum $L=1$

$$\varphi_{odd}(r) = const \cdot r \tag{1.61}$$

in the odd channels are a good choice for small r.

We shall determine two-body minimized correlators using these trial states. In channels with a bound state the energy minimum is achieved with a correlator of finite range. Because of the restriction imposed by the parameterization of the correlation function we will even

find a minimum if the attraction is not strong enough to establish a bound state. In purely repulsive channels a correlator that minimizes the energy will shift the nucleons as far outwards as possible because this lowers the energy to zero, the lowest possible energy. But as the correlator should only describe the short range behavior we impose an additional restriction on the correlation range in order to keep the three-body contributions in the many-body system small.

Minimizing the Energy in the Many-Body System

From the perspective of the variational principle the correlator should be treated as an additional degree of freedom in the many-body trial state. The expectation value of the Hamiltonian

$$E = \langle \Phi \left| \underset{\sim}{C}^{\dagger} H \underset{\sim}{C} \right| \Phi \rangle \tag{1.62}$$

calculated with the variational ansatz $\underset{\sim}{C}\left| \Phi \right\rangle$ is then minimized with respect to the shape of $\underset{\sim}{C}$ for the short range and with respect to the degrees of freedom in the antisymmetrized many-body state $\left| \Phi \right\rangle$, usually a Slater determinant or a superposition of determinants, relating to the long range properties. The optimal correlator is obtained in this sense by simultaneous variation of the parameters of the uncorrelated many-body state and the correlator. This simultaneous variation with respect to correlators and many-body trial state is in practice only possible if an analytic expression for the Hamiltonian is known and the uncorrelated trial state depends only on a small number of parameters. We will use shell model states for ^{4}He, ^{16}O and ^{40}Ca, where the Hamiltonian can be evaluated analytically with the help of the Talmi transformation and where the uncorrelated many-body state depends only on the oscillator parameter, to perform this minimization.

We face the problem that for the calculation of the energy we have to use a truncation of the cluster expansion and hence the Ritz variational principle is only approximately fulfilled, the exact ground state energy is no longer a rigorous lower limit. It has to be checked that the range of the correlator is short enough so that the omission of the higher-order contributions is justified.

Our studies show that the use of many-body optimized correlators provide a clear improvement only for very light nuclei like ^{4}He. The heavier nuclei like ^{16}O and ^{40}Ca have a smooth density distribution and the uncorrelated two-body density is almost constant in the even channels or quadratic in the odd channels at short distances $r \leq 1$ fm between the nucleons, as can be seen in Fig. 1.12. The correlators determined in the two-body system using constant trial functions in the even and linear trial functions in the odd channels are then almost identical to the many-body optimized correlators.

1.6.4 Parameterization of the Correlation Function

For technical reasons it is advantageous to work with parameterizations of the correlation functions. The parameterization has to be flexible enough to represent the correlators determined for example by the zero energy scattering solution. We usually use the parameterization

$$R_+(r) = r + \alpha \left(\frac{r}{\beta}\right)^{\eta} \exp\left\{-\exp\left\{\frac{r}{\beta}\right\}\right\} \tag{1.63}$$

where the range of the correlation function can be tuned with the parameter β. The behavior close to the origin is determined by the parameter η and α governs the overall strength of the correlation function.

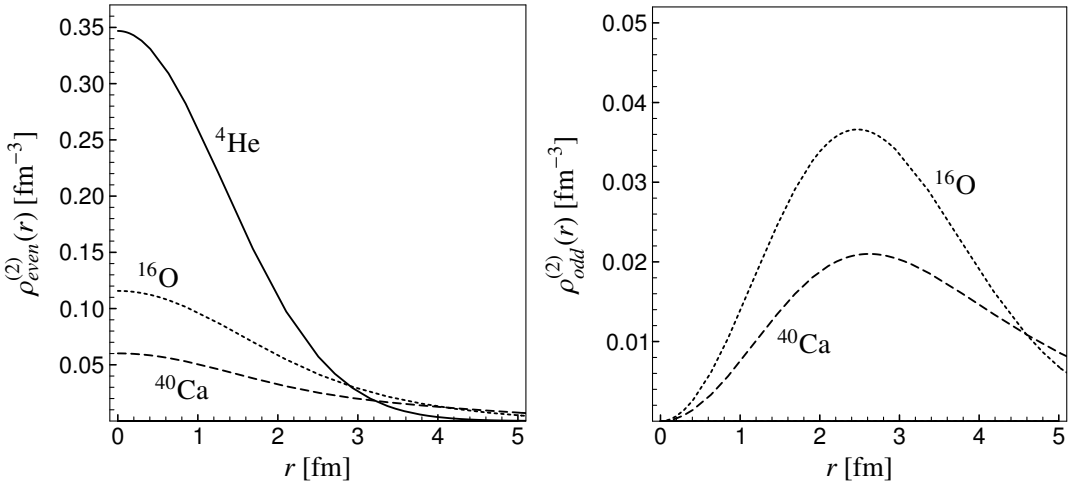

Figure 1.12: Two-body distribution functions for shell model states in odd and even channels. The width of the oscillator basis has been adjusted to the experimental radii. The densities are normalized to identity by dividing the two-body densities by the number of pairs in the respective channels.

For the correlation functions in purely repulsive odd channels we use another parameterization with an exponential decay at large distances

$$R_+(r) = r + \alpha\gamma^\eta\left(1 - \exp\left\{-\left(\frac{r}{\gamma}\right)^\eta\right\}\right)\exp\left\{-\frac{r}{\beta}\right\} . \tag{1.64}$$

If we restrict the correlation range in these channels a variation of the above parameterization with a double exponential tail is used

$$R_+(r) = r + \alpha\gamma^\eta\left(1 - \exp\left\{-\left(\frac{r}{\gamma}\right)^\eta\right\}\right)\exp\left\{-\exp\left\{\frac{r}{\beta}\right\}\right\} . \tag{1.65}$$

The parameter η is an integer for these parameterizations.

The correlation functions determined from the scattering solutions will be fitted with the above parameterizations. The energy minimized correlation functions are obtained by minimizing the energy with respect to the parameters of the parameterizations.

All correlation functions appearing in this work are given in appendix D.

UCOM and Jastrow Correlators Compared

It is illustrative to compare the UCOM method with the well known Jastrow correlation functions. The correlated wave function is obtained in the Jastrow method by multiplying the uncorrelated relative wave function in the two-body system $\varphi(r)$ by a correlation function $f(r)$. The correlated wave function obtained in this manner is of course no longer normalized. In order to construct the equivalent UCOM correlation function $R_-(r)$ or $R_+(r)$ to a given Jastrow correlation function we have to renormalize the Jastrow wave function explicitly

$$\langle\, r \,|\, \underset{\sim}{C} \,|\, \varphi \,\rangle = \frac{R_-(r)}{r}\sqrt{R'_-(r)}\varphi(R_-(r)) \stackrel{!}{=} \frac{f(r)\varphi(r)}{\int \mathrm{d}r\; r^2 f^2(r)\varphi^2(r)} . \tag{1.66}$$

The result of this procedure for a typical Jastrow correlation function using a Gaussian as uncorrelated wave function is shown in Fig. 1.13 together with the UCOM correlation function

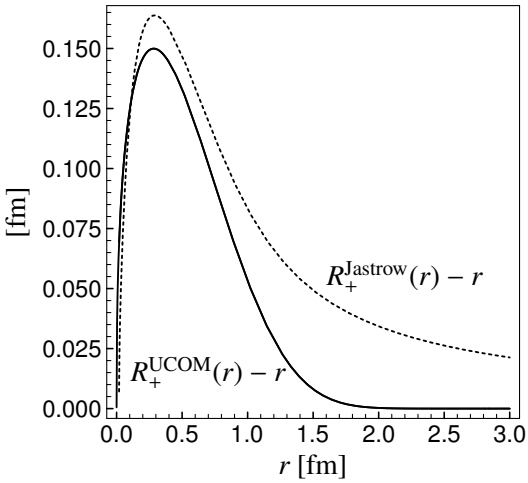

Figure 1.13: Correlation functions for the MTV potential. R_+^{Jastrow} corresponds to the Jastrow correlation function, R_+^{UCOM} is the correlation function obtained with the UCOM method. Contrary to the UCOM correlation function the Jastrow correlation is not of finite range. This is the result of the non-unitarity which necessarily leads to a renormalization.

for the same system. The need for an explicit renormalization of the Jastrow wave function means that the Jastrow correlation is in principle of infinite range despite a finite healing length of the correlation function f(r). The unitary correlator conserves the norm of the correlated state and therefore allows us to used the two-body approximation for low enough densities.

1.7 Many-Body Calculations

Many-body calculations are performed using Slater determinants and the correlated interaction $\hat{\underset{\sim}{H}}^{C2}$ in two-body approximation as explained in section 1.2.1.

In the case of the doubly magic nuclei ^{4}He, ^{16}O and ^{40}Ca the harmonic oscillator shell model states with fully occupied shells provide a very good trial state for the uncorrelated many-body state

$$\left|{}^4\text{He}\right\rangle = \left|(1s)^4\right\rangle \tag{1.67}$$

$$\left|{}^{16}\text{O}\right\rangle = \left|(1s)^4(1p)^{12}\right\rangle \tag{1.68}$$

$$\left|{}^{40}\text{Ca}\right\rangle = \left|(1s)^4(1p)^{12}(2s)^4(1d)^{20}\right\rangle . \tag{1.69}$$

The explicit form of the harmonic oscillator single particle wave functions

$$\phi^a_{nlm}(\mathbf{r}) = \frac{R_{nl}(a)(r)}{r} Y^l_m(\hat{\mathbf{r}}) \tag{1.70}$$

is given by Eq. (C.1).

The only free parameter of these many-body states is the oscillator parameter a that is related to the uncorrelated radii of the nuclei, see appendix C.3.

The expectation value of the Hamilton operator in two-body approximation involves one- and two-body matrix elements that are summed over all occupied harmonic oscillator states

$$\begin{aligned}\left\langle \hat{\underset{\sim}{H}}^{C2} \right\rangle = &\sum_{nlm\xi\chi} \left\langle nlm\chi\xi \left| \hat{\underset{\sim}{h}}^{[1]} \right| nlm\chi\xi \right\rangle \\ &+ \frac{1}{2} \sum_{\substack{n_1 l_1 m_1 \xi_1 \chi_1 \\ n_2 l_2 m_2 \xi_2 \chi_2}} \left\langle n_1 l_1 m_1 \xi_1 \chi_1; n_2 l_2 m_2 \xi_2 \chi_2 \left| \hat{\underset{\sim}{h}}^{[2]} \right| n_1 l_1 m_1 \xi_1 \chi_1; n_2 l_2 m_2 \xi_2 \chi_2 \right\rangle_a .\end{aligned} \tag{1.71}$$

The harmonic oscillator basis has the unique property that the relative and center of mass motion of a two-body state can be separated

$$\phi^a_{n_1 l_1 m_1}(\mathbf{r}_1)\phi^a_{n_2 l_2 m_2}(\mathbf{r}_2) = \sum_{NLMnlm} \left\langle \begin{matrix} n_1 l_1 m_1 \\ n_2 l_2 m_2 \end{matrix} \middle| \begin{matrix} NLM \\ nlm \end{matrix} \right\rangle \phi^{a/2}_{NLM}(\mathbf{R})\, \phi^{2a}_{nlm}(\mathbf{r}) \,. \tag{1.72}$$

With the help of this so called Talmi transformation (see appendix C) we can simplify the evaluation of the two-body matrix elements significantly and gain explicit expressions for the expectation value of two-body operators.

In the case of ^{4}He we get for example

$$\begin{aligned} \langle\, {}^4\mathrm{He} \,|\, \underset{\sim}{\hat{H}}^{[2]} \,|\, {}^4\mathrm{He} \,\rangle = &\sum_{M_T} \langle\, 1;(00)00,1M_T \,|\, \underset{\sim}{\hat{h}}^{[2]} \,|\, 1;(00)00,1M_T \,\rangle \\ &+ \sum_{M} \langle\, 1;(01)1M,00 \,|\, \underset{\sim}{\hat{h}}^{[2]} \,|\, 1;(01)1M,00 \,\rangle \,, \end{aligned} \tag{1.73}$$

The matrix elements do not depend on the M and M_T quantum numbers and we can write the ^{4}He expectation value as

$$\langle\, {}^4\mathrm{He} \,|\, \underset{\sim}{\hat{H}}^{[2]} \,|\, {}^4\mathrm{He} \,\rangle = 3\langle\, 1;(00)0,1 \,|\, \underset{\sim}{\hat{h}}^{[2]} \,|\, 1;(00)0,1 \,\rangle + 3\langle\, 1;(01)1,0 \,|\, \underset{\sim}{\hat{h}}^{[2]} \,|\, 1;(01)1,0 \,\rangle \,. \tag{1.74}$$

The relative wave functions of the two-body states $|\, n;(LS)JM,TM_T \,\rangle$

$$\langle\, \mathbf{r} \,|\, n;(LS)JM,TM_T \,\rangle = \sum_{M_L,M_S} \mathrm{C}\left(\begin{matrix} L & S \\ M_L & M_S \end{matrix} \middle| \begin{matrix} J \\ M \end{matrix} \right) \phi^{2a}_{nLM_L}(\mathbf{r}) \otimes |\, S\,M_S \,\rangle \otimes |\, T,M_T \,\rangle \tag{1.75}$$

are harmonic oscillator wave functions with twice the variance of the single-particle states in coordinate space.

Explicit expressions for expectation values of two-body operators in ^{16}O and ^{40}Ca are given in appendix C.2.

1.7.1 Malfliet-Tjon V Potential

The Malfliet Tjon V potential [MT69] is a central potential independent of spin and isospin. It has been used as a test case for spin and isospin independent correlations. Although we do not regard it as a physical meaningful nuclear interaction we take it as a first benchmark for the unitary correlation operator as several calculations are available in the literature to compare with.

Following our prescription we get the correlation functions displayed in Fig. 1.14. $R^{zero}_+(r)$ is the correlation function obtained by mapping a Gaussian trial wave function onto the zero-energy scattering solution in the even channels with $L = 0$. The correlation function $R^{min}_+(r)$ is obtained by minimizing the energy in the two-body system with a constant trial function. Finally $R^{^4\mathrm{He}}_+(r)$ is the energy minimized correlation function for the ^{4}He nucleus in two-body approximation and with a harmonic oscillator trial wave function whose width has been fixed to reproduce the radius obtained in the GFMC calculation. The parameters for all correlation functions are given in appendix D.2.

The distinct correlation functions have a similar radial dependence, the ^{4}He optimized correlator being a little bit stronger than the other two. The results of the ^{4}He and ^{16}O many-body calculations with these correlation functions are shown in Fig. 1.15 where the binding energy

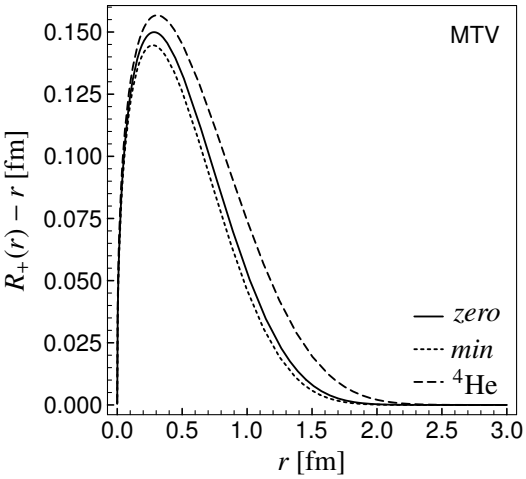

Figure 1.14: Correlation functions for the MTV potential. R_+^{zero} is derived from the zero energy scattering solution. R_+^{min} is obtained by minimizing the energy in the two-body system with a constant trial function and $R_+^{^4\mathrm{He}}$ is the result of minimizing the ^{4}He energy using a harmonic oscillator shell model state whose width is fixed to the GFMC result.

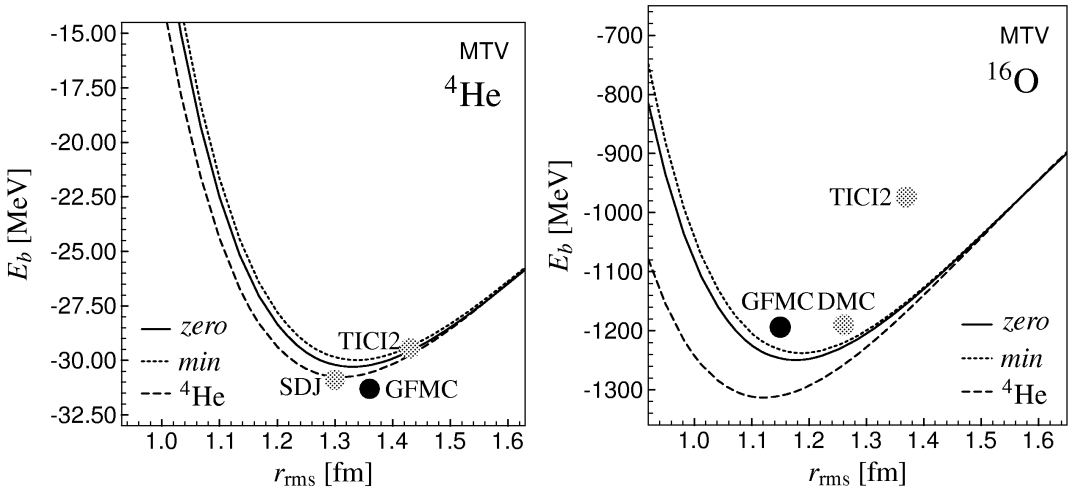

Figure 1.15: Binding energy versus radius r_{rms} for ^{4}He on the left and ^{16}O on the right hand side obtained with the MTV potential. Three different correlators have been used. Reference results for the GFMC, TICI2 and SDJ methods are shown for ^{4}He and GFMC, DMC and TICI2 results for ^{16}O.

is plotted as a function of r_{rms} radius. The same correlation function is used in both the odd channels and the even channels. The UCOM results agree very well with results from Green's Function Monte Carlo calculations (GFMC) [HZ85], the TICI2 method [GMN+96], HNC calculations using state dependent Jastrow correlations (SDJ) [GP98], and a Diffusion Monte Carlo calculation (DMC) [CK93]. This is very encouraging when we consider the simplicity of our trial state.

The best binding in ^{4}He is achieved, as expected, with the correlator optimized for this specific nucleus though the differences are rather small. The fact that the ^{4}He optimized correlator gives the largest binding energy also in ^{16}O is an artifact of the MTV interaction. Because of the absence of repulsion in the odd channels the radius of the ^{16}O nucleus is even smaller than that of the ^{4}He nucleus. This small radius corresponds to an extremely high density. The fact that our binding energies seem to be reasonable even at these extreme high densities strengthens our believe in the validity of the two-body approximation.

1.7.2 Modified Afnan-Tang S3 Potential

The modified Afnan-Tang S3 (ATS3M) potential [GFMP81] is a central nucleon-nucleon interaction with spin and isospin dependence but without tensor interactions and spin-orbit interactions and it is considered as a benchmark for central state-dependent correlators.

The correlators obtained in the even channels are shown in Fig. 1.16, the correlator for the odd channels – the ATS3M potential is equal in both odd channels – is shown in Fig. 1.17. The parameterizations for all correlation functions are given in appendix D.3. Whereas the correlation functions in the even channels are similar to the MTV correlation functions, the ATS3M potential is purely repulsive in the odd channels and the correlator determined from the zero-energy scattering solution has a very long range. Three other correlators have been obtained by minimizing the energy in the two-body system with constraints

$$\int \mathrm{d}r\, r^2\, (R_+(r) - r) \stackrel{!}{=} \begin{cases} 0.1\,\mathrm{fm}^3 & ; \quad \alpha \\ 0.2\,\mathrm{fm}^3 & ; \quad \beta \\ 0.5\,\mathrm{fm}^3 & ; \quad \gamma \end{cases} \tag{1.76}$$

on the correlation range.

In Fig. 1.18 we show the result of out ^{4}He calculations. As the odd channel of the interaction does not contribute to the ^{4}He binding energy in two-body approximation the results depend only on the correlation functions in the even channels. The strongest binding is of course obtained using the ^{4}He optimized correlator. For reference the results of the Stochastic Variational Method (SVM) [VS95], the TICI2 method [GMN+96] and HNC calculations using state dependent Jastrow correlations (SDJ) [GP98] are shown. Again the agreement is astonishingly good considering the simplicity of our approach.

The results for the ^{16}O and ^{40}Ca nuclei are shown in Fig. 1.19. In the even channels we use the correlation functions $R_+^{min}(r)$ minimized in the two-body system. In contrast to the ^{4}He nucleus the many-body optimal correlators give almost no improvement in the binding

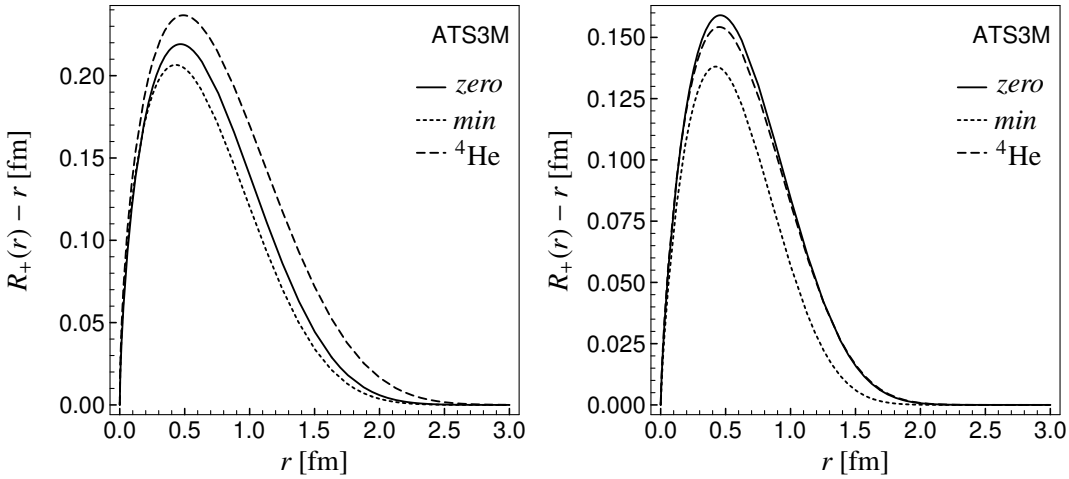

Figure 1.16: The correlation functions in $S, T = 0, 1$ (left hand side) and $S, T = 1, 0$ channels (right hand side) for the ATS3M potential. R_+^{zero} is derived from the zero energy scattering solution. R_+^{min} is obtained by minimizing the energy in the two-body system with a constant trial function and $R_+^{^4\mathrm{He}}$ is the result of minimizing the ^{4}He energy using a harmonic oscillator shell model state.

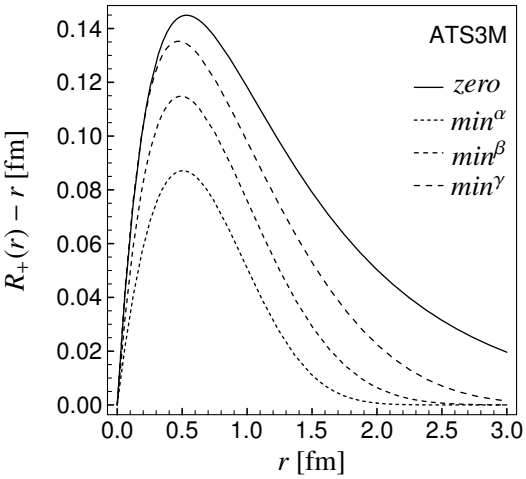

Figure 1.17: Correlation functions in the odd channels for the ATS3M interaction. R_+^{zero} is derived from the zero energy scattering solution. The three other correlation functions are obtained by minimizing the energy in the two-body system with a linear trial function and restricted correlation ranges.

energy. In the odd channels the correlation function determined from the zero-energy scattering solution and the three correlators obtained by minimizing the energy in the two-body system and a restriction on the correlation range are used. The influence of the correlation range on the binding energy is clearly visible. The correlator determined from the zero-energy scattering solution apparently gives too much binding. Considering the extremely long range of this correlator we do not believe in the validity of the two-body approximation. The results with the three other correlators of restricted range demonstrate the uncertainty in our correlator choice. To become more selective the explicit evaluation of the three-body contributions would be necessary.[4]

For comparison the results of Brueckner-Hartree-Fock (BHF) calculations [GFMP81], the TICI2 method [GMN+96] and Correlated Basis Function calculations CBF^a, CBF^b [CFFdS96], and CBF^c [FdSCF98] are shown in Fig. 1.18 and Fig. 1.19. Unfortunately we cannot reliably use the reference calculations as a fix point in our considerations as they differ strongly from each other.

The CBF results clearly display uncertainties stemming from different choices of the parameterization of the correlation functions and the trial state. The CBF calculations have not been minimized with respect to the radius but used fixed single-particle states (Woods-Saxon for CBF^a, CBF^b and harmonic oscillator for CBF^c). The CBF^a and CBF^b calculations differ by the choice of the Jastrow correlation functions, CBF^a uses Euler correlation functions determined from the two-body problem, CBF^b uses a Gaussian parameterization of the correlation function.

[4] The dependence of the binding energy on the correlation range in the odd channels is less pronounced in case of realistic interactions. In the $S,T=0,0$ channel the repulsion of these interactions is similarly strong as with the ATS3M potential, but in the $S,T=1,1$ channel, which appears with a nine times higher weight, the repulsion is much weaker.

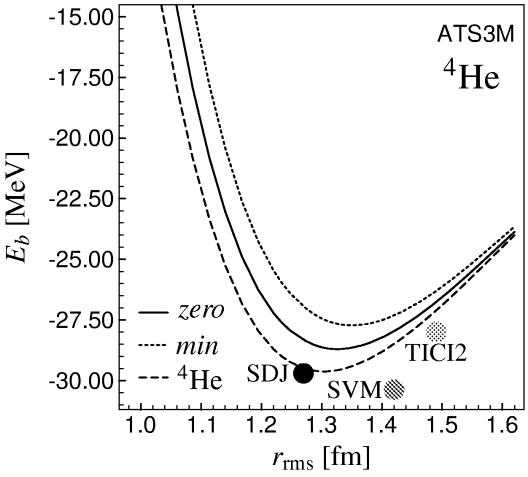

Figure 1.18: Binding energy for the ^{4}He nucleus versus the $r_{\rm rms}$ radius. Correlation functions determined from the scattering solutions *zero*, obtained by minimizing the energy in the two-body system with a constant trial function *min* and by minimizing the ^{4}He energy with a harmonic oscillator shell model state are used. Results of reference calculations for the TICI2, SVM and SDJ methods are shown.

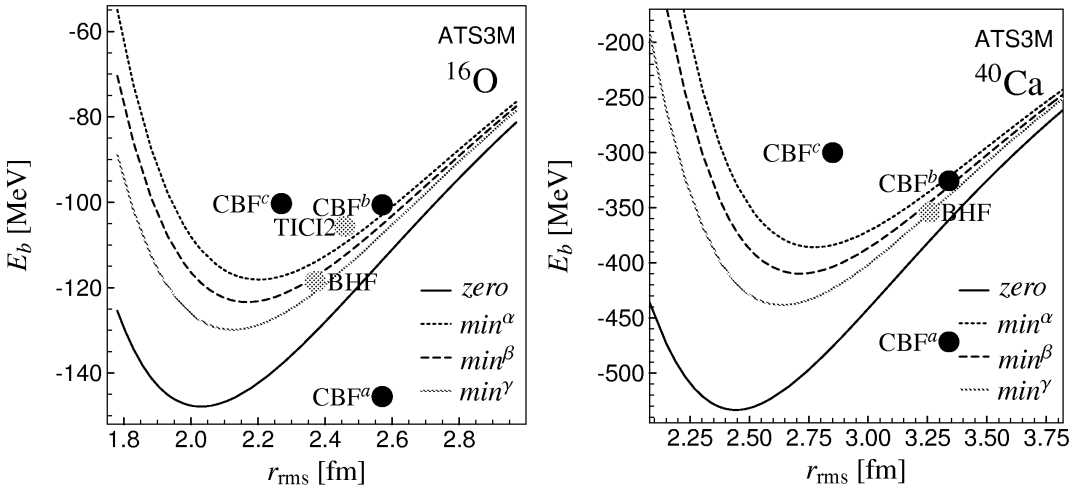

Figure 1.19: Binding energy versus radius $r_{\rm rms}$ for ^{16}O (left hand side) and ^{40}Ca (right hand side) obtained with the ATS3M potential. In the even channels the correlator derived by minimizing the energy in the two-body system with a constant trial function is used. In the odd channels the correlated obtained from the zero-energy scattering solution and three different correlators with constraints on the correlation range are used. Reference results for the BHF, TICI2 and CBF calculations are shown.

1.8 Tensor Correlations

All realistic nucleon-nucleon interactions possess a strong tensor force that is mainly due to the exchange of pions. It operates only in the $S = 1$ channels and induces there a strong correlation between the spatial orientation of the nucleons and the orientation of their spins. The tensor force is crucial for a successful description of the nucleus, without the tensor force nuclei are not bound.

To get a basic understanding of this correlation between the spins and the relative orientation of the nucleons one can investigate a system of two magnets. The dipole-dipole interaction between two magnets has the same structure as the tensor force. The magnets will align their orientations and therefore their spin along the distance vector as illustrated in Fig. 1.20.

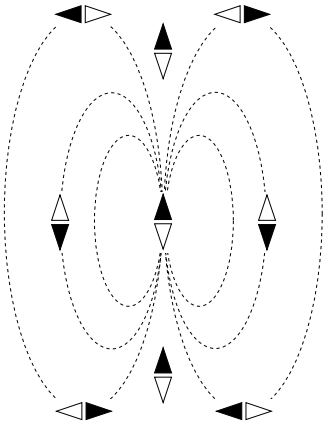

Figure 1.20: The dipole-dipole interaction between two magnets causes a correlation between the positions of the magnets and their orientation. In this picture the orientation of the magnet in the center is fixed. The second magnet will adjust its orientation according to its position.

Moving a magnet to a different position will also result in a reorientation of the magnets and therefore the spins. In the case of the nucleons basically the same will happen but now we have to consider also the kinetic energy of the zero-point motion of the two-body system – the system will adjust itself in such a way that the sum of the potential energy, which favors a total alignment, and the kinetic energy, which prefers a smooth wave function, is minimal.

A single Slater determinant, where the spin direction of a single particle state depends at most on the position $\mathbf{r}_i$ and not on the relative coordinate $\mathbf{r}_{ij} = \mathbf{r}_i - \mathbf{r}_j$ of two nucleons, cannot reflect the correlations between spins and relative orientation of the nucleons. We face a similar problem as with the short-range correlations. A single Slater determinant does not have the proper degrees of freedom needed for the description of the physical system. Since the Slater determinants form a complete basis the appropriate state can always be written as a superposition of determinants. One needs however a huge number of those for a successful description. For example in second order perturbation theory the tensor interaction scatters to intermediate states with energies of about 300 MeV which would mean that about $30\hbar\omega$ excitations have to be included in shell model calculations [Bro71].

Our aim is, as with the short-range correlations, to include the tensor correlations into the many-body state by means of a unitary correlation operator.

1.8.1 Deuteron Tensor Correlator

For the repulsive core the unitary correlation operator performs a radial shift. In the case of the tensor correlator the form of the generator is not as obvious because one needs to correlate the spins of the nucleons with the relative orientation of the nucleons.

The tensor correlations can be studied explicitly in case of the deuteron, where the known exact solution has a d-wave admixture because of the tensor force. We thus make the ansatz

$$\langle r \,|\, \hat{d} \rangle = \frac{\hat{u}(r)}{r} \Big| (01)1 \Big\rangle + \frac{\hat{w}(r)}{r} \Big| (21)1 \Big\rangle \tag{1.77}$$

for the correlated deuteron wave function. Here r denotes the distance between proton and neutron and $\Big| (LS)J \Big\rangle$ a basis for the angular and spin part of the state.

The Schrödinger equation with this ansatz gives the Rarita-Schwinger equations which we solve by diagonalizing the Hamiltonian on a grid in coordinate space. The deuteron wave functions for the Bonn-A and Argonne V18 interaction are shown in Fig. 1.21.

The correlation between spins and relative orientation of the nucleons is observable in the

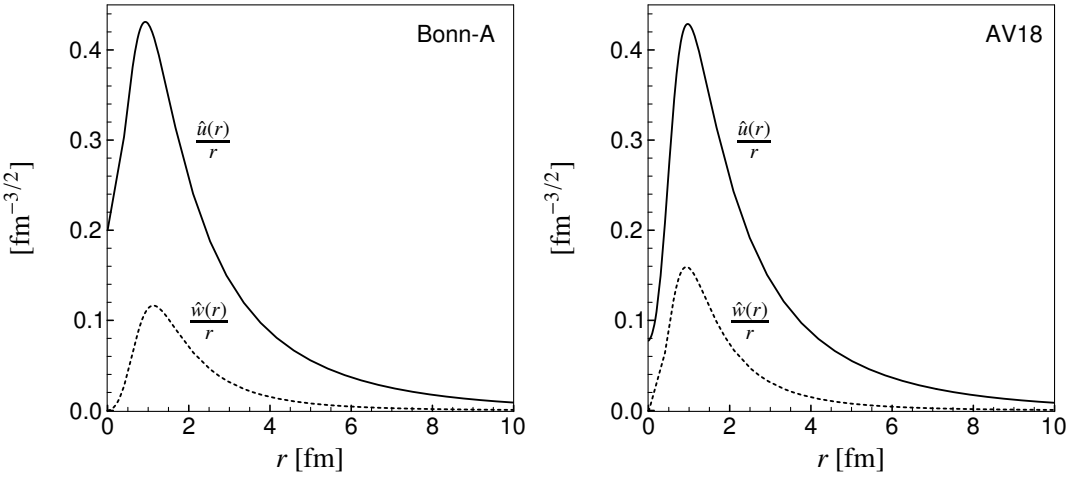

Figure 1.21: The deuteron wave function. Plotted are $\frac{\hat{u}(r)}{r}$ and $\frac{\hat{w}(r)}{r}$ for the Bonn-A (left) and the Argonne V18 (right) interaction. There is a noticeable difference in the d-wave admixture, the Argonne V18 interaction has stronger tensor correlations. The behavior of the wave function at the origin shows a larger correlation hole caused by the stronger repulsive core of the Argonne V18 as compared to that of the Bonn-A interaction.

d-wave component, where the orbital angular momentum $L=2$ is coupled with the spin $S=1$ to the total angular momentum $J=1$.

To define our unitary tensor correlator we start with an ansatz $\big|\, d\,\big\rangle$ for the uncorrelated deuteron state that has only a $L=0$ component.

$$\big\langle\, r \,\big|\, d\,\big\rangle = \frac{u(r)}{r}\big|\,(01)1\,\big\rangle \tag{1.78}$$

The $L=2$ component of the correlated deuteron state has to be generated by the tensor correlator $\underset{\sim}{c}_\Omega$ that maps $\big|\, d\,\big\rangle$ onto the exact solution $\big|\,\hat{d}\,\big\rangle$

$$\big|\,\hat{d}\,\big\rangle = \underset{\sim}{c}_\Omega\big|\, d\,\big\rangle = \exp\{-i\underset{\sim}{g}_\Omega\}\big|\, d\,\big\rangle\,. \tag{1.79}$$

The generator $\underset{\sim}{g}_\Omega$ has to be a scalar operator as the total angular momentum J is not changed. In coordinate space it has to be a tensor operator of rank two, there is no other possibility to connect $L=0$ with $L=2$ states. If it is of rank two in coordinate space it also has to be of rank two in spin space. In the two-body spin space there is only one operator of rank two so there is no freedom left. We restrict the coordinate space part of the generator by demanding that the correlator should make shifts perpendicular to the relative orientation of the nucleons only. Radial shifts are already treated by the central correlator.

In order to achieve shifts perpendicular to the relative orientation we decompose the momentum operator

$$\underset{\sim}{\mathbf{p}} = \underset{\sim}{\mathbf{p}}_r + \underset{\sim}{\mathbf{p}}_\Omega \tag{1.80}$$

in the radial momentum

$$\underset{\sim}{\mathbf{p}}_r \overset{\mathbf{r}}{\Rightarrow} \frac{\mathbf{r}}{r}p_r = \frac{\mathbf{r}}{r}\frac{1}{i}\Big(\frac{1}{r} + \frac{\partial}{\partial r}\Big) \tag{1.81}$$

and the remaining part,

$$\underset{\sim}{\mathbf{p}}_\Omega \overset{\mathbf{r}}{\Rightarrow} \frac{1}{2r}\Big(\mathbf{l}\times\frac{\mathbf{r}}{r} - \frac{\mathbf{r}}{r}\times\mathbf{l}\Big) \tag{1.82}$$

$s_{12}(\mathbf{r},\mathbf{p}_\Omega)$	$\vert(11)0\rangle$	$\vert(01)1\rangle$	$\vert(11)1\rangle$	$\vert(21)1\rangle$	$\vert(11)2\rangle$	$\vert(21)2\rangle$	$\vert(31)2\rangle$
$\langle(11)0\vert$	0	0	0	0	0	0	0
$\langle(01)1\vert$	0	0	0	$-3i\sqrt{2}$	0	0	0
$\langle(11)1\vert$	0	0	0	0	0	0	0
$\langle(21)1\vert$	0	$3i\sqrt{2}$	0	0	0	0	0
$\langle(11)2\vert$	0	0	0	0	0	0	$-3i\sqrt{6}$
$\langle(21)2\vert$	0	0	0	0	0	0	0
$\langle(31)2\vert$	0	0	0	0	$3i\sqrt{6}$	0	0

Table 1.1: Matrixelements of $s_{12}(\mathbf{r},\mathbf{p}_\Omega)$ in angular momentum eigenstates $\vert(LS)J\rangle$.

which we call *orbital momentum*. It should not be confused with the orbital angular momentum $\underset{\sim}{\mathbf{l}}$. Both $\underset{\sim}{\mathbf{p}}_r$ and $\underset{\sim}{\mathbf{p}}_\Omega$ are Hermitian. We have summarized some properties of these operators in appendix B.2.

With the orbital momentum operator we define the generator $\underset{\sim}{g}_\Omega$

$$\begin{aligned}\underset{\sim}{g}_\Omega &\overset{\mathbf{r}}{\Rightarrow} \vartheta(r)s_{12}(\mathbf{r},\mathbf{p}_\Omega)\\ &= \vartheta(r)\Big(\frac{3}{2}(\boldsymbol{\sigma}_1\cdot\mathbf{p}_\Omega)(\boldsymbol{\sigma}_2\cdot\mathbf{r})+\frac{3}{2}(\boldsymbol{\sigma}_1\cdot\mathbf{r})(\boldsymbol{\sigma}_2\cdot\mathbf{p}_\Omega)-(\boldsymbol{\sigma}_1\cdot\boldsymbol{\sigma}_2)\frac{1}{2}(\mathbf{p}_\Omega\cdot\mathbf{r}+\mathbf{r}\cdot\mathbf{p}_\Omega)\Big)\,.\end{aligned} \tag{1.83}$$

This operator has indeed all the required properties. It is a scalar operator of rank two in coordinate and spin-space and does not shift the relative wave function radially. The strength of the tensor correlation can be adjusted with the tensor correlation function $\vartheta(r)$ for each distance r independently. Like the correlation function $R_+(r)$ in the case of central correlations $\vartheta(r)$ will depend on the potential and on the system under investigation.

It is very illustrative to look at the generator $\underset{\sim}{g}_\Omega$ in angular momentum representation. The angular and spin dependence of $\underset{\sim}{g}_\Omega$ is contained in the $s_{12}(\mathbf{r},\mathbf{p}_\Omega)$ operator. Its matrix elements[5] in the lowest angular momentum states are displayed in Tab. 1.1. We notice that all diagonal matrix elements are zero. The operator $s_{12}(\mathbf{r},\mathbf{p}_\Omega)$ and therefore also the generator $\underset{\sim}{g}_\Omega$ only connects states with $L-L'=\pm2$ and the same total angular momentum J.

Using these matrix elements we can immediately write the correlated deuteron wave function as

$$\langle r\,\vert\,\underset{\sim}{c}_\Omega\,\vert\,d\rangle = \cos\big(3\sqrt{2}\,\vartheta(r)\big)\frac{u(r)}{r}\vert(01)1\rangle+\sin\big(3\sqrt{2}\,\vartheta(r)\big)\frac{u(r)}{r}\vert(21)1\rangle\,. \tag{1.84}$$

We compare this to the exact deuteron solution Eq. (1.77) and find the deuteron correlation function

$$\vartheta_d(r)=\frac{1}{3\sqrt{2}}\arctan\frac{\hat{w}(r)}{\hat{u}(r)}\,. \tag{1.85}$$

The deuteron correlation functions for the Bonn-A and the Argonne V18 potential are shown in Fig. 1.22.

[5] The calculation of the matrix elements is outlined in appendix B.4.

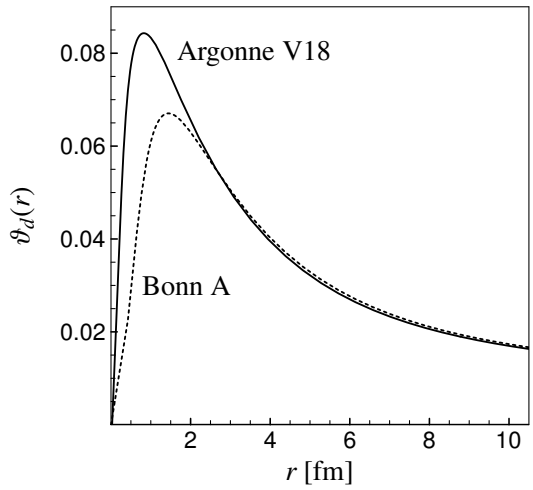

Figure 1.22: The deuteron correlation functions $\vartheta_d(r)$ for the Bonn-A and Argonne V18 interactions. The correlations are stronger in case of the Argonne V18 interaction at short distances and show a different behavior for $r \to 0$.

The uncorrelated deuteron trial state Eq. (1.78) has no $L=2$ admixture. Thus the "optimal" deuteron correlator which maps the trial state onto the exact deuteron solution has to generate the entire radial wave function $\hat{w}(r)$. It is therefore very long ranged and will induce three- and higher-body correlations in many-body states. In order to avoid the higher-body terms one should not put all responsibility for creating long-ranged or low-momentum $L=2$ admixtures on the correlator, but should include those into the degrees of freedom of the uncorrelated many-body trial state. Only the short-range or high-momentum part of the tensor correlations should be taken care of by the correlator $\underset{\sim}{C}_\Omega$. Such a correlator can be used efficiently in many-body calculations because the two-body approximation is valid when the correlation range is short enough.

Nevertheless the tensor correlations seem to be very strong up to $3-4\,\mathrm{fm}$. The question whether we can describe the essential part of the tensor correlations with a tensor correlation operator of restricted range has to be checked in many-body systems.

1.8.2 Correlations in the Deuteron Wave Function

The tensor correlations can be studied particularly easy for the deuteron. The two-body distribution function $\rho^{(2)}_{1M_S}(\mathbf{r})$ defined in Eq. (1.23), where we omit the isospin indices, is calculated easily. We are only interested in the intrinsic correlations and therefore calculate the two-body distribution function in a superposition of all spatial orientations [6]

$$\rho^{(2)}_{1M_S}(\mathbf{r}) = \frac{1}{3}\sum_{M=-1}^{1} \left| \langle\, \mathbf{r}, S=1, M_S \,|\, \hat{d}, 1M \,\rangle \right|^2 . \tag{1.86}$$

With the deuteron wave function Eq. (1.77) this equates to

$$\rho^{(2)}_{1M_S}(\mathbf{r}) = \frac{1}{3}\Bigg[\frac{\hat{u}^2(r)}{r^2} Y^\star_{00}(\hat{\mathbf{r}}) Y_{00}(\hat{\mathbf{r}}) + 2\frac{\hat{u}(r)\hat{w}(r)}{r^2} \mathrm{C}\begin{pmatrix} 2 & 1 & \\ 0 & M_S & M_S \end{pmatrix} \mathrm{Re}\{ Y^\star_{00}(\hat{\mathbf{r}}) Y_{20}(\hat{\mathbf{r}}) \}$$
$$+ \frac{\hat{w}^2(r)}{r^2} \sum_{M=-1}^{1} \mathrm{C}\begin{pmatrix} 2 & 1 & \\ M-M_S & M_S & M \end{pmatrix}^2 Y^\star_{2(M-M_S)}(\hat{\mathbf{r}}) Y_{2(M-M_S)}(\hat{\mathbf{r}}) \Bigg] . \tag{1.87}$$

[6] Otherwise the two-body distribution function would depend on the orientation of the deuteron in space.

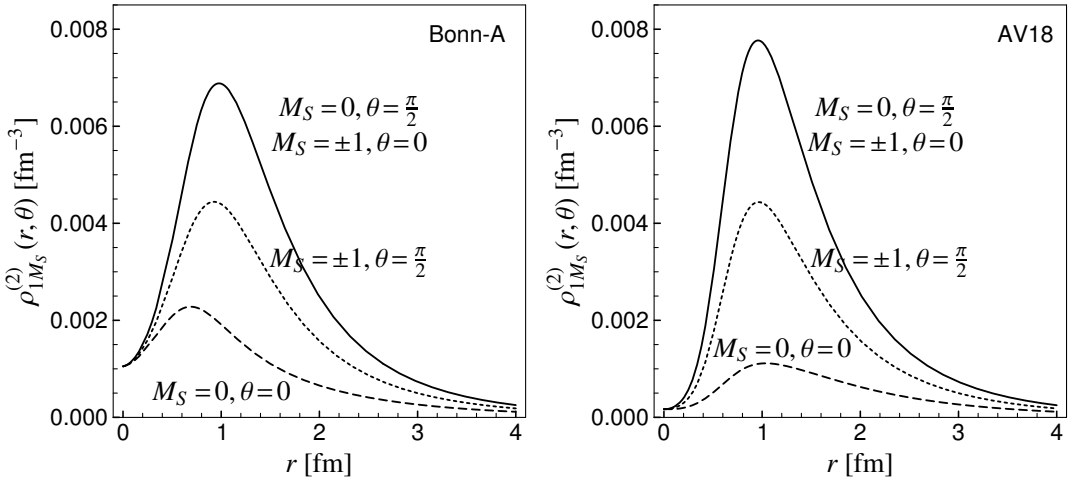

Figure 1.23: Deuteron two-body density as a function of the orientation in coordinate and spin-space for the Bonn-A interaction (left hand side) and the Argonne V18 interaction (right hand side).

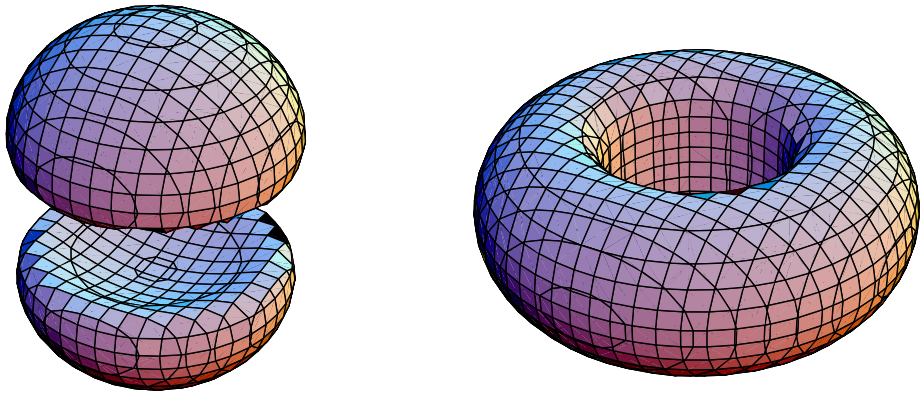

Figure 1.24: Surfaces of constant density in the deuteron ($\rho^{(2)}_{1M_S} = 0.005\text{fm}^{-3}$) for $M_S = \pm 1$ on the left and $M_S = 0$ on the right. The plots are done for the Argonne V18 interaction.

The deuteron two-body densities for the Bonn-A and the Argonne V18 interactions are shown in Fig. 1.23. The strong attraction of the tensor force in the deuteron causes an alignment of the nucleons along the spin orientation. Perhaps more illustrative is Fig. 1.24 where isodensity surfaces for different orientations of the total spin are shown. The famous dumbbell ($M_S = \pm 1$) and donut shapes ($M_S = 0$) make clearly visible the effect of the core (the correlation hole in the two-body density) and the tensor force (the alignment of density with the spin).

1.8.3 Combination of Central and Tensor Correlations

In the discussion of the tensor correlations in the deuteron the central correlations have not been considered explicitly. The central correlations already had been built into the "tensor-uncorrelated" state $\left| d \right\rangle$.

In a many-body calculation we start with a many-body state $\left|\Psi\right\rangle$ which is uncorrelated with respect to both central and tensor correlations. The correlated many-body state is then defined as

$$\left|\hat{\Psi}\right\rangle = \underset{\sim}{C}\left|\Psi\right\rangle = \underset{\sim}{C}_{\Omega}\underset{\sim}{C}_{r}\left|\Psi\right\rangle , \tag{1.88}$$

where the central correlator is applied first, followed by the tensor correlator. In the spirit of the variational principle the best approximation to the true ground state is achieved by a simultaneous variation of the central and the tensor correlator. We assume that the central and tensor correlators can be determined independently as they act within different domains. The central correlator has to describe the effects of the short-range repulsion in the interaction by means of a radial shift, while the tensor correlator generates correlations between the spins and the relative orientation of the nucleons by means of tangential shifts.

Two-Body Matrix Elements

For the evaluation of centrally correlated two-body matrix elements it is more convenient to work with correlated operators rather than with correlated states. Therefore we make use of the unitarity of the central correlation operator $\underset{\sim}{c}_{r}$ in the two-body system and evaluate correlated two-body matrix elements as

$$\begin{aligned}\left\langle \phi\right|\underset{\sim}{c}_{r}^{\dagger}\underset{\sim}{c}_{\Omega}^{\dagger}\underset{\sim}{a}\underset{\sim}{c}_{\Omega}\underset{\sim}{c}_{r}\left|\psi\right\rangle &= \left\langle \phi\right|(\underset{\sim}{c}_{r}^{\dagger}\underset{\sim}{c}_{\Omega}^{\dagger}\underset{\sim}{c}_{r})(\underset{\sim}{c}_{r}^{\dagger}\underset{\sim}{a}\underset{\sim}{c}_{r})(\underset{\sim}{c}_{r}^{\dagger}\underset{\sim}{c}_{\Omega}\underset{\sim}{c}_{r})\left|\psi\right\rangle \\ &= \left\langle \phi\right|(\underset{\sim}{c}_{r}^{\dagger}\underset{\sim}{c}_{\Omega}\underset{\sim}{c}_{r})^{\dagger}(\underset{\sim}{c}_{r}^{\dagger}\underset{\sim}{a}\underset{\sim}{c}_{r})(\underset{\sim}{c}_{r}^{\dagger}\underset{\sim}{c}_{\Omega}\underset{\sim}{c}_{r})\left|\psi\right\rangle .\end{aligned} \tag{1.89}$$

Using this trick centrally correlated operators $\underset{\sim}{c}_{r}^{\dagger}\underset{\sim}{a}\underset{\sim}{c}_{r}$ can be used in tensor correlated states which are uncorrelated with respect to the short-range repulsion. The centrally correlated tensor correlator

$$\begin{aligned}\underset{\sim}{c}_{r}^{\dagger}\underset{\sim}{c}_{\Omega}\underset{\sim}{c}_{r} &\overset{\mathbf{r}}{\Rightarrow} \underset{\sim}{c}_{r}^{\dagger}\exp\{-i\vartheta(r)s_{12}(\mathbf{r},\mathbf{p}_{\Omega})\}\underset{\sim}{c}_{r} \\ &= \exp\{-i\underset{\sim}{c}_{r}^{\dagger}\vartheta(r)\underset{\sim}{c}_{r}s_{12}(\mathbf{r},\mathbf{p}_{\Omega})\} \\ &= \exp\{-i\vartheta(R_{+}(r))s_{12}(\mathbf{r},\mathbf{p}_{\Omega})\}\end{aligned} \tag{1.90}$$

differs only by a transformed radial dependence of the tensor correlation function $\vartheta(r)$. The technical advantage of unitary correlations is quite obvious in this example.

For the sake of convenience we introduce a shorthand notation for the matrix elements of the generator $\underset{\sim}{g}_{\Omega}$

$$\theta^{(J)}_{L',L}(r) \equiv \frac{1}{i}\left\langle (L'1)J\right|\underset{\sim}{g}_{\Omega}\left|(L1)J\right\rangle = \vartheta(r)\left\langle (L'1)J\right|\frac{1}{i}s_{12}(\mathbf{r},\mathbf{p}_{\Omega})\left|(L1)J\right\rangle . \tag{1.91}$$

$s_{12}(\mathbf{r},\mathbf{p}_{\Omega})$ connects only states with $S=1$ and the same J. In addition we must have $|L'-L|=2$ with $L'=J-1$ and $L=J+1$ or vice versa. Therefore we can simplify our notation even further

$$\theta^{(J)}(r) \equiv \theta^{(J)}_{J+1,J-1}(r) = -\theta^{(J)}_{J-1,J+1}(r) . \tag{1.92}$$

1.8.4 Tensor Correlations in Angular Momentum Eigenstates

The action of the tensor correlator can be evaluated explicitly in two-body angular momentum eigenstates $\left|(LS)J\right\rangle$ that are used for example in shell model calculations.

As the generator $\underset{\sim}{g}_\Omega$ does only connect states $L{=}\pm1$ with $L{=}\mp1$ the tensor correlator will not affect states with $L{=}J$

$$\left\langle \mathbf{r} \middle| \underset{\sim}{c}_\Omega \middle| (J1)J \right\rangle = \left\langle \mathbf{r} \middle| (J1)J \right\rangle , \tag{1.93}$$

but only states with $L{=}J{\mp}1$ that are tensor correlated as

$$\left\langle \mathbf{r} \middle| \underset{\sim}{c}_\Omega \middle| (J{\mp}1,1)J \right\rangle = \cos(\theta^{(J)}(r)) \left\langle \mathbf{r} \middle| (J{\mp}1,1)J \right\rangle \pm \sin(\theta^{(J)}(r)) \left\langle \mathbf{r} \middle| (J{\pm}1,1)J \right\rangle \tag{1.94}$$

with the shorthand notation Eq. (1.92).

Correlated Operators in Angular Momentum Eigenstates

With the inclusion of the tensor correlations it is no longer possible to give the general closed form for the correlated interaction. In section 1.11 this will be discussed in detail. However, it is possible to evaluate the correlated interaction in angular momentum eigenstates exactly. This can be used for example in the harmonic oscillator shell model.

As a consequence of Eq. (1.93) the interaction in the states $\left|(J1)J\right\rangle$ will not be influenced by the tensor correlations

$$\left\langle (J1)J \middle| \underset{\sim}{c}_r^\dagger \underset{\sim}{c}_\Omega^\dagger \underset{\sim}{h} \underset{\sim}{c}_\Omega \underset{\sim}{c}_r \middle| (J1)J \right\rangle = \left\langle (J1)J \middle| \underset{\sim}{c}_r^\dagger \underset{\sim}{h} \underset{\sim}{c}_r \middle| (J1)J \right\rangle . \tag{1.95}$$

Therefore only the projection on the states $\left|(J\pm1,1)J\right\rangle$ is of interest. The projected correlated interaction is constructed, following Eq. (1.89), by evaluating the centrally correlated interaction in the tensor correlated angular momentum states Eq. (1.94).

The kinetic energy in the relative motion in the two-body system is decomposed into kinetic energy of radial motion and kinetic energy of orbital motion.

$$\underset{\sim}{t}_{\mathrm{rel}} = \underset{\sim}{t}_r + \underset{\sim}{t}_\Omega \overset{\mathbf{r}}{\Rightarrow} \frac{p_r^2}{m} + \frac{1}{m}\frac{\mathbf{l}^2}{r^2} \tag{1.96}$$

The correlated kinetic energy of the radial motion in the two-body system

$$\begin{aligned}\left\langle (J{\mp}1,1)J \middle| \underset{\sim}{\hat{t}}_r^{[2]} \middle| (J{\mp}1,1)J \right\rangle &= \left\langle (J{\mp}1,1)J \middle| \underset{\sim}{c}_r^\dagger \underset{\sim}{c}_\Omega^\dagger \underset{\sim}{t}_r \underset{\sim}{c}_\Omega \underset{\sim}{c}_r - \underset{\sim}{t}_r \middle| (J{\mp}1,1)J \right\rangle \\ &\overset{\mathbf{r}}{\Rightarrow} \frac{1}{2}\left[p_r^2 \frac{1}{2\hat{\mu}_r(r)} + \frac{1}{2\hat{\mu}_r(r)} p_r^2\right] + \frac{1}{m}\left(\frac{d}{dR_+(r)}\theta^{(J)}(R_+(r))\right)^2 + \hat{u}(r)\end{aligned} \tag{1.97}$$

has an additional potential-like term originating from the radial dependence of the tensor correlation function when compared to the centrally correlated kinetic energy Eq. (1.41). "Radial mass" $\hat{\mu}_r(r)$ and potential term $\hat{u}(r)$ are unchanged from Eq. (1.42) and Eq. (1.43).

The mixture of different angular momenta by the tensor correlator changes the correlated kinetic energy of the orbital motion in the two-body system

$$\begin{aligned}\left\langle (J{\mp}1,1)J \middle| \underset{\sim}{\hat{t}}_\Omega^{[2]} \middle| (J{\mp}1,1)J \right\rangle &= \left\langle (J{\mp}1,1)J \middle| \underset{\sim}{c}_r^\dagger \underset{\sim}{c}_\Omega^\dagger \underset{\sim}{t}_\Omega \underset{\sim}{c}_\Omega \underset{\sim}{c}_r - \underset{\sim}{t}_\Omega \middle| (J{\mp}1,1)J \right\rangle \\ &\overset{\mathbf{r}}{\Rightarrow} \frac{1}{m}\left(\cos^2(\theta^{(J)}(R_+(r)))\frac{(J{\mp}1)(J{\mp}1{+}1)}{R_+(r)^2} + \sin^2(\theta^{(J)}(R_+(r)))\frac{(J{\pm}1)(J{\pm}1{+}1)}{R_+(r)^2}\right) \\ &\quad - \frac{1}{m}\left(\frac{(J{\mp}1)(J{\mp}1{+}1)}{r^2}\right)\end{aligned} \tag{1.98}$$

compared to Eq. (1.44) without tensor correlations.

The central potentials $\underset{\sim}{v}^c \overset{\mathbf{r}}{\Rightarrow} v^c(r)$ are not affected by the tensor correlations

$$\left\langle (J\mp1,1)J \left| \underset{\sim}{c}^\dagger_r \underset{\sim}{c}^\dagger_\Omega \underset{\sim}{v}^c \underset{\sim}{c}_\Omega \underset{\sim}{c}_r \right| (J\mp1,1)J \right\rangle \overset{\mathbf{r}}{\Rightarrow} v^c(R_+(r)) \,. \tag{1.99}$$

Whereas for the spin-orbit interactions $\underset{\sim}{v}^b \overset{\mathbf{r}}{\Rightarrow} v^b(r)\,\mathbf{l}\cdot\mathbf{s}$ only diagonal contributions from the distinct L channels of the correlated states have to be considered

$$\begin{aligned}\left\langle (J\mp1,1)J \left| \underset{\sim}{c}^\dagger_r \underset{\sim}{c}^\dagger_\Omega \underset{\sim}{v}^b \underset{\sim}{c}_\Omega \underset{\sim}{c}_r \right| (J\mp1,1)J \right\rangle \overset{\mathbf{r}}{\Rightarrow}& \\ v^b(R_+(r)) \Big\{ \cos^2(\theta^{(J)}(R_+(r))) \left\langle (J\mp1,1)J \left| \mathbf{l}\cdot\mathbf{s} \right| (J\mp1,1)J \right\rangle& \\ + \sin^2(\theta^{(J)}(R_+(r))) \left\langle (J\pm1,1)J \left| \mathbf{l}\cdot\mathbf{s} \right| (J\pm1,1)J \right\rangle \Big\}& \,,\end{aligned} \tag{1.100}$$

the matrix elements of the correlated tensor interactions $\underset{\sim}{v}^t \overset{\mathbf{r}}{\Rightarrow} v^t(r)\; s_{12}(\hat{\mathbf{r}},\hat{\mathbf{r}})$ also include contributions from the off-diagonal matrix elements between the L channels of the correlated state

$$\begin{aligned}&\left\langle (J\mp1,1)J \left| \underset{\sim}{c}^\dagger_r \underset{\sim}{c}^\dagger_\Omega \underset{\sim}{v}^t \underset{\sim}{c}_\Omega \underset{\sim}{c}_r \right| (J\mp1,1)J \right\rangle \overset{\mathbf{r}}{\Rightarrow} \\ &\quad v^t(R_+(r)) \Big\{ \cos^2(\theta^{(J)}(R_+(r))) \left\langle (J\mp1,1)J \left| s_{12}(\hat{\mathbf{r}},\hat{\mathbf{r}}) \right| (J\mp1,1)J \right\rangle \\ &\qquad \pm 2\cos(\theta^{(J)}(R_+(r))) \sin(\theta^{(J)}(R_+(r))) \left\langle (J\mp1,1)J \left| s_{12}(\hat{\mathbf{r}},\hat{\mathbf{r}}) \right| (J\pm1,1)J \right\rangle \\ &\qquad + \sin^2(\theta^{(J)}(R_+(r))) \left\langle (J\pm1,1)J \left| s_{12}(\hat{\mathbf{r}},\hat{\mathbf{r}}) \right| (J\pm1,1)J \right\rangle \Big\} \,.\end{aligned} \tag{1.101}$$

The correlation of the other interaction components and of other operators has to be performed accordingly.

1.8.5 Choice of Correlator

The addition of the tensor correlations does not change the strategy we use for the determination of the correlators. As described in section 1.6.3 we either fix the correlators on the zero-energy scattering solutions or perform an energy minimization in the two- or the many-body system.

As before the correlators will be determined in the lowest angular momentum states of the respective spin and isospin channels as these channels have the biggest weight in many-body calculations. Furthermore the influence of the correlations decreases with increasing orbital angular momentum L as the centrifugal barrier suppresses significantly the two-body density at short distances.

In the $S,T = 0,0$ and the $S,T = 0,1$ channels where we do not have to deal with tensor correlations the correlators are therefore fixed with $\left|(10)1\right\rangle$ and $\left|(00)0\right\rangle$ trial states. In the $S,T = 1,0$ channel our uncorrelated trial state will be $\left|(01)1\right\rangle$. The tensor correlator will admix the $\left|(21)1\right\rangle$ state. In the $S,T = 1,1$ channel the situation is more complicated. The lowest orbital angular momentum $L=1$ can be coupled with the spin $S=1$ to the total angular momenta $J = 0,1,2$. Only for $J = 2$ we have to deal with tensor correlations which will admix $\left|(31)2\right\rangle$ states. As the potentials are different for each J channel it would be conceivable to define different correlators for all of these channels. However we prefer to have a single correlator in the $S,T = 1,1$ channel and use the following concept: The tensor correlator will be fixed on the zero-energy scattering solution in the $J=2$ channel. The central correlator will be fixed using the scattering solution obtained with the central part of the interaction. Therewith the non-central components of the interaction have no influence on the central correlations. For the determination of the energy-minimized correlators we use a similar idea. The trial state will

be a mixture of the $\big|(11)J\big\rangle$ states with weights of 1,3,5 for $J = 0, 1, 2$. The tensor correlator will admix the $\big|(31)2\big\rangle$ state. The energy minimized correlator is then optimized for spherically symmetric nuclei.

1.8.6 Parameterization of the Tensor Correlation Function

The parameterizations of the tensor correlation functions $\vartheta(r)$ are similar to the parameterizations of the central correlation functions.

If the range of the tensor correlator is not constrained we use the parameterization

$$\vartheta(r) = \alpha\gamma^n \left(1 - \exp\left\{-\left(\frac{r}{\gamma}\right)^\eta\right\}\right) \exp\left\{-\frac{r}{\beta}\right\} \tag{1.102}$$

with an exponential decay at large distances r. For correlators with a restricted range the parameterization

$$\vartheta(r) = \alpha\gamma^n \left(1 - \exp\left\{-\left(\frac{r}{\gamma}\right)^n\right\}\right) \exp\left\{-\exp\left\{\frac{r}{\beta}\right\}\right\} \tag{1.103}$$

with a double-exponential is used.

1.9 Bonn-A and Argonne V18 Correlators

Following the principles outlined in the last section we will determine now the central and tensor correlators for the Bonn-A and the Argonne V18 interaction. By comparing the correlators side-by-side a better understanding of common and specific properties of the different nuclear interactions and the correlations can be achieved.

The Argonne V8' interaction is by construction identical to the Argonne V18 interaction in the lowest L channels. As we fix our correlators in these channels the Argonne V18 correlators presented are identical to the Argonne V8' correlators.

Many-body optimized correlators will only be given for the ^{4}He nucleus. For heavier nuclei like ^{16}O and ^{40}Ca they are nearly indistinguishable from the two-body optimized correlators.

The correlation functions determined from the zero-energy scattering solutions will be fitted for the use in many-body calculations by the parameterizations given in section 1.6.4 and section 1.8.6. The correlation functions resulting from minimizing the energy use the same parameterizations for the variation. A summary of all correlation parameters is given in appendix D.4 for the Bonn-A interaction and in appendix D.5 for the Argonne V18 interaction.

1.9.1 $S, T = 0, 0$ Channel

According to our prescription we have to fix the correlator for the lowest angular momentum, which is $L = 1$ in this channel. Both, the Bonn-A and the Argonne V18 interaction show a strong repulsion in the $S, T = 0, 0$ channel. This can be seen in the zero-energy scattering solutions $\hat{\varphi}^{zero}(r)$ plotted in the upper part of Fig. 1.25. We observe a remarkable difference in the Bonn-A and the Argonne V18 scattering solutions. Whereas the local Argonne interaction strongly suppresses the scattering solution at small distances the more momentum dependent repulsion of the Bonn interaction sets in only at distances of about 0.5 fm. This difference manifests itself also in the correlation functions $R_+^{zero}(r)$ derived from mapping the trial function $\varphi(r) = r$ onto the scattering solutions. The Argonne correlation function increases steeply for small r whereas the Bonn correlation function starts to rise at greater distances as seen in the lower

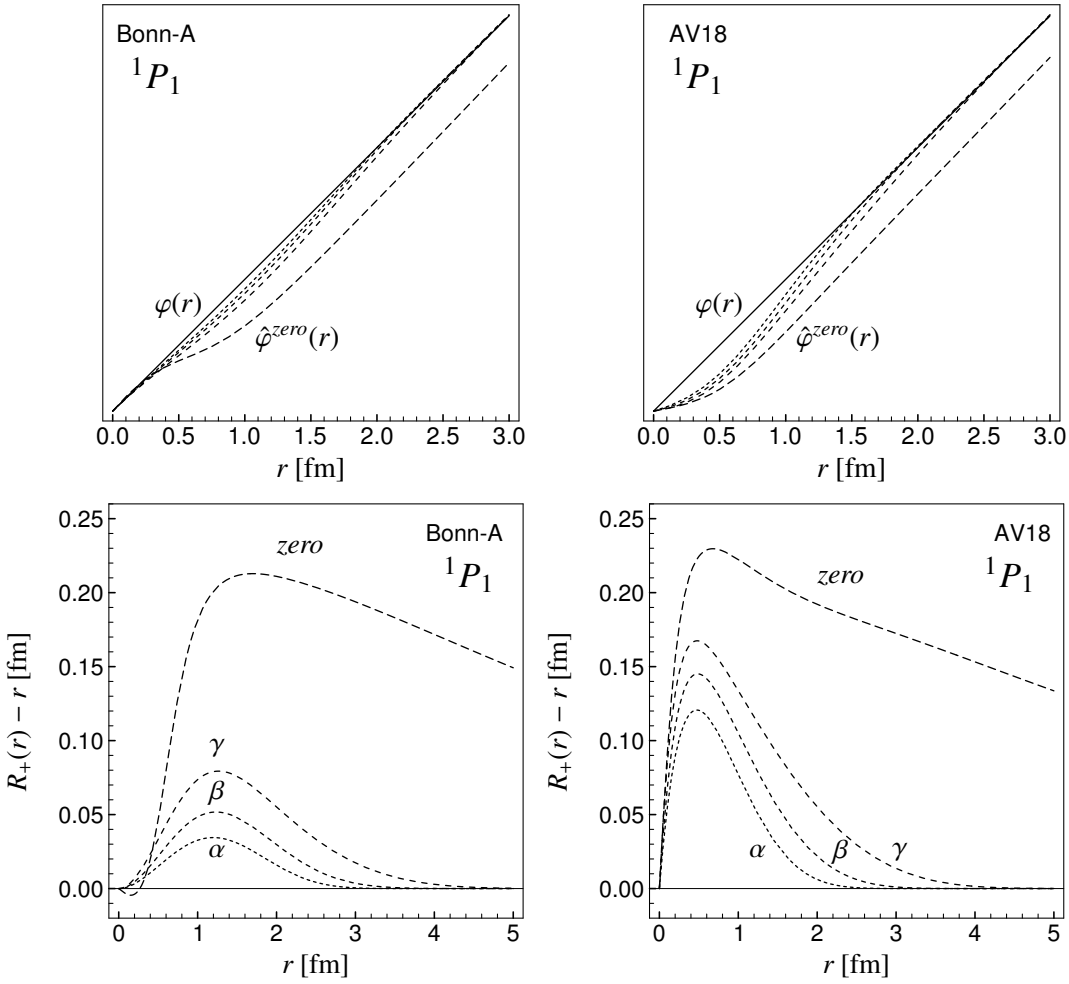

Figure 1.25: Zero-energy scattering solutions and central correlation functions in the $S, T = 0, 0$ channel for the Bonn-A interaction (left hand side) and the Argonne V18 interaction (right hand side). The trial state $\varphi(r)$ is mapped onto the zero-energy scattering solution $\hat{\varphi}^{zero(r)}$ with the correlation function $R_+^{zero}(r)$. Minimizing the energy in the two-body system with additional constraints on the correlation range leads to the correlation functions labeled by α, β and γ.

part of Fig. 1.25. The correlation functions $R_+^{zero}(r)$ are extremely long ranged and cannot be used meaningfully in a many-body calculation.

By minimizing the energy in the two-body system with the trial function $\varphi(r)$ with additional constraints

$$\int \mathrm{d}r\, r^2\, (R_+(r) - r) \stackrel{!}{=} \begin{cases} 0.1\,\mathrm{fm}^3 & ; \quad \alpha \\ 0.2\,\mathrm{fm}^3 & ; \quad \beta \\ 0.5\,\mathrm{fm}^3 & ; \quad \gamma \end{cases} \tag{1.104}$$

on the correlation range we obtain the correlators α, β and γ. The difference to the zero-energy scattering solution correlator can be seen in the upper part of Fig. 1.25 where they have been applied to the trial wave function $\varphi(r)$. The constraint on the correlation range influences the long-range part but has only a small effect on the short-range behavior of the correlation functions.

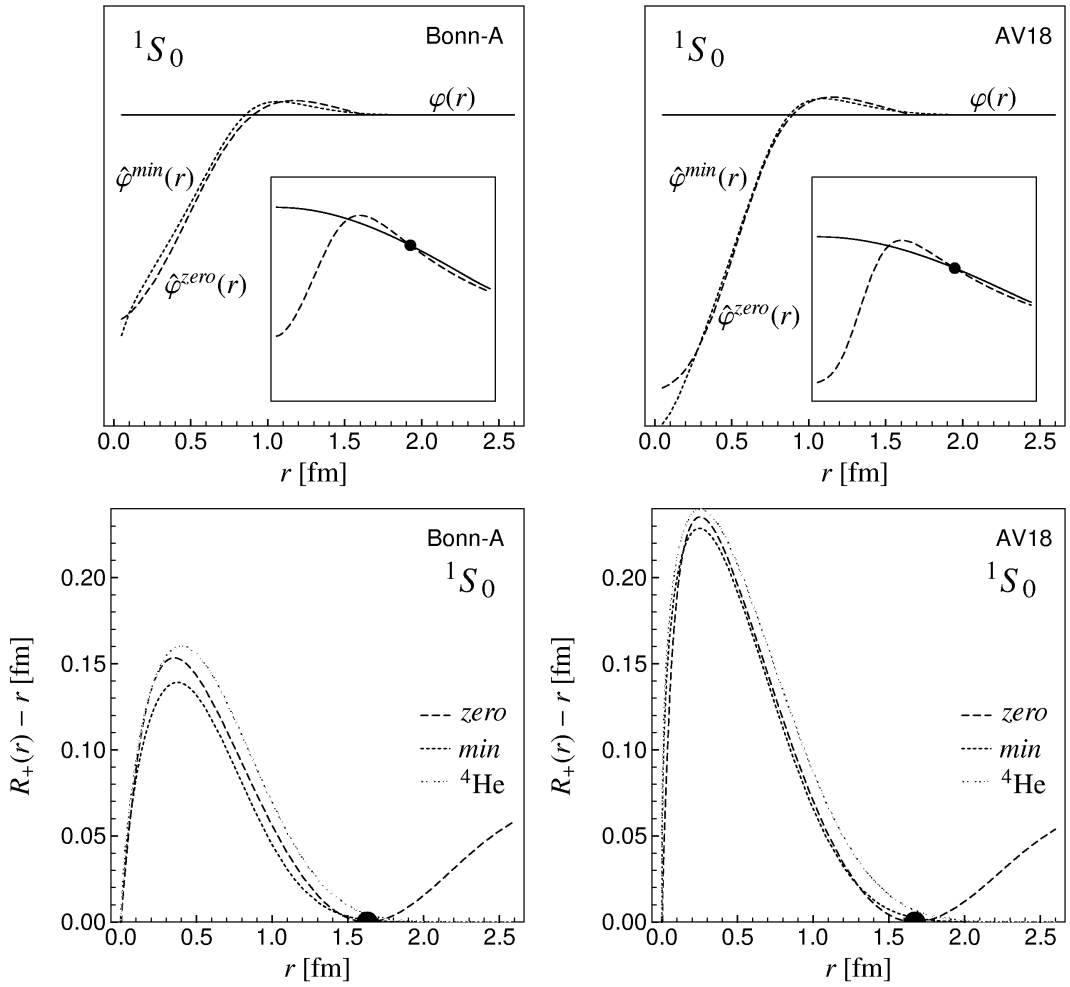

Figure 1.26: Central correlations in the $S, T = 0, 1$ channel for the Bonn-A (left hand side) and the Argonne V18 interaction (right hand side). In the upper part $\hat{\varphi}^{min}(r)$ is obtained by minimizing the energy with the constant trial function $\varphi(r)$. Mapping a Gaussian trial function onto the zero-energy scattering solution as displayed in the insets of the upper part defines the correlation function *zero*. Applying this correlation function on the constant trial function $\varphi(r)$ results in $\hat{\varphi}^{zero}(r)$. The correlation functions are displayed in the lower part together with the ^{4}He optimized correlation function.

In many-body calculations we will only present results obtained with the correlator α. It is comparable in range to the central correlators in the even channel. Because of the small weight of the $S, T = 0, 0$ channel the final many-body results depend only weakly on the particular choice of the correlation function.

1.9.2 $S, T = 0, 1$ Channel

In the $S, T = 0, 1$ channel the correlators are fixed with $L = 0$ trial functions. We obtain the correlators labelled "*zero*" from the mapping of a Gaussian trial function onto the scattering solution and the correlators labeled "*min*" by minimizing the energy in the two-body system with a constant trial function. These procedures are illustrated in the upper part of Fig. 1.26. In

addition we determine a correlator optimized for the ^{4}He nucleus in two-body approximation. Here we use a harmonic oscillator shell model trial state which reproduces the experimental radius of the ^{4}He nucleus. Comparing the Bonn with the Argonne correlators we again observe considerable differences. The depletion of the Argonne scattering solution at small distances r is much stronger than in case of the Bonn potential. The correlation functions of the Argonne interaction are correspondingly stronger but of the same range as the Bonn correlation functions. We can also observe that the ^{4}He optimized correlators are very similar to the two-body optimized correlators.

1.9.3 $S, T = 1, 0$ Channel

In the $S, T = 1, 0$ channel we have to deal with central and tensor correlation functions. The zero-energy scattering solution allows us to define tensor and central correlators in a two-step process. In the first step we deduce the tensor correlator. To do this we take the zero energy scattering solution that has in addition to the s- a d-wave component induced by the tensor force

$$\langle\, r \,\big|\, \hat{\varphi}^{zero} \,\rangle = \frac{\hat{u}(r)}{r}\Big|\,(01)1\,\rangle + \frac{\hat{w}(r)}{r}\Big|\,(21)1\,\rangle\,. \tag{1.105}$$

Following the procedure described in section 1.8.1 for the deuteron correlator we define the tensor correlator $\vartheta^{zero}(r)$ for the zero-energy scattering state by mapping the $L = 0$ "tensor-decorrelated" wave function $u(r)$

$$u^2(r) = \hat{u}^2(r) + \hat{w}^2(r) \tag{1.106}$$

onto the full scattering solution.

The tensor correlation function $\vartheta^{zero}(r)$ is then given by

$$\vartheta^{zero}(r) = \frac{1}{3\sqrt{2}} \arctan \frac{\hat{w}(r)}{\hat{u}(r)}\,. \tag{1.107}$$

The scattering solutions together with the tensor correlation functions are plotted in Fig. 1.27.

The naive idea to create the d-wave component only with the tensor correlator leads to extremely long ranged correlation functions that extend even outside the range of the interaction. Since $\hat{u}(r)$ goes through zero at $r = 5.4$ fm there is even a pole in $\vartheta^{zero}(r)$. However at short distances up to about $r \approx 2$ fm the deuteron tensor correlation functions $\vartheta^d(r)$ are almost identical to the tensor correlation functions derived from the scattering solutions. Therefore we consider the deuteron tensor correlators as the reference correlators when comparing with tensor correlators of restricted range.

As already indicated for the central correlations we could construct shorter ranged tensor correlators starting from the scattering solution (or the deuteron solution) with a trial function that has the correct asymptotic behavior, that means the right d-admixture at large distances. The tensor correlator would then have to describe the tensor correlations only for small distances or high momenta.

In a second step we derive the central correlation function for the zero-energy scattering state. It is defined by the mapping of a Gaussian trial function onto the wave function $\frac{u(r)}{r}$ that takes the role of the scattering solution with respect to the central correlations. This mapping is indicated in the insets of Fig. 1.28.

The energy minimized correlators in the two-body system can be determined in principle by simultaneously minimizing the energy with a constant trial function $\varphi(r) = const$

$$\min_{R_+(r),\vartheta(r)} \langle\, \varphi \,\big|\, \underset{\sim}{c}_r^\dagger \underset{\sim}{c}_\Omega^\dagger \underset{\sim}{\sim} h \underset{\sim}{c}_\Omega \underset{\sim}{c}_r \,\big|\, \varphi \,\rangle \tag{1.108}$$

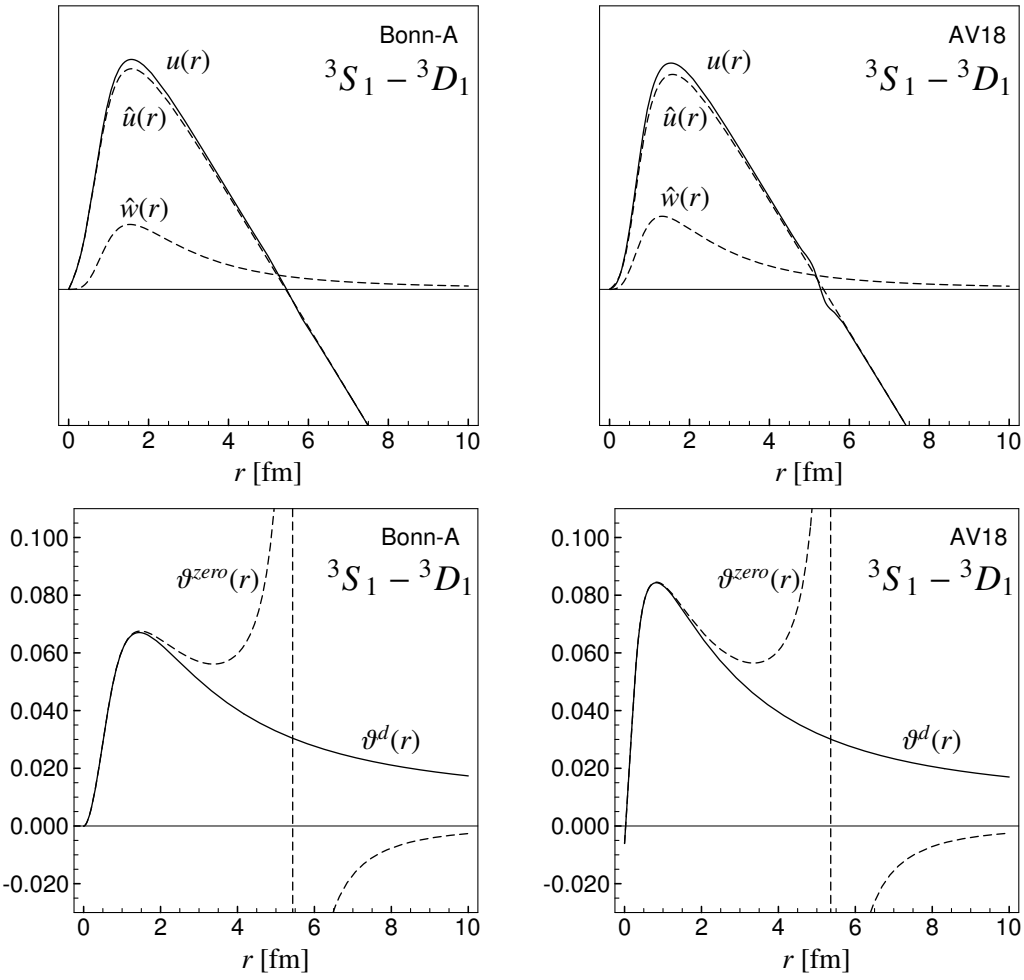

Figure 1.27: The zero energy scattering solution in the $S, T = 1, 0$ channel for the Bonn-A (upper left) and the Argonne V18 (upper right) interaction. They define the tensor correlation functions $\vartheta^{zero}(r)$ plotted below together with the deuteron tensor correlation functions $\vartheta^d(r)$.

with respect to central and tensor correlations and additional constraints concerning the correlation range in case of the tensor correlator. In practice we proceed in two steps. In the first step we determine the central correlation function $R_+(r)$ using the deuteron tensor correlation function $\vartheta^d(r)$ in Eq. (1.108). From the perspective of the central correlator the long range behavior of the tensor correlator is not relevant. It therefore makes no real difference whether we use here the deuteron tensor correlator or a tensor correlator that has a restricted range. In a second step we vary the energy in the two-body system with respect to the tensor correlation function.

We proceed in the same way for the determination of the ^{4}He optimized correlators, where the energy in a harmonic oscillator shell model trial state is minimized with respect to central and tensor correlators[7]

$$\min_{R_+(r),\vartheta(r)} \langle\, {}^4\mathrm{He} \,\big|\, [\underset{\sim}{C}^\dagger_r \underset{\sim}{C}^\dagger_\Omega \underset{\sim}{H} \underset{\sim}{C}_\Omega \underset{\sim}{C}_r]^{C2} \,\big|\, {}^4\mathrm{He} \,\rangle \,. \tag{1.109}$$

[7] The evaluation of this expectation value is discussed in detail in section 1.10.

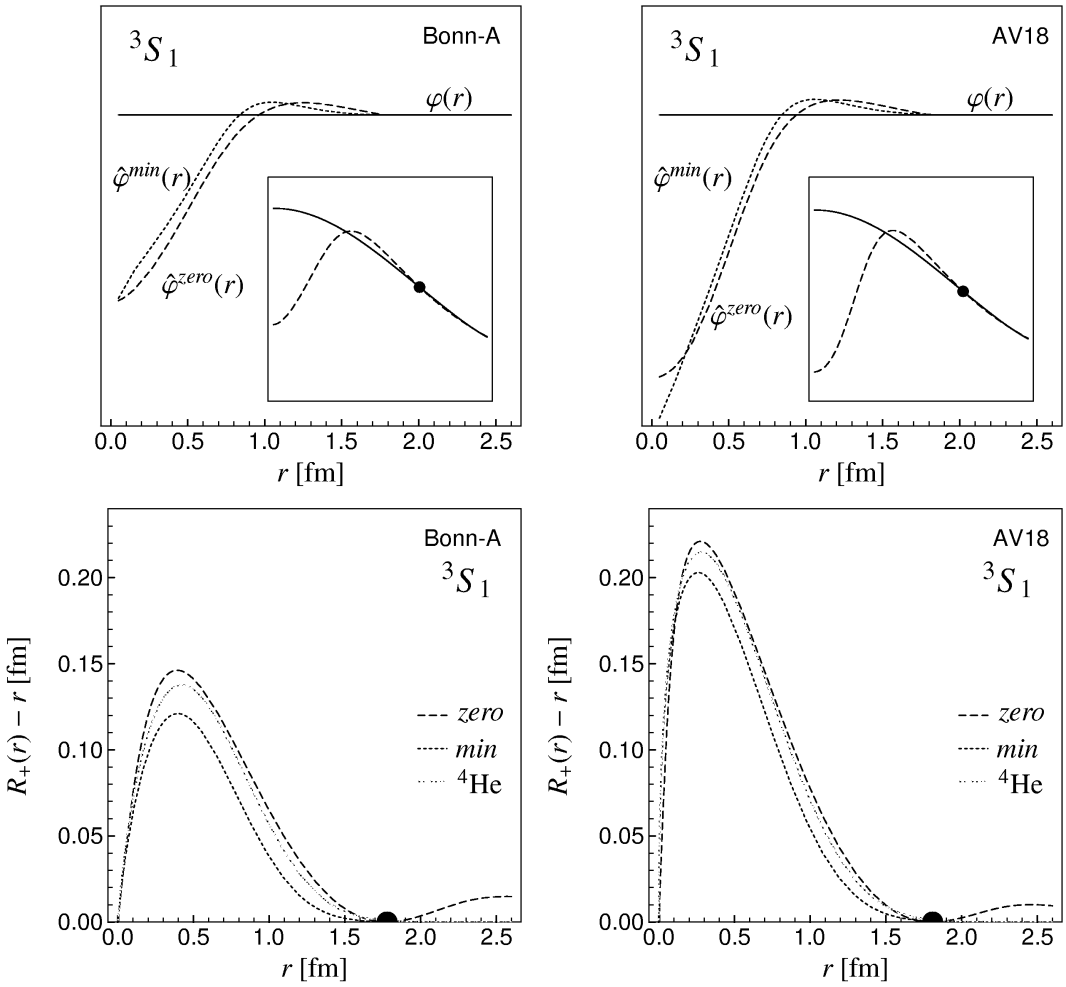

Figure 1.28: Central correlation functions $R_+(r)$ in the $S, T = 1, 0$ channel for Bonn-A interaction (left) and the Argonne V8' interaction (right). Applying the central correlation functions *min* and *zero* to the constant trial function $\varphi(r)$ results in $\hat{\varphi}_{min}(r)$ and $\hat{\varphi}_{zero}(r)$. In the insets the mapping of the Gaussian trial function onto the "tensor-decorrelated" scattering solution $\frac{u(r)}{r}$ is indicated. The central correlation functions optimized for the ^{4}He are shown in addition to the zero-energy scattering and the two-body optimized correlation functions in the lower part.

We end up with the central correlators shown in Fig. 1.28. The central correlation functions $R_+(r)$ obtained with the three methods turn out to be all very similar for the Bonn-A and the Argonne V18 interaction respectively. But as in the other channels we can observe that the Argonne interaction induces stronger correlations, the correlation hole is deeper.

The tensor correlation functions $\vartheta(r)$ are displayed in Fig. 1.29. Besides the deuteron tensor correlators we see tensor correlation functions α, β and γ that are obtained by minimizing the energy in the two-body system with a constant trial function or by minimizing the energy with the ^{4}He trial state in the two-body approximation. An additional constraint on the correlation

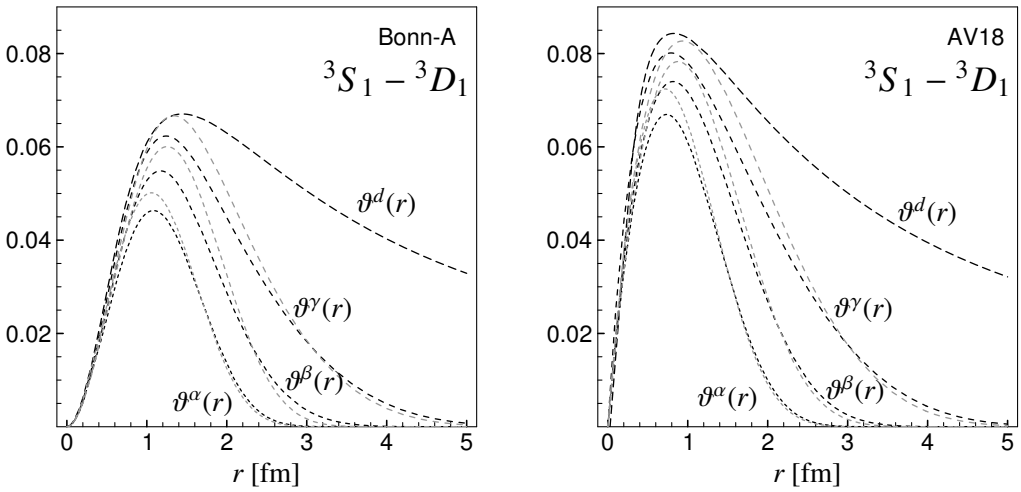

Figure 1.29: Tensor correlation functions for Bonn-A interaction (left hand side) and Argonne V18 interaction (right hand side). The tensor correlation functions α, β and γ are the result of a minimization of the energy of the energy in the two-body system (black dotted lines) or in ^{4}He trial state (gray dotted lines) with additional constraints on the range of the correlators.

range

$$\int \mathrm{d}r\, r^2\, \vartheta(r) \stackrel{!}{=} \begin{cases} 0.1\,\mathrm{fm}^3 & ; \quad \alpha \\ 0.2\,\mathrm{fm}^3 & ; \quad \beta \\ 0.5\,\mathrm{fm}^3 & ; \quad \gamma \end{cases} \tag{1.110}$$

is imposed for these correlators.

1.9.4 $S, T = 1, 1$ Channel

The lowest orbital angular momentum $L = 1$ in the $S, T = 1, 1$ channel can be coupled to an total angular momentum of $J = 0, 1, 2$. Tensor correlations affect only the $J = 2$ channel. We can therefore determine the tensor correlator from the zero-energy scattering solution in the $^3P_2 - {}^3F_2$ channel. As we want a central correlator that is independent of J we fix the central correlator not on the scattering solution for one particular J but on the zero-energy scattering solution obtained with the central part of the interaction only.

Minimizing the energy in the two-body system defines our second set of correlators. Here we minimize the energy

$$E = \frac{1}{9}\langle (11)0 \left| \underset{\sim}{c}_r^\dagger \underset{\sim\sim}{h} \underset{\sim}{c}_r \right| (11)0 \rangle + \frac{3}{9}\langle (11)1 \left| \underset{\sim}{c}_r^\dagger \underset{\sim\sim}{h} \underset{\sim}{c}_r \right| (11)1 \rangle + \frac{5}{9}\langle (11)2 \left| \underset{\sim}{c}_r^\dagger \underset{\sim}{c}_\Omega^\dagger \underset{\sim\sim}{h} \underset{\sim\sim}{c}_\Omega \underset{\sim}{c}_r \right| (11)2 \rangle \tag{1.111}$$

averaged over the different angular momenta J. Like in the $S, T = 1, 0$ channel we first minimize the energy with respect to the central correlator using the tensor correlation function $\vartheta^{zero}(r)$ derived from the $^3P_2 - {}^3F_2$ scattering solution. In a second step the energy is minimized with respect to the tensor correlator.

In contrast to the $S, T = 0, 0$ channel where the central correlator determined from the zero-energy scattering solution is extremely long ranged the central correlator in the $S, T = 1, 1$ channel is essentially short-ranged, see Fig. 1.30. We therefore do not have to impose a constraint on the correlation range for the energy minimized correlator. The tensor correlations

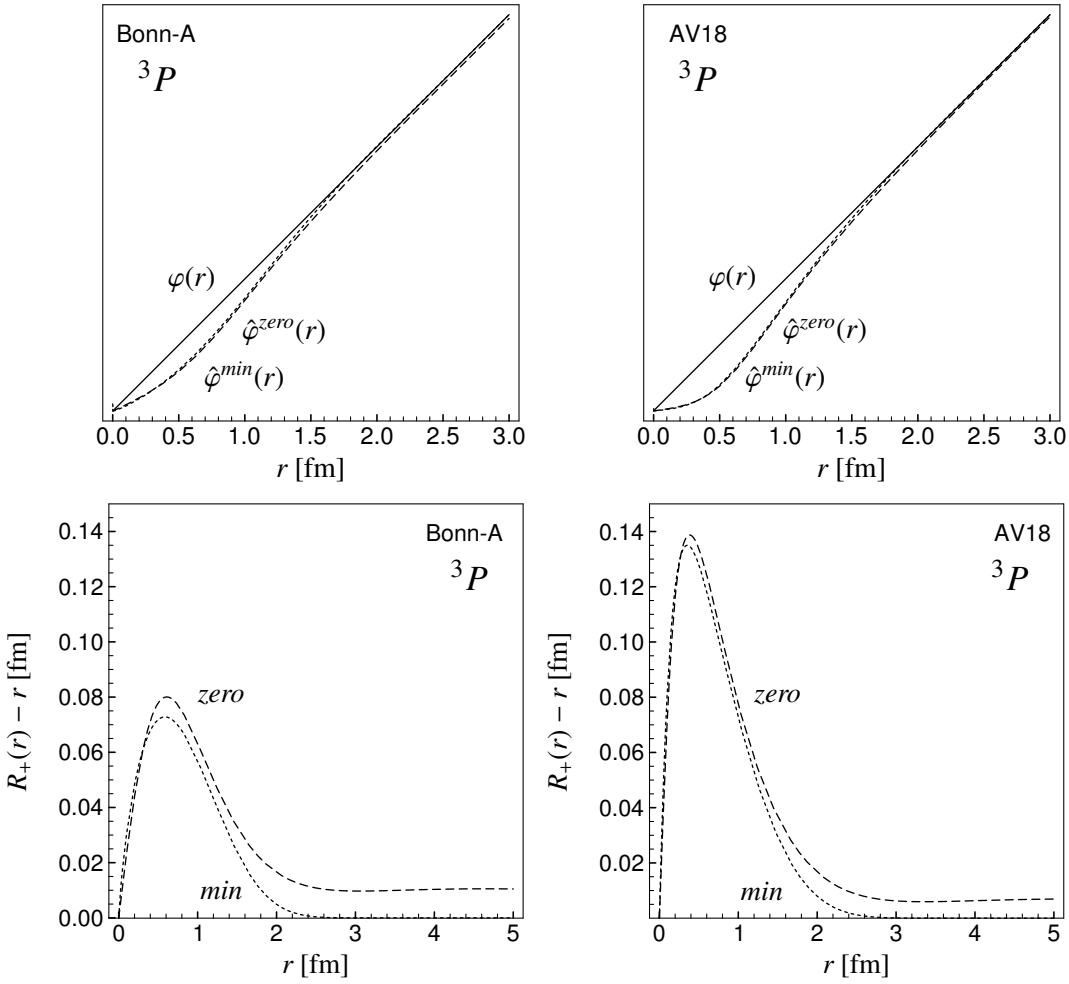

Figure 1.30: Central correlation functions $R_+(r)$ in the $S, T = 1, 1$ channel for Bonn-A interaction (left hand side) and the Argonne V18 interaction (right hand side). The zero-energy scattering solution $\hat{\varphi}^{zero(r)}$ (dashed line) is determined neglecting the non-central parts of the interaction. $\varphi(r)$ is the free zero-energy scattering solution. Besides the correlator which maps the free scattering solution onto the interacting scattering solution (*zero*) the correlator resulting from minimizing the energy in the two-body system is shown.

are also very weak compared to the $S, T = 1, 0$ channel and we refrain from imposing additional constraints on the range of the tensor correlator. The tensor correlators are displayed in Fig. 1.31.

As in all the other channels we can observe stronger correlations in case of the Argonne interaction.

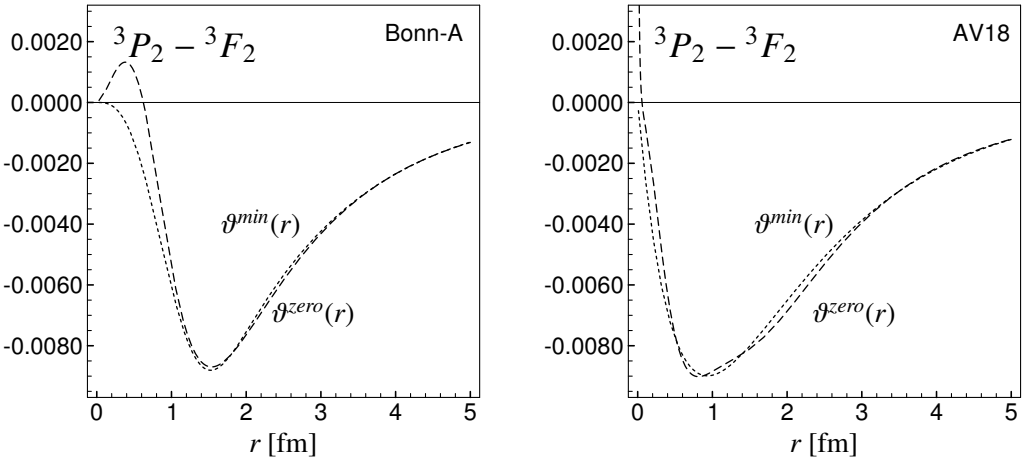

Figure 1.31: Tensor correlation functions in the $S, T = 1, 1$ channel for the Bonn-A (left) and Argonne V18 (right) interaction. Shown are the correlation functions $\vartheta^{zero}(r)$ (dashed line) determined from the scattering solutions in the $^3P_2 - {}^3F_2$ channel and $\vartheta^{min}(r)$ (dotted line) determined from the energy minimization in the two-body system. Because of the small tensor correlations no constraints on the correlation range have been imposed.

1.10 Many-Body Calculations

In this section Many-body calculations of the ground state properties of the doubly magic nuclei ^{4}He, ^{16}O and ^{40}Ca are performed using the Bonn-A and Argonne V18 interactions and their corresponding correlators determined in section 1.9. Of particular interest is the role of the tensor correlator. The tensor correlator derived from the deuteron or the zero-energy scattering solution is of very long range. As we want to use the two-body approximation we have to restrict the range of the correlator. To study the influence of the correlation range we will compare the results obtained with the three differently ranged tensor correlators α, β and γ. We investigate the question how long ranged the correlator must be to successfully describe the tensor correlations and how short ranged it has to be if we want to restrict ourselves to the two-body approximation.

1.10.1 The ^{4}He Nucleus

The many-body calculations are done with the harmonic oscillator shell model trial states as defined in section 1.7. The correlated interactions are used in two-body approximation and we can use the correlated operators given in section 1.8.4. We will discuss the calculations in the ^{4}He nucleus in some detail to illustrate the formalism.

The uncorrelated trial state $\left|\,^4\mathrm{He}\,\right\rangle$ is the product of a harmonic oscillator ground state wave function with different spins and isospins. The only parameter of the trial state is the oscillator width a, that is related to the radius of the ^{4}He nucleus.

This uncorrelated ^{4}He trial state has only s-wave components in its relative wave functions. In the uncorrelated trial state the tensor and spin-orbit forces therefore do not contribute to the expectation value $\left\langle\,^4\mathrm{He}\,\middle|\,\underset{\sim}{H}_{intr}\,\middle|\,^4\mathrm{He}\,\right\rangle$ of the Hamilton operator. The d-wave admixtures in the relative wave functions of the ^{4}He nucleus have to be generated by the tensor correlator.

With the Talmi transformation (C.7) we can calculate the ^{4}He expectation value of the Hamil-

ton operator in two-body approximation

$$\begin{aligned}
&\langle\, ^4\mathrm{He} \,|\, [\underset{\sim}{C}^\dagger_r \underset{\sim}{C}^\dagger_\Omega \underset{\sim}{H}_{intr} \underset{\sim}{C}_\Omega \underset{\sim}{C}_r]^{C2} \,|\, ^4\mathrm{He} \,\rangle = \langle\, ^4\mathrm{He} \,|\, \underset{\sim}{T} - \underset{\sim}{T}_{cm} \,|\, ^4\mathrm{He} \,\rangle \\
&+ 3\langle\, 1;(00)0,1 \,|\, \underset{\sim}{c}^\dagger_r \underset{\sim}{\underset{\sim}{t}} \underset{\sim}{c}_r - \underset{\sim}{t} \,|\, 1;(00)0,1 \,\rangle + 3\langle\, 1;(01)1,0 \,|\, \underset{\sim}{c}^\dagger_r \underset{\sim}{c}^\dagger_\Omega \underset{\sim}{\underset{\sim}{t}} \underset{\sim}{c}_\Omega \underset{\sim}{c}_r - \underset{\sim}{t} \,|\, 1;(01)1,0 \,\rangle \\
&+ 3\langle\, 1;(00)0,1 \,|\, \underset{\sim}{c}^\dagger_r \underset{\sim}{\underset{\sim}{v}} \underset{\sim}{c}_r \,|\, 1;(00)0,1 \,\rangle + 3\langle\, 1;(01)1,0 \,|\, \underset{\sim}{c}^\dagger_r \underset{\sim}{c}^\dagger_\Omega \underset{\sim}{\underset{\sim}{v}} \underset{\sim}{c}_\Omega \underset{\sim}{c}_r \,|\, 1;(01)1,0 \,\rangle \,.
\end{aligned} \tag{1.112}$$

The expectation value $\langle\, ^4\mathrm{He} \,|\, \underset{\sim}{T} - \underset{\sim}{T}_{cm} \,|\, ^4\mathrm{He} \,\rangle$ can be calculated analytically, see Eq. (C.10). The relative wave function of the two-body states $|\, n;(LS)J,T \,\rangle$ are Gaussians with twice the variance of the single-particle states.

In the $S = 0$ channel, where we only have to deal with central correlations, we get for the two-body matrix element of the correlated kinetic energy

$$\begin{aligned}
&\langle\, 1;(00)0,1 \,|\, \underset{\sim}{c}^\dagger_r \underset{\sim}{\underset{\sim}{t}} \underset{\sim}{c}_r - \underset{\sim}{t} \,|\, 1;(00)0,1 \,\rangle = \\
&-\int dr\, R_{10}(2a)(r) \frac{1}{m} \Big(\frac{1}{R^{01\prime}_+(r)^2} - 1 \Big) R''_{10}(2a)(r) + \int dr\, R^2_{10}(2a)(r) \frac{1}{m} \Big(\frac{7R^{01\prime\prime}_+(r)^2}{4R^{01\prime}_+(r)^4} - \frac{R^{01\prime\prime\prime}_+(r)}{2R^{01\prime}_+(r)^3} \Big) ,
\end{aligned} \tag{1.113}$$

see Eq. (1.41). Here $R^{ST}_+(r)$ is the central correlation function in the S,T channel and

$$R_{10}(2a)(r) = r \left(\frac{2}{\pi a^3} \right)^{\frac{1}{4}} \exp\left\{ -\frac{r^2}{4a} \right\} \tag{1.114}$$

the radial wave function of the relative motion.

In the $S = 1$ channel also the tensor correlations have to be considered and we get with help of Eq. (1.97) and Eq. (1.98)

$$\begin{aligned}
&\langle\, 1;(01)1,0 \,|\, \underset{\sim}{c}^\dagger_r \underset{\sim}{c}^\dagger_\Omega \underset{\sim}{\underset{\sim}{t}} \underset{\sim}{c}_\Omega \underset{\sim}{c}_r - \underset{\sim}{t} \,|\, 1;(01)1,0 \,\rangle = -\int dr\, R_{10}(2a)(r) \frac{1}{m} \Big(\frac{1}{R^{10\prime}_+(r)^2} - 1 \Big) R''_{10}(2a)(r) \\
&+ \int dr\, R^2_{10}(2a)(r) \frac{1}{m} \Big(\frac{7R^{10\prime\prime}_+(r)^2}{4R^{10\prime}_+(r)^4} - \frac{R^{10\prime\prime\prime}_+(r)}{2R^{10\prime}_+(r)^3} \Big) + \int dr\, R^2_{10}(2a)(r) \frac{1}{m} [\theta^{(1)\prime}(R^{10}_+(r))]^2 \\
&+ \int dr\, R^2_{10}(2a)(r) \sin^2\left(\theta^{(1)}(R^{10}_+(r)) \right) \frac{1}{m} \frac{1}{R^{10}_+(r)^2} \langle\, (21)1 \,|\, \underset{\sim}{\mathbf{l}}^2 \,|\, (21)1 \,\rangle \,.
\end{aligned} \tag{1.115}$$

In the $S,T = 1,0$ channel only the central part contributes to the matrix element of the potential

$$\langle\, 1;(00)0,1 \,|\, \underset{\sim}{c}^\dagger_r \underset{\sim}{\underset{\sim}{v}} \underset{\sim}{c}_r \,|\, 1;(00)0,1 \,\rangle = \int dr\, R^2_{10}(2a)(r)\, v^c_{01}(R^{01}_+(r)) \,, \tag{1.116}$$

but in the $S,T = 1,0$ channel we have to consider also the spin-orbit and tensor force. The expectation value of the central force does not change when including the tensor correlation. The spin-orbit force has only diagonal matrix elements in the $L = 2$ states whereas the tensor force has strong off-diagonal contributions between the $L = 0$ and $L = 2$ states, see Eqs. (1.99-

1.101):

$$\begin{aligned}\langle\, 1;(01)1,0 \,|\, \underset{\sim}{c}^\dagger_r \underset{\sim}{c}^\dagger_\Omega v \underset{\sim}{c}_\Omega \underset{\sim}{c}_r \,|\, 1;(01)1,0 \,\rangle &= \int dr\, R^2_{10}(2a)(r) v^c_{10}(R^{10}_+(r)) \\ &+ \int dr\, R^2_{10}(2a)(r) \sin^2\left(\theta^{(1)}(R^{10}_+(r))\right) \langle\, (21)1,0 \,|\, \underset{\sim}{\mathbf{l}}\cdot\underset{\sim}{\mathbf{s}} \,|\, (21)1,0 \,\rangle\, v^b_{10}(R^{10}_+(r)) \\ &+ 2\int dr\, R^2_{10}(2a)(r) \cos\left(\theta^{(1)}(R^{10}_+(r))\right) \sin\left(\theta^{(1)}(R^{10}_+(r))\right) \\ &\qquad \times \langle\, (01)1,0 \,|\, \underset{\sim}{s}_{12}(\hat{\mathbf{r}},\hat{\mathbf{r}}) \,|\, (21)1,0 \,\rangle\, v^t_{10}(R^{10}_+(r)) \\ &+ \int dr\, R^2_{10}(2a)(r) \sin^2\left(\theta^{(1)}(R^{10}_+(r))\right) \langle\, (21)1,0 \,|\, \underset{\sim}{s}_{12}(\hat{\mathbf{r}},\hat{\mathbf{r}}) \,|\, (21)1,0 \,\rangle\, v^t_{10}(R^{10}_+(r)) \,.\end{aligned} \tag{1.117}$$

Other components of the interaction have to be treated accordingly.

The uncorrelated ^{4}He trial state has only s-wave components but the tensor correlator induces a d-wave admixture. The percentages of s-wave and d-wave components define the measures P_s and P_d. The total orbital angular momentum of the ^{4}He nucleus can then be expressed as

$$\langle\, \underset{\sim}{\mathbf{L}}^2 \,\rangle = 0 \cdot P_s + 2(2+1) \cdot P_d \,. \tag{1.118}$$

The total orbital angular momentum of the correlated ^{4}He nucleus calculated in the two-body approximation is given by

$$\begin{aligned}&\langle\, {}^4\mathrm{He} \,|\, \left[\underset{\sim}{C}^\dagger_r \underset{\sim}{C}^\dagger_\Omega \underset{\sim}{\mathbf{L}}^2 \underset{\sim}{C}_\Omega \underset{\sim}{C}_r\right]^{C2} \,|\, {}^4\mathrm{He} \,\rangle = \\ &\quad 3\langle\, 1;(00)0,1 \,|\, \underset{\sim}{c}^\dagger_r \underset{\sim}{\mathbf{l}}^2 \underset{\sim}{c}_r - \underset{\sim}{\mathbf{l}}^2 \,|\, a;(00)0,1 \,\rangle + 3\langle\, 1;(01)1,0 \,|\, \underset{\sim}{c}^\dagger_r \underset{\sim}{c}^\dagger_\Omega \underset{\sim}{\mathbf{l}}^2 \underset{\sim}{c}_\Omega \underset{\sim}{c}_r - \underset{\sim}{\mathbf{l}}^2 \,|\, 1;(01)1,0 \,\rangle \,.\end{aligned} \tag{1.119}$$

There are no contributions from the one-body part (one-body states have $l=0$) of the cluster expansion. From the two-body part the only non-vanishing contribution is in the tensor correlated $S,T=1,0$ channel with its $L=2$ admixture (Eq. (1.94))

$$\langle\, {}^4\mathrm{He} \,|\, [\underset{\sim}{C}^\dagger_r \underset{\sim}{C}^\dagger_\Omega \underset{\sim}{\mathbf{L}}^2 \underset{\sim}{C}_\Omega \underset{\sim}{C}_r]^{C2} \,|\, {}^4\mathrm{He} \,\rangle = 2(2+1) \int dr\, R^2_{10}(2a)(r) \sin^2\left(\theta^{(1)}(R^{10}_+(r))\right) \,. \tag{1.120}$$

The correlations also influence the radius of the nucleus. The R_{rms} radius is defined as

$$R^2_{\mathrm{rms}} = \frac{1}{A}\langle \sum_i (\underset{\sim}{\mathbf{r}}_i - \underset{\sim}{\mathbf{R}}_{cm})^2 \,\rangle \tag{1.121}$$

and can be calculated analytically for the uncorrelated trial state, see Eq. (C.12). The correlated radius $\hat{R}_{\mathrm{rms}}$ is obtained in two-body approximation as

$$\begin{aligned}4\hat{R}^2_{\mathrm{rms}} &= \langle\, {}^4\mathrm{He} \,|\, \sum_i (\underset{\sim}{\mathbf{r}}_i - \underset{\sim}{\mathbf{R}}_{cm})^2 \,|\, {}^4\mathrm{He} \,\rangle \\ &+3\langle\, 1;(00)0,1 \,|\, \frac{1}{2}(\underset{\sim}{c}^\dagger_r \underset{\sim}{r}^2 \underset{\sim}{c}_r - \underset{\sim}{r}^2) \,|\, 1;(00)0,1 \,\rangle + 3\langle\, 1;(01)1,0 \,|\, \frac{1}{2}(\underset{\sim}{c}^\dagger_r \underset{\sim}{c}^\dagger_\Omega \underset{\sim}{r}^2 \underset{\sim}{c}_\Omega \underset{\sim}{c}_r - \underset{\sim}{r}^2) \,|\, 1;(01)1,0 \,\rangle \,.\end{aligned} \tag{1.122}$$

The tensor correlator $\underset{\sim}{c}_\Omega$ commutes with r^2 and we obtain

$$\hat{R}^2_{\mathrm{rms}} = R^2_{\mathrm{rms}} + \frac{3}{4}\int dr\, R^2_{10}(2a)(r) \frac{1}{2}\left((R^{01}_+(r))^2 - r^2\right) + \frac{3}{4}\int dr\, R^2_{10}(2a)(r) \frac{1}{2}\left((R^{10}_+(r))^2 - r^2\right) \,. \tag{1.123}$$

Results - Argonne V8'

The Argonne V8' is simpler in its operator structure than the full Argonne V18 interaction and has been used recently as a benchmark potential for many-body calculations of the ^{4}He nucleus [KNG+01]. The predictions of all the quasi-exact many-body methods presented in this paper agree in binding energy and radius of the ^{4}He nucleus and we can therefore use this as a reliable reference.

Figure 1.32: ^{4}He binding energies with the Argonne V8' interaction (without Coulomb interaction) as a function of the matter radius $r_{\rm rms}$. The black solid line is obtained using two-body optimized central correlators and the deuteron tensor correlator. For the gray solid line ^{4}He optimized central correlators and a ^{4}He optimized tensor correlator, that is very similar to the deuteron correlator, are used. The black dotted lines use two-body minimized central correlators and the three two-body optimized tensor correlators with restricted range (labeled with α, β and γ). The gray dotted lines use the ^{4}He optimized central and tensor correlators. The result of the reference calculations [KNG+01] is indicated.

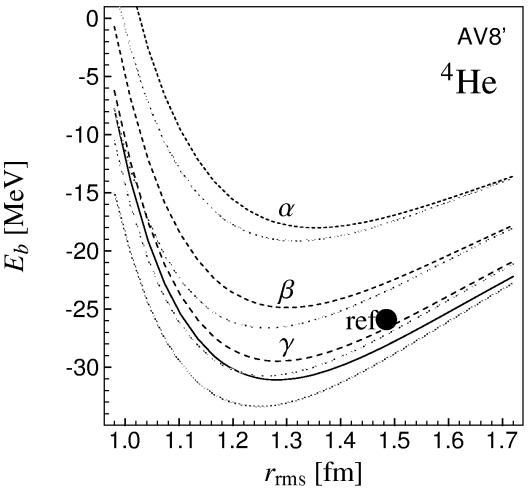

Figure 1.33: Contributions of the various interaction parts to the binding energy with the Argonne V8' interaction. Reference values are given by the dots. The ^{4}He optimized correlators are used. For the intrinsic kinetic energy $\langle T - T_{cm} \rangle$, the spin-orbit $\langle V^b \rangle$ and the tensor potential $\langle V^t \rangle$ three curves for the tensor correlators α, β and γ are shown. The central interaction $\langle V^c \rangle$ (solid line and grey point) is not influenced by the tensor correlations.

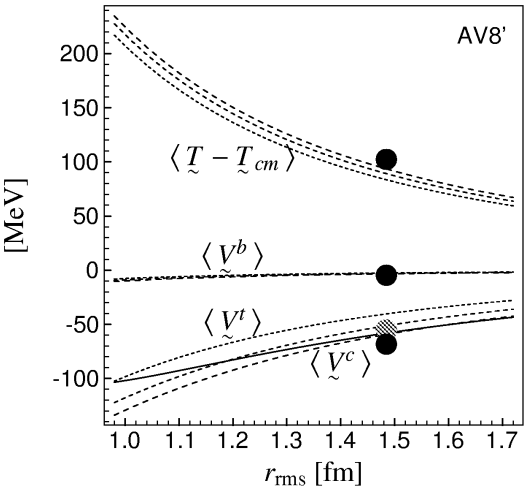

In Fig. 1.32 the binding energy of ^{4}He calculated with the correlated Argonne V8' interaction is shown. As expected the binding energy increases with the range of the tensor correlator. We can also observe that a small but significant increase of about 2 MeV in binding is achieved when using the ^{4}He optimized correlators instead of the correlators derived with constant trial functions in the two-body system. The ^{4}He optimized correlators have been fixed in this calculation for a trial state that reproduces the rms radius of the reference calculations. An additional increase in binding is achieved with tensor correlators of unrestricted range.

One should note that this strong increase in binding with many-body optimized correlators is specific for very light nuclei. In heavier nuclei the two-nucleon distribution function is much smoother and only an insignificant increase in binding can be achieved by using many-body optimized correlators.

When we compare the binding energy at the rms radius of the reference result we see a fair agreement with the results of the long ranged tensor correlator γ. This is affirmed by the contributions of the individual interaction parts, as shown in Fig. 1.33 and the d-wave probability P_d of 13.9% which agrees well with the γ tensor correlator.

Although our calculations reproduce fairly well the binding energy at the ^{4}He reference width, our minimum of the binding energy is obtained at a smaller radius and has about 4 MeV more binding. Also for the shorter ranged tensor correlators β and α we observe radii that are too small. This effect may be explained to some extent by our extremely simple ansatz for the uncorrelated trial state. We only have $L=0$ components in our uncorrelated trial function and the tensor correlator only admixes $L=2$ contributions. The reference calculations conclude for example on a 0.37% p-wave probability in the ^{4}He nucleus.

Of much greater importance is however the fact that we have to use rather long ranged tensor correlators to get sufficient binding. The higher-order contributions cannot be neglected for the long ranged correlators especially for smaller radii which correspond to higher densities. Additional repulsion from three-body contributions could shift the minimum up in energy and towards larger radii. A qualitative discussion of this effect is presented in section 1.10.3.

We want to emphasize the fact that we are discussing small effects resulting from the sum of large positive and negative contributions, as seen in Fig. 1.33, to the total binding energy. It should also be noted that the correlators are absolutely essential. The energy obtained with the uncorrelated trial state is

$$\langle\, ^4\mathrm{He} \,|\, \underset{\sim}{H}_{intr} \,|\, ^4\mathrm{He} \,\rangle = +73\,\mathrm{MeV} \tag{1.124}$$

and the energy of a trial state correlated only with the central correlator

$$\langle\, ^4\mathrm{He} \,|\, [\underset{\sim}{C}_r^\dagger \underset{\sim}{H}_{intr} \underset{\sim}{C}_r]^{C2} \,|\, ^4\mathrm{He} \,\rangle = +11\,\mathrm{MeV}\ , \tag{1.125}$$

calculated for the radius $r_{\mathrm{rms}} = 1.48$ fm. The tensor correlator alone brings the system from an unbound configuration with +11 MeV down to

$$\langle\, ^4\mathrm{He} \,|\, [\underset{\sim}{C}_r^\dagger \underset{\sim}{C}_\Omega^\dagger \underset{\sim}{H}_{intr} \underset{\sim}{C}_\Omega \underset{\sim}{C}_r]^{C2} \,|\, ^4\mathrm{He} \,\rangle = -27\,\mathrm{MeV}\ , \tag{1.126}$$

for the long ranged tensor correlator γ.

Results – Bonn-A and Argonne V18

In Fig. 1.34 we show our results for the ^{4}He nucleus using the Bonn-A and the Argonne V18 interactions. The Argonne V18 nuclear interaction is identical to the Argonne V8' in the channels relevant in the two-body approximation and the results will differ therefore only because of the Coulomb force. For reference we show results of VMC and GFMC calculations [Wir92] with the Argonne V18 interaction. As in the case of the Argonne V8' interactions we observe that our radii are somewhat smaller. One should however also note the large difference in the radii of the VMC and the GFMC calculations. At the reference radius of the GFMC calculation the long range tensor correlator γ reproduces the GFMC binding energy. The differences between the GFMC calculation and the experimental binding energy and radius are usually interpreted as an indication for the necessity of genuine three-body forces.

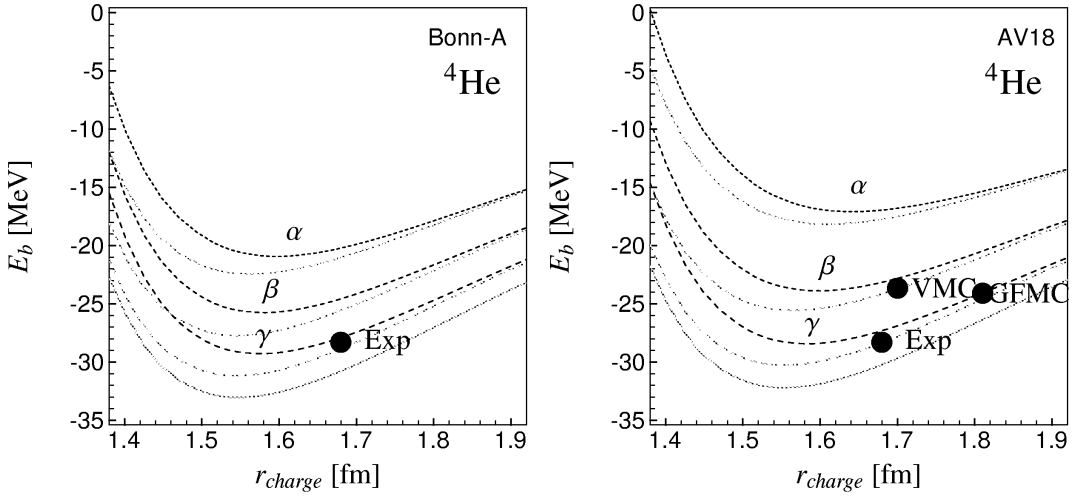

Figure 1.34: The ^{4}He nucleus calculated with the Bonn-A (left hand side) and the Argonne V18 (right hand side) interaction. The differences between the Argonne V18 and the Argonne V8' results shown in Fig. 1.32 are due to the Coulomb force. Black dotted lines are obtained using the two-body optimized central correlator and the two-body optimized tensor correlators of restricted range. The gray dotted lines use the ^{4}He optimized correlators instead. The gray solid line is obtained with the ^{4}He optimized central correlator and a ^{4}He optimized tensor correlator without range constraints. For the Argonne V18 we indicate the results of VMC and GFMC calculations [Wir92].

For the Bonn-A interaction there are no reference calculations but the results are very similar to the Argonne V18 calculations, except that the Bonn-A interaction is more attractive with the shorter tensor correlators α and β.

1.10.2 Doubly Magic Nuclei: ^{16}O and ^{40}Ca

The doubly magic nuclei are calculated with the harmonic oscillator shell model trial states given in section 1.7 using the two-body approximation. The evaluation of the two-body matrix elements is done with the correlated interaction in angular momentum eigenstates given in section 1.8.4 and as it was illustrated for the ^{4}He nucleus.

Results – Argonne V8'

In Fig. 1.35 our results with the Argonne V8' interaction are displayed. The FHNC/SOC calculations we show for reference were done with a Hamiltonian consisting of the Argonne V8' potential together with the Urbana IX three-body force. Therefore we can unfortunately only compare the expectation values of the Argonne V8' potential at the radii obtained in the FHNC/SOC calculations. At those radii the β and γ tensor correlators yield very similar energies.

Results – Bonn-A and Argonne V18

In Fig. 1.36 and Fig. 1.37 the results of many-body calculations using the Bonn-A and the Argonne V18 interaction are presented. In case of the Bonn-A interaction the results of a

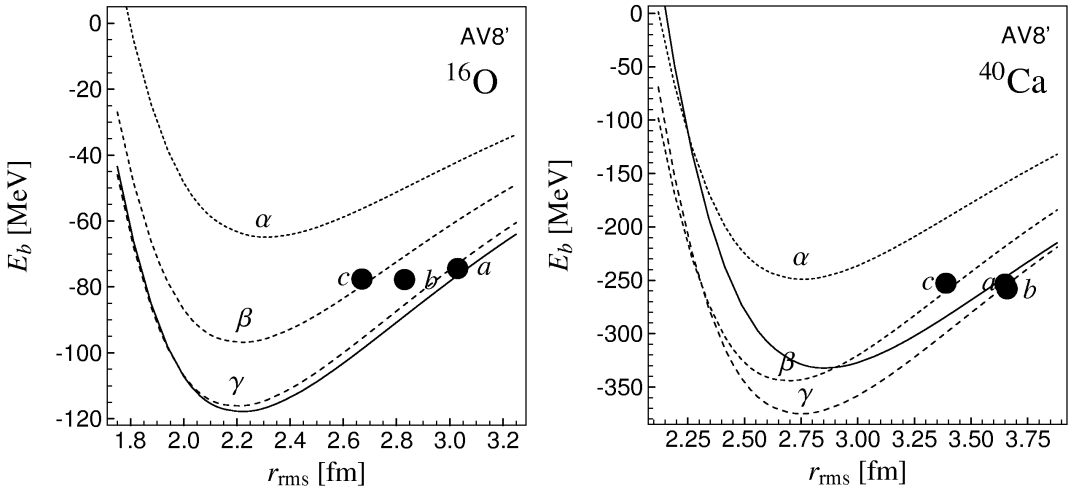

Figure 1.35: Calculations for the ^{16}O and ^{40}Ca nuclei using the Argonne V8' interaction (including the Coulomb force). The dotted lines show the results with the two-body optimized central correlator and the three two-body optimized tensor correlators α, β and γ. The solid lines are obtained with the deuteron tensor correlator. The points denote FHNC/SOC calculations. The radii for the points *a* and *b* represent minima of the energy where additional three-body forces are added to the Argonne V8'. The calculation *c* used a trial state that reproduces the experimental radius. Calculation *a* used harmonic oscillator states, the calculations *b* and *c* Woods-Saxon states.

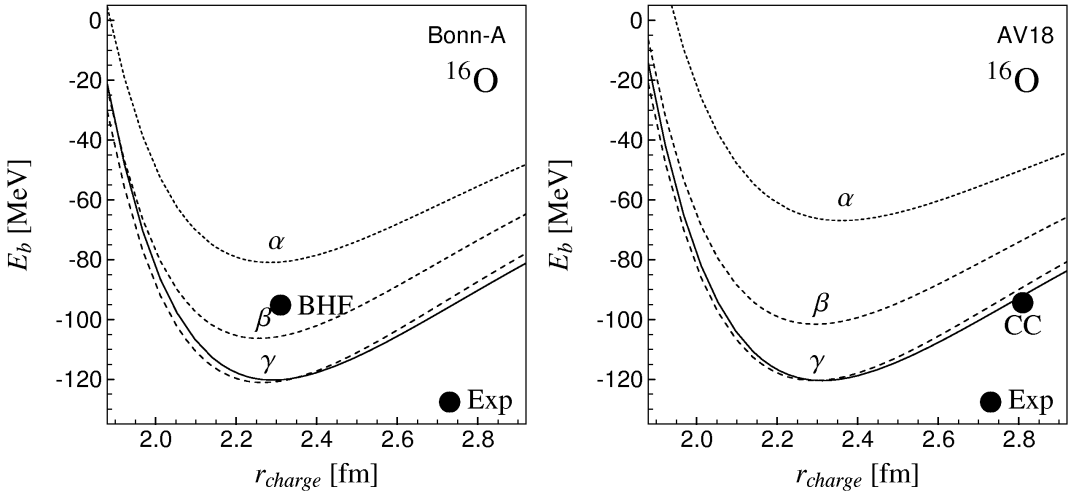

Figure 1.36: Calculations for the ^{16}O nucleus using the Bonn-A (left) and the Argonne V18 (right) interaction. The two-body optimized central correlators are used together with two-body optimized tensor correlators with restricted range (dotted lines) or the deuteron tensor correlators (solid line). For the Bonn-A interaction the result of a Brueckner Hartree Fock (BHF) calculation [MP00] and for the Argonne V18 potential the result of a Coupled Cluster (CC) calculation [HM99] are indicated.

BHF calculation [MP00] and for the Argonne V18 a Coupled Cluster Calculation [HM99] are included for reference.

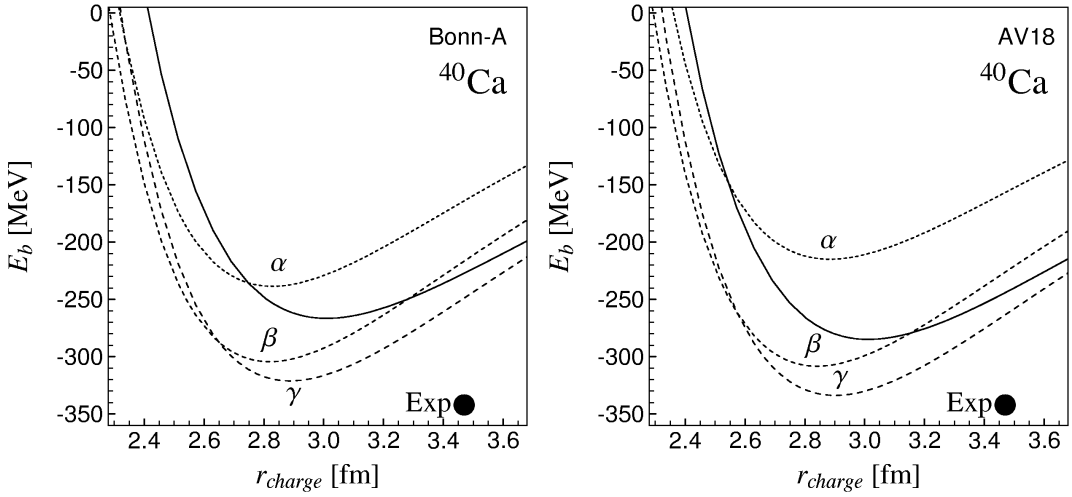

Figure 1.37: The ^{40}Ca nucleus calculated with the Bonn-A (left) and the Argonne V18 (right) interaction. The two-body optimized central correlators are used together with two-body optimized tensor correlators with restricted range (dotted lines) or the deuteron tensor correlators (solid line).

In the case of ^{16}O the uncorrelated energies for the Bonn-A and the Argonne V18 interaction are +212 MeV and +321 MeV, in case of ^{40}Ca they are +622 MeV and +933 MeV respectively. But when the tensor correlators β and γ are used the correlated Bonn-A and Argonne V18 interactions give very similar results. It seems that the unitary correlators which are interaction specific map the two different interactions on the same correlated interaction. This is illustrated further in section 1.12 where the low-momentum behavior of the correlated interaction is discussed.

Another interesting observation is the fact that the tensor correlator of unrestricted range which is optimal in the two-body system actually gives less binding for the heavier nuclei than the correlator γ that is restricted in range. In the two-body system we only consider a $L=0$ trial state but in the two-body densities of the heavier nuclei also higher relative angular momenta appear. The additional angular momentum dependence which comes with the tensor correlations gives then, increasing with the correlation range and decreasing with the radius, more repulsion which overcompensates the increased binding in the $L=0$ channels. This effect cannot be observed with the short ranged tensor correlator as the probability density at short distances is already strongly suppressed by the centrifugal barrier.

We can further notice that neither the correlated Argonne V18 nor the correlated Bonn-A interaction can reproduce the experimental binding energies at the experimental radii. It is known from GFMC calculations of light nuclei ($A < 10$) that the Argonne V18 interaction does not provide enough binding and additional genuine three-body forces are needed to reproduce the experimental radii and binding energies.

1.10.3 Higher Order Contributions

The study of the nuclei ^{4}He, ^{16}O and ^{40}Ca shows that the tensor correlations are indeed long ranged and it has to be questioned whether they can by treated solely by the unitary correlator in the two-body approximation. Instead of starting the tedious job of calculating three-body terms we want to discuss what we can expect from the three-body contributions.

The three-body parts of the correlated interaction will be induced mainly by the tensor correlator in the $S = 1, T = 0$ channel because of the strength and long range of this correlator.

We simulate the three-body contributions by a three-body delta force. The expectation value

$$\langle \underset{\sim}{V}^{(3)} \rangle = V_0 \int \mathrm{d}^3 r \, \rho^3(r) \tag{1.127}$$

can be evaluated analytically and we get as three-body contributions at the experimental radii:

$$^4\mathrm{He}: \qquad \langle \underset{\sim}{V}^{(3)} \rangle / A = 0.0188 \, \mathrm{fm}^{-6} V_0 \tag{1.128}$$

$$^{16}\mathrm{O}: \qquad \langle \underset{\sim}{V}^{(3)} \rangle / A = 0.0112 \, \mathrm{fm}^{-6} V_0 \tag{1.129}$$

$$^{40}\mathrm{Ca}: \qquad \langle \underset{\sim}{V}^{(3)} \rangle / A = 0.0141 \, \mathrm{fm}^{-6} V_0 \tag{1.130}$$

The effect of such a three-body contribution with $V_0 = 35$ MeV fm^6 and $V_0 = 70$ MeV fm^6 is displayed in Fig. 1.38. If we adjust V_0 to reproduce the binding energy of quasi-exact calculations in ^{4}He we estimate three-body contributions at the experimental radii in the order of $1 - 1.5$ MeV per nucleon. At smaller radii (higher densities) the three-body contributions are much larger and consequently the locations of the minima are noticeably shifted to larger radii compared to the radii obtained in two-body approximation.

If we include such a three-body correction in our calculations we are missing about $2-3$ MeV binding energy per nucleon when compared to the experimental values. This difference, that is also observed in the GFMC calculations for light nuclei up to $A = 10$, might be explained by genuine three-body forces [PPWC01]. A very rough extrapolation of the three-body contributions obtained in GFMC calculations of light nuclei to ^{16}O and ^{40}Ca is compatible with our estimation of $2 - 3$ MeV per nucleon. Compared to the total binding energy this may seem like a large correction, but compared to the large contribution of the two-body force alone, this is only a small correction.

Summarizing these considerations we conclude that the treatment of the tensor correlations in the UCOM approach is working. Unfortunately the tensor correlations are not so short ranged that the two-body approximation is sufficient. There are two possible conclusions: The first is to restrict the range of the tensor correlator in order to ensure the validity of the two-body approximation. The effect of the long range part of tensor correlations has then to be included in the many-body trial state. One can think of configuration mixing shell model calculations. The second possibility is to use the long ranged tensor correlator and try to evaluate the three-body contributions in a certain approximation. This would be the preferred approach for applications of the correlated interaction if one wants to work with a single or only a small set of Slater determinants.

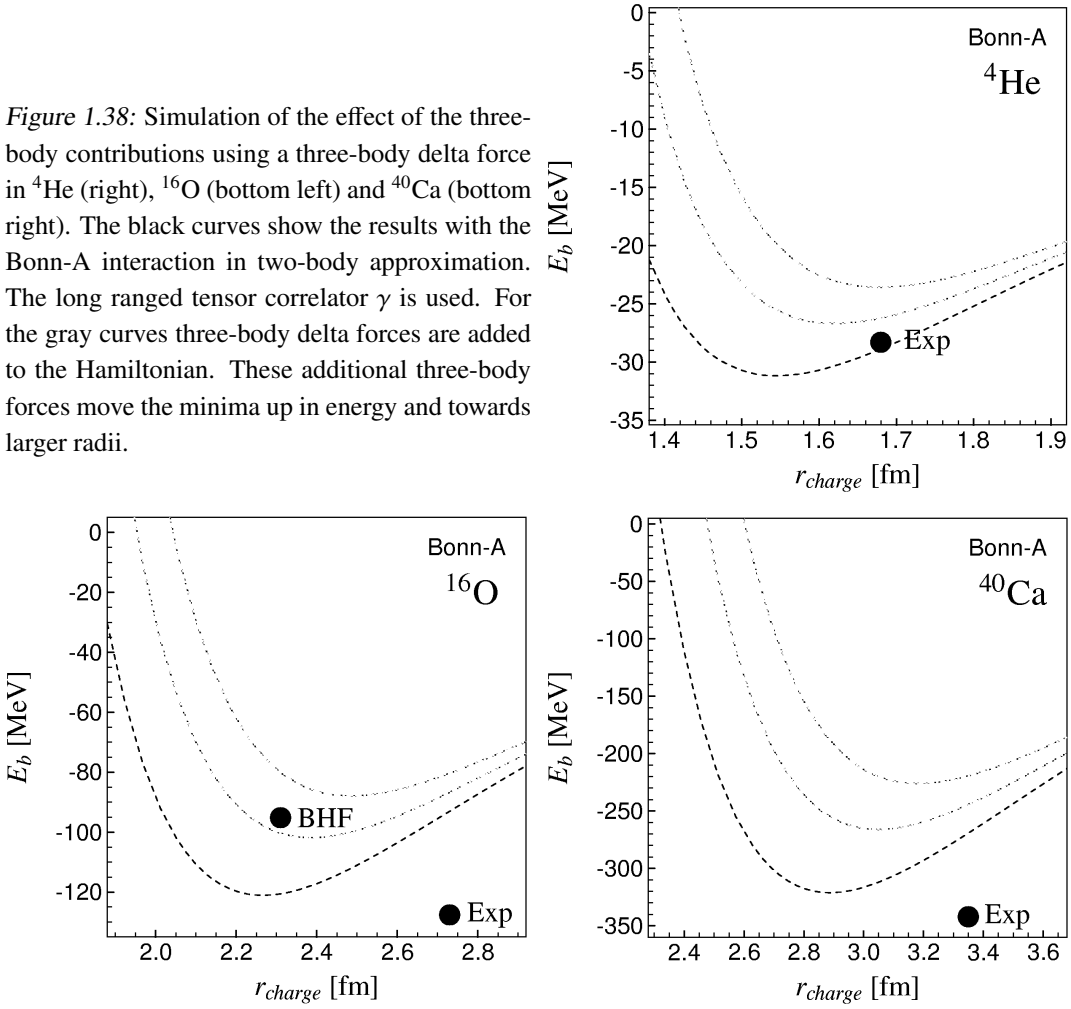

Figure 1.38: Simulation of the effect of the three-body contributions using a three-body delta force in ^{4}He (right), ^{16}O (bottom left) and ^{40}Ca (bottom right). The black curves show the results with the Bonn-A interaction in two-body approximation. The long ranged tensor correlator γ is used. For the gray curves three-body delta forces are added to the Hamiltonian. These additional three-body forces move the minima up in energy and towards larger radii.

1.11 Correlated Operators

When using a harmonic oscillator shell model basis the two-body states can easily be written in angular momentum eigenstates of relative and center of mass coordinates. The unitary tensor correlations acting on the relative coordinates can be performed explicitly in these states. However if we are not dealing with angular momentum eigenstates it is technically advantageous to correlate the operators. The centrally and tensorically correlated interaction can then be used in many-body calculations (Hartree-Fock, FMD).

A fully correlated operator $\hat{\underset{\sim}{A}}$ is given by

$$\hat{\underset{\sim}{A}} = \underset{\sim}{C}^\dagger \underset{\sim}{A} \underset{\sim}{C} = \underset{\sim}{C}_r^\dagger \underset{\sim}{C}_\Omega^\dagger \underset{\sim}{A} \underset{\sim}{C}_\Omega \underset{\sim}{C}_r \ . \tag{1.131}$$

The tensor correlated operator in the two-body space is calculated with the Baker-Campbell-Hausdorff formula

$$\begin{aligned} \underset{\sim}{c}_\Omega^\dagger \underset{\sim}{a} \underset{\sim}{c}_\Omega &= e^{i\underset{\sim}{g}_\Omega} \underset{\sim}{a} e^{-i\underset{\sim}{g}_\Omega} \\ &= \underset{\sim}{a} + i[\underset{\sim}{g}_\Omega, \underset{\sim}{a}]_- + \frac{i^2}{2}[\underset{\sim}{g}_\Omega, [\underset{\sim}{g}_\Omega, \underset{\sim}{a}]_-]_- + \dots \\ &= e^{\mathrm{L}_\Omega} \underset{\sim}{a} \ , \end{aligned} \tag{1.132}$$

where we use the superoperator $\mathsf{L}_\Omega = i[\underset{\sim}{g_\Omega}, \circ]_-$ to rewrite the expression. For the explicit calculation we have to evaluate the repeated application of L_Ω. In the case of the Hamilton operator the commutators of the generator $\underset{\sim}{g_\Omega}$ with the kinetic energy and all components of the potential have to be calculated. All interaction components are scalar two-body operators (STB) with respect to rotations. In coordinate and spin-space they are of rank 0 (e.g. central potential), rank 1 (e.g. spin-orbit potential) or rank 2 (e.g. tensor potential). The calculation of the commutators of the operators is performed by recoupling the tensor components and is given in detail in appendix B.

The uncorrelated Bonn and Argonne interactions have potential components with Π_1, $\mathbf{l}^2$, $\mathbf{l}\cdot\mathbf{s}$, $(\mathbf{l}\cdot\mathbf{s})^2$ and $s_{12}(\hat{\mathbf{r}}, \hat{\mathbf{r}})$ operators. Unfortunately operators with increasing order in angular momenta are generated by the repeated application of L_Ω.

A special situation occurs for the radial part of the kinetic energy in the two-body space. Here the Baker-Campbell-Hausdorff series terminates after the second iteration

$$[g_\Omega, p_r^2]_- = i\,(p_r\vartheta'(r) + \vartheta'(r)p_r)\,s_{12}(\mathbf{r}, \mathbf{p}_\Omega) \tag{1.133}$$

$$[g_\Omega, [g_\Omega, p_r^2]_-]_- = -2\vartheta'(r)^2\left[(18 + 6\,\mathbf{l}^2)\Pi_1 + \frac{45}{2}\mathbf{l}\cdot\mathbf{s} + \frac{3}{2}s_{12}(\mathbf{l}, \mathbf{l})\right] \tag{1.134}$$

$$[g_\Omega, [g_\Omega, [g_\Omega, p_r^2]_-]_-]_- = 0\ . \tag{1.135}$$

The tensor operators $s_{12}(\mathbf{r}, \mathbf{p}_\Omega)$ and $s_{12}(\mathbf{l}, \mathbf{l})$ are defined as

$$s_{12}(\mathbf{r}, \mathbf{p}_\Omega) = \frac{1}{2}(3(\boldsymbol{\sigma}_1\cdot\mathbf{r})(\boldsymbol{\sigma}_2\cdot\mathbf{p}_\Omega) + 3(\boldsymbol{\sigma}_1\cdot\mathbf{p}_\Omega)(\boldsymbol{\sigma}_2\cdot\mathbf{r}) - (\boldsymbol{\sigma}_1\cdot\boldsymbol{\sigma}_2)(\mathbf{r}\cdot\mathbf{p}_\Omega) - (\boldsymbol{\sigma}_1\cdot\boldsymbol{\sigma}_2)(\mathbf{p}_\Omega\cdot\mathbf{r})) \tag{1.136}$$

and

$$s_{12}(\mathbf{l}, \mathbf{l}) = 3(\boldsymbol{\sigma}_1\cdot\mathbf{l})(\boldsymbol{\sigma}_2\cdot\mathbf{l}) - (\boldsymbol{\sigma}_1\cdot\boldsymbol{\sigma}_2)\mathbf{l}^2\ . \tag{1.137}$$

In case of the angular part of the kinetic energy and the potential part of the interactions we have to deal with the commutators

$$[g_\Omega, \Pi_1]_- = 0 \tag{1.138}$$

$$[g_\Omega, s_{12}(\hat{\mathbf{r}}, \hat{\mathbf{r}})]_- = i\vartheta(r)[-24\,\Pi_1 - 18\,\mathbf{l}\cdot\mathbf{s} + 3\,s_{12}(\hat{\mathbf{r}}, \hat{\mathbf{r}})] \tag{1.139}$$

$$[g_\Omega, \mathbf{l}\cdot\mathbf{s}]_- = i\vartheta(r)[-\bar{s}_{12}(\mathbf{p}_\Omega, \mathbf{p}_\Omega)] \tag{1.140}$$

$$[g_\Omega, \mathbf{l}^2]_- = i\vartheta(r)[2\,\bar{s}_{12}(\mathbf{p}_\Omega, \mathbf{p}_\Omega)] \tag{1.141}$$

$$[g_\Omega, s_{12}(\mathbf{l}, \mathbf{l})]_- = i\vartheta(r)[7\,\bar{s}_{12}(\mathbf{p}_\Omega, \mathbf{p}_\Omega)]\ , \tag{1.142}$$

where $\bar{s}_{12}(\mathbf{p}_\Omega, \mathbf{p}_\Omega)$ is a short-hand notation for the combination

$$\bar{s}_{12}(\mathbf{p}_\Omega, \mathbf{p}_\Omega) = 2r^2 s_{12}(\mathbf{p}_\Omega, \mathbf{p}_\Omega) + s_{12}(\mathbf{l}, \mathbf{l}) - \frac{1}{2}s_{12}(\hat{\mathbf{r}}, \hat{\mathbf{r}})\ . \tag{1.143}$$

In higher orders of the series the commutators

$$[g_\Omega, \bar{s}_{12}(\mathbf{p}_\Omega, \mathbf{p}_\Omega)]_- = i\vartheta(r)[(96\,\mathbf{l}^2 + 108)\Pi_1 + (36\,\mathbf{l}^2 + 153)\,\mathbf{l}\cdot\mathbf{s} + 15\,s_{12}(\mathbf{l}, \mathbf{l})] \tag{1.144}$$

$$[g_\Omega, \mathbf{l}^2\mathbf{l}\cdot\mathbf{s}]_- = i\vartheta(r)[-3\,\bar{s}_{12}(\mathbf{p}_\Omega, \mathbf{p}_\Omega) - \mathbf{l}^2\bar{s}_{12}(\mathbf{p}_\Omega, \mathbf{p}_\Omega)] \tag{1.145}$$

$$\begin{aligned}[g_\Omega, \mathbf{l}^2\bar{s}_{12}(\mathbf{p}_\Omega, \mathbf{p}_\Omega)]_- = i\vartheta(r)[&324\,\Pi_1 + 477\,\mathbf{l}\cdot\mathbf{s} + 600\,\mathbf{l}^2 + 51\,s_{12}(\mathbf{l}, \mathbf{l}) + 477\,\mathbf{l}^2\mathbf{l}\cdot\mathbf{s} \\ &+ 144\,\mathbf{l}^4 + 27\,\mathbf{l}^2 s_{12}(\mathbf{l}, \mathbf{l}) + 36\,\mathbf{l}^4\mathbf{l}\cdot\mathbf{s}]\end{aligned} \tag{1.146}$$

contribute. With the repeated application of the generator operators of higher order in angular momentum are generated. We will restrict our calculation to operators up to third power in

angular momentum, that means that we neglect the last three operators in Eq. (1.146). The considered operators define a vector space of finite dimension. The operator L_Ω can be represented in this basis by a matrix and the Baker-Hausdorff series can be evaluated explicitly by calculating the matrix exponential.

In the basis $\left\{\Pi_1, \mathbf{l}^2\Pi_1, \mathbf{l}\cdot\mathbf{s}, s_{12}(\hat{\mathbf{r}},\hat{\mathbf{r}}), s_{12}(\mathbf{l},\mathbf{l}), \bar{s}_{12}(\mathbf{p}_\Omega,\mathbf{p}_\Omega), \mathbf{l}^2\mathbf{l}\cdot\mathbf{s}, \mathbf{l}^2\bar{s}_{12}(\mathbf{p}_\Omega,\mathbf{p}_\Omega)\right\}$ we get

$$\mathsf{L}_\Omega = i\vartheta(r)\begin{pmatrix} 0 & 0 & 0 & -24 & 0 & 108 & 0 & 324 \\ 0 & 0 & 0 & 0 & 0 & 96 & 0 & 600 \\ 0 & 0 & 0 & -18 & 0 & 153 & 0 & 477 \\ 0 & 0 & 0 & 3 & 0 & 0 & 0 & 0 \\ 0 & 0 & 0 & 0 & 0 & 15 & 0 & 51 \\ 0 & 2 & -1 & 0 & 7 & 0 & -3 & 0 \\ 0 & 0 & 0 & 0 & 0 & 36 & 0 & 477 \\ 0 & 0 & 0 & 0 & 0 & 0 & -1 & 0 \end{pmatrix}. \tag{1.147}$$

Together with the contribution of the radial part of the kinetic energy we thus have an explicit expression for the correlated interaction.

The truncation of the operator basis is justified by looking at the binding energy obtained with the so calculated correlated interaction. With the restriction to the given basis going up to third order in angular momentum the deuteron energy is reproduced with an error of 0.005 MeV. Using the basis $\left\{\Pi_1, \mathbf{l}^2\Pi_1, \mathbf{l}\cdot\mathbf{s}, s_{12}(\hat{\mathbf{r}},\hat{\mathbf{r}}), s_{12}(\mathbf{l},\mathbf{l}), \bar{s}_{12}(\mathbf{p}_\Omega,\mathbf{p}_\Omega)\right\}$ the deuteron energy deviates by 0.05 MeV. It should be noted that in the deuteron with the $L = 0$ trial state the deviation is not caused by the explicit contributions of the neglected higher order operators but by the correlated central part of the interaction as the repeated application of L_Ω to higher-order operators gives also contributions to the central part of the interaction. Omitting the operators of higher order in angular momentum is justified also for heavier nuclei as the correlations and therefore also the correlated interaction parts with higher order in angular momentum are of short range whereas the relative wave function for large angular momenta is suppressed at short radii because of the centrifugal barrier. We could in principle enlarge the basis of the operator space but obviously the results will not change noticeable.

The effect of the central and tensor correlations on the central part of the interaction is shown in Fig. 1.39 for the $S, T = 1, 0$ channel of the Bonn-A interaction. We can see how the repulsive core of the local potential $v^c_{10}(r)$ has been tamed by the central correlations and the additional attraction generated by the tensor correlator. The increased attraction in the local part of the correlated interaction is accompanied by an increased repulsion in the momentum-dependent parts of the interaction. While the original $\mathbf{l}^2$ term $v^{l^2}_{10}(r)$ sets in around $r \approx 0.8$ fm the correlated $\mathbf{l}^2$ potential $\hat{v}^{l^2}_{10}(r)$ due to the long range tensor correlations reaches out to about $r \approx 2$ fm. The radial momentum part $\hat{v}^{p_r^2}_{10}(r)$ is also shifted further out.

In Fig. 1.40 the noncentral components of the Bonn-A interaction are shown. The tensor correlations do not only change the tensor component $\hat{v}^t_{10}(r)$ of the interaction but also the spin-orbit part $\hat{v}^b_{10}(r)$ of the interaction. In addition we get interaction components of higher order in angular momentum shown in the lower right part of Fig. 1.40. Interaction components of this operator structure are not present in the uncorrelated interaction.

The analysis of the interaction components in the r-representation is not very illustrative. The differences between correlated and uncorrelated interaction can be visualized better by comparing matrix elements. As the interactions will be used in shell model calculations matrix

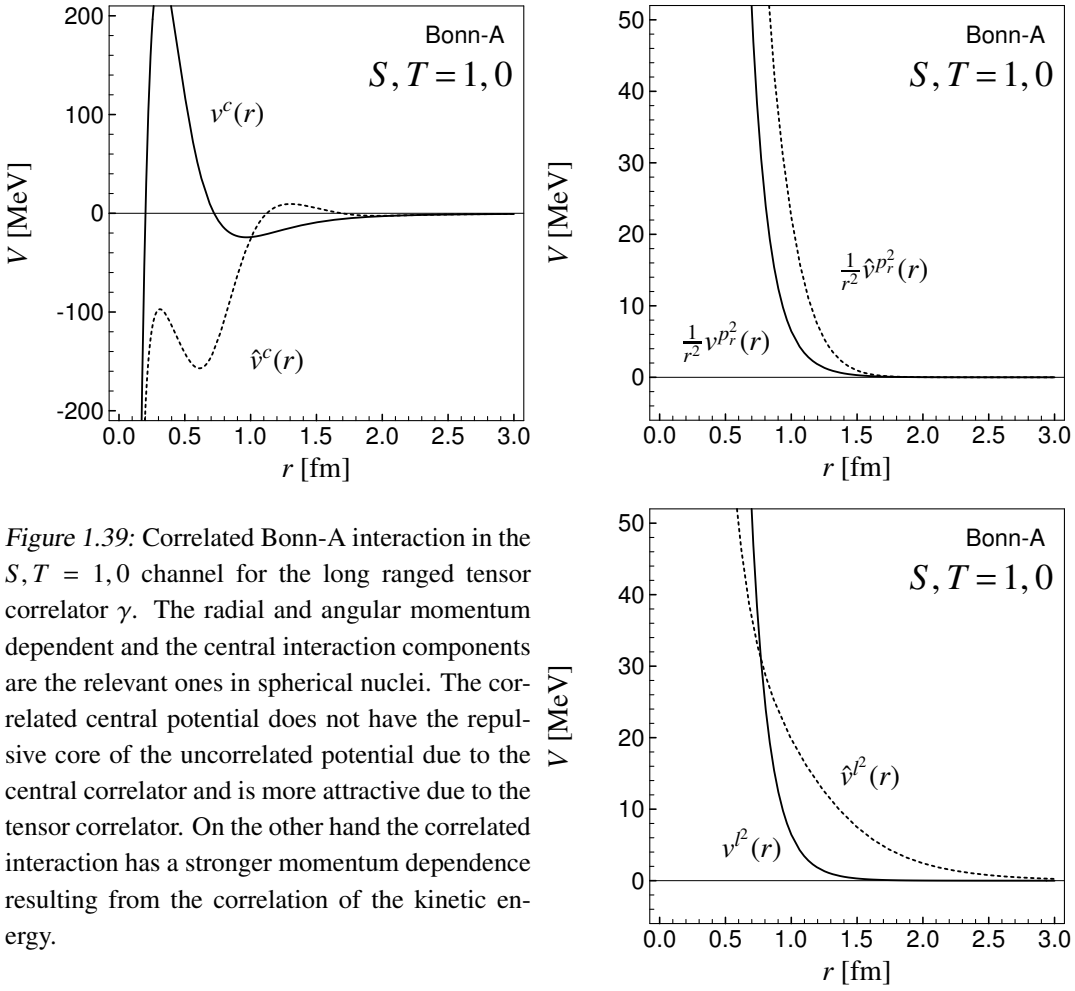

Figure 1.39: Correlated Bonn-A interaction in the $S,T = 1,0$ channel for the long ranged tensor correlator γ. The radial and angular momentum dependent and the central interaction components are the relevant ones in spherical nuclei. The correlated central potential does not have the repulsive core of the uncorrelated potential due to the central correlator and is more attractive due to the tensor correlator. On the other hand the correlated interaction has a stronger momentum dependence resulting from the correlation of the kinetic energy.

elements are calculated in relative harmonic oscillator states $\left|2a;n(LS)J\right\rangle$ for $n = 1$ and the lowest angular momenta in the respective channels as a function of the oscillator parameter a. The oscillator parameters of the doubly magic nuclei reproducing the empirical charge radii provide an orientation. To avoid too much redundancy only the results for the Bonn-A interaction will be shown. The Argonne V18 results differ only slightly.

Nucleus	^{4}He	^{16}O	^{40}Ca
a [fm^2]	1.74	3.06	3.77

The matrix elements for the central part of the uncorrelated and correlated Bonn-A interaction are shown in Fig. 1.41. In spherical nuclei the non-central components vanish in a shell model state and the binding energy is determined by the central part of the interaction alone.

In all channels one can observe the general trend of decreasing matrix elements with increasing relative angular momentum – the probability density of the higher angular momentum states is shifted to larger distances outside the range of the interaction.

In the odd channels the effect of the correlations is not as pronounced as in the even channels. The centrifugal barrier suppresses the probability to find two nucleons in the vicinity of the repulsive core and the effect of the central correlations is rather weak. In the strongly repulsive

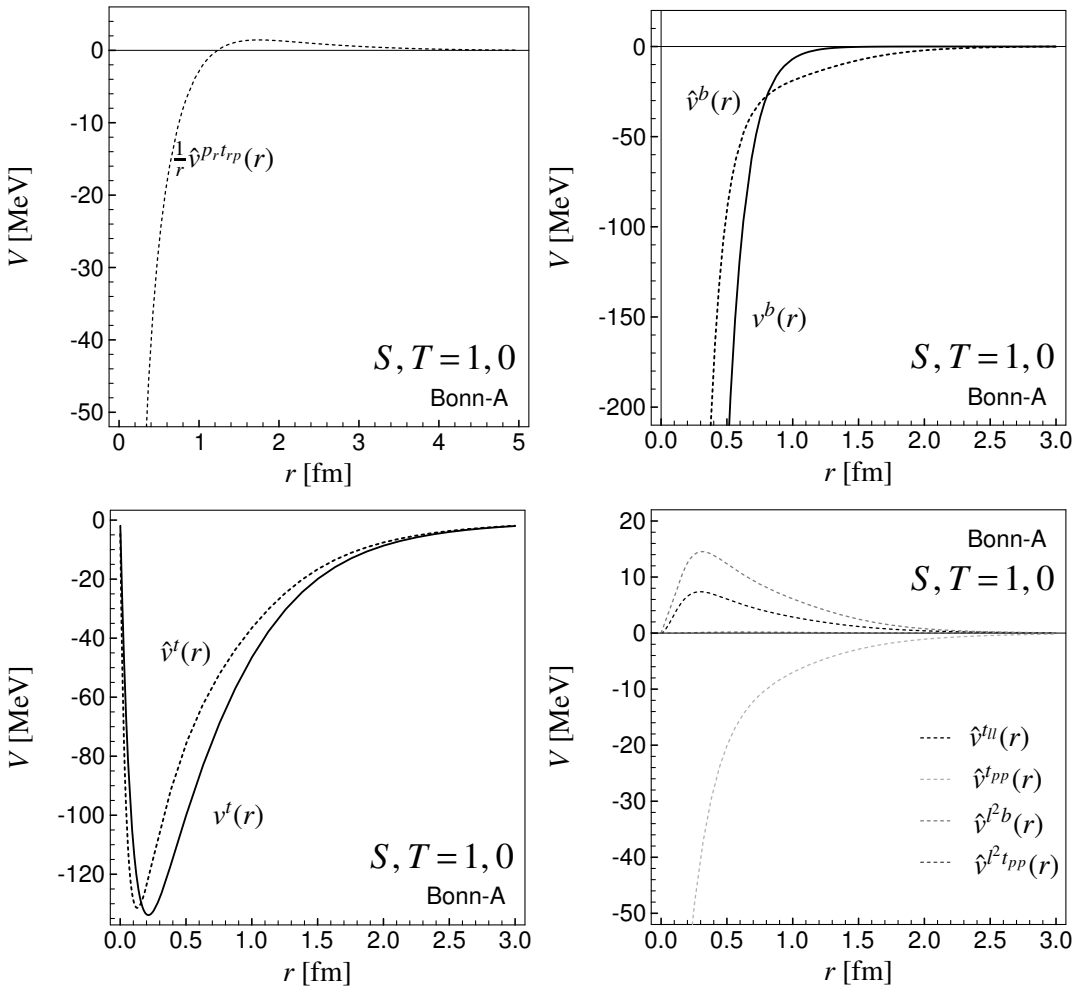

Figure 1.40: Non central components of the correlated Bonn-A interaction in the $S,T=1,0$ channel using the long-ranged correlator γ. Full lines denote the uncorrelated interaction, dotted lines the correlated interaction.

$S,T=0,0$ channel the effect of the correlator is almost not noticeable. In the $S,T=1,1$ channel the repulsive core is weaker to begin with and the tensor correlator provides additional attraction in this channel. The matrix elements in higher angular momentum states are nearly vanishing in this channel (not the change in the energy scale).

In the even channels the repulsive core of the uncorrelated interaction leads to strongly repulsive matrix elements at small oscillator parameters. The matrix elements of the correlated interaction are much more attractive. In the $S,T=0,1$ channel this is achieved by central correlations alone. For $L=0$ the effect is dramatic, for $L=2$ due to the centrifugal barrier it is rather small. In the $S,T=1,0$ channel the tensor correlator contributes strongly to the central part of the correlated interaction. In the $L=0$ case the difference between the different ranges of the tensor correlators appears on the scale of the matrix element. But on the scale of the net binding energy where we have big cancellations between kinetic and potential energy this seemingly small difference translates to the big differences seen in the calculations for ^{4}He, ^{16}O and ^{40}Ca. For $L=2$ the matrix elements for the different correlators differ significantly only

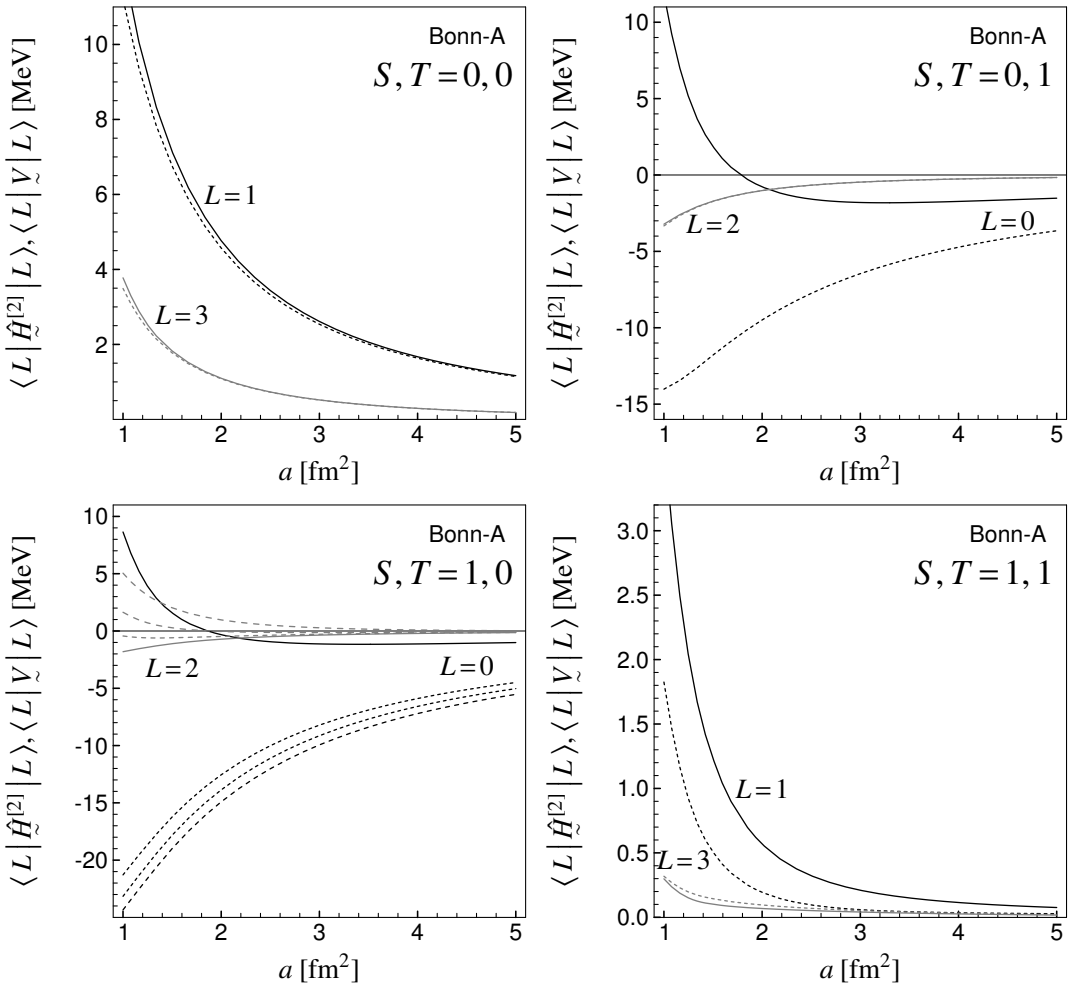

Figure 1.41: Expectation values of the central part of the uncorrelated (full lines) and the correlated (dashed lines) Bonn-A interaction in relative harmonic oscillator states. For $S,T=1,0$ the effects of the three tensor correlators α,β and γ are shown.

for small oscillator parameters. With increasing correlator range the matrix elements become more repulsive.

The non-central interaction components have diagonal and off-diagonal matrix elements. Diagonal matrix elements are shown in Fig. 1.42. The first non-vanishing matrix element is obtained for $L=2$ in the $S,T=1,0$ channel. The matrix elements using the short-ranged tensor correlator differ only slightly from the uncorrelated ones. With increasing correlation range and decreasing oscillator parameter the differences between the correlated and uncorrelated matrix elements become more pronounced. In the $S,T=1,1$ channel the effect of the tensor correlator is visible only in the channel of lowest angular momentum $L=1$.

The off-diagonal matrix elements are displayed in Fig. 1.43. Here we can see a strong effect of the tensor correlations. The rather large off-diagonal matrix elements between the $\big|\,1(01)1\,\rangle$ and $\big|\,1(21)1\,\rangle$ are reduced dramatically by the tensor correlator. The matrix elements are getting smaller with increasing range of the tensor correlator. This strength reduction of the off-diagonal matrix elements enlightens the operation of the tensor correlator once more –

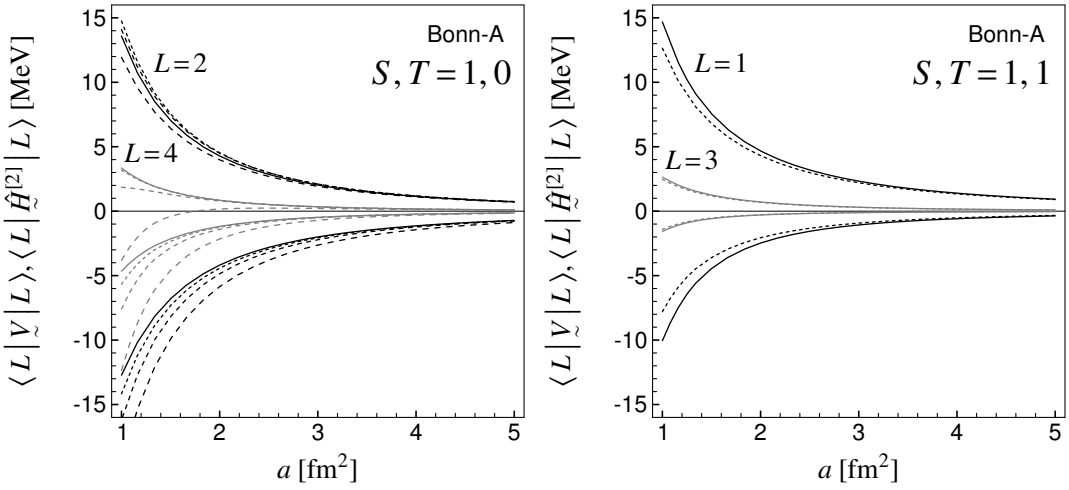

Figure 1.42: Diagonal matrix elements of the non-central two-body components of the uncorrelated (solid lines) and correlated Bonn-A interaction (dotted lines) in the $\big|\, 1(L1)J = L \,\big\rangle$ and the $\big|\, 1(L1)J = L+1 \,\big\rangle$ state. The matrix elements in the $\big|\, 1(L1)J = L-1 \,\big\rangle$ state are not shown to avoid to much clutter.

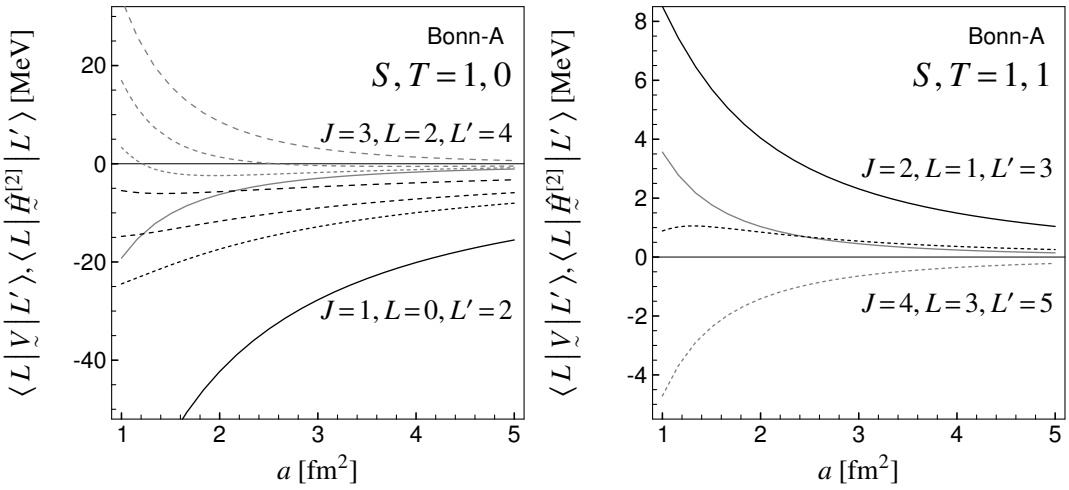

Figure 1.43: Off-diagonal matrix elements of the non-central two-body components of the uncorrelated (solid lines) and correlated (dotted lines) Bonn-A interaction between $\big|\, 1(J-1,1)J \,\big\rangle$ and $\big|\, 1(J+1,1)J \,\big\rangle$ states.

the tensor correlator "diagonalizes" the tensor interaction. Using the uncorrelated interaction the most important part of the deuteron binding energy comes from the off-diagonal matrix elements of the tensor interaction between the s- and the d-wave. In the correlated interaction the binding is achieved by the central part of the correlated interaction and we have no d-wave in the uncorrelated deuteron state. As we have to use tensor correlators of restricted range we cannot achieve a total vanishing of the off-matrix elements. In the $S,T=1,1$ channel we can see in principle the same behavior but the off-diagonal matrix elements are much weaker in this channel.

1.12 Momentum Space Representation of the Interaction

The effect of unitary correlations on the interaction can also be studied in the momentum space representation. To do this, correlated interaction and uncorrelated potential are evaluated in eigenstates of momentum and angular momentum

$$\langle kLM \left| \underset{\sim}{V} \right| k'L'M' \rangle = i^L i^{L'} m \int \mathrm{d}^3x \int \mathrm{d}^3x' \; Y^\star_{LM}(\hat{\mathbf{x}}) j_L(kx) \langle \mathbf{x} \left| \underset{\sim}{V} \right| \mathbf{x}' \rangle j_{L'}(k'x') Y_{L'M'}(\hat{\mathbf{x}}') \,, \tag{1.148}$$

$$\langle kLM \left| \hat{\underset{\sim}{H}}^{[2]} \right| k'L'M' \rangle = i^L i^{L'} m \int \mathrm{d}^3x \int \mathrm{d}^3x' \; Y^\star_{LM}(\hat{\mathbf{x}}) j_L(kx) \langle \mathbf{x} \left| \hat{\underset{\sim}{H}}^{[2]} \right| \mathbf{x}' \rangle j_{L'}(k'x') Y_{L'M'}(\hat{\mathbf{x}}') \,. \tag{1.149}$$

For the correlated interaction the potential consists of the two-body part of the correlated kinetic energy and the correlated potential.

The momentum space representation of the interaction in the $S, T = 0, 1$ and $L = 0$ state obtained in this manner is shown in Fig. 1.44 for the uncorrelated and correlated Bonn-A and Argonne V18 interaction. Although the uncorrelated interactions differ significantly, both, the diagonal and the off-diagonal matrix elements are almost indistinguishable for the correlated interaction.

We can compare our correlated potential to the V_{lowk} potential [BKS+01]. V_{lowk} is obtained by integrating out the high relative momentum modes in the sense of the renormalization group, while preserving the half-on-shell T-matrix and bound state properties of the bare potential. V_{lowk} has momentum components only lower than the cutoff.

In Fig. 1.45 the diagonal and off-diagonal matrix elements of V_{lowk} in the $S, T = 0, 1$ and $L = 0$ channel are shown for the Bonn-A and the Argonne V18 interaction as well as for the Paris potential and the chiral potential by Machleidt and Entem [EM01]. Obviously the matrix elements of the V_{lowk} compare favorably to our correlated interaction Fig. 1.44.

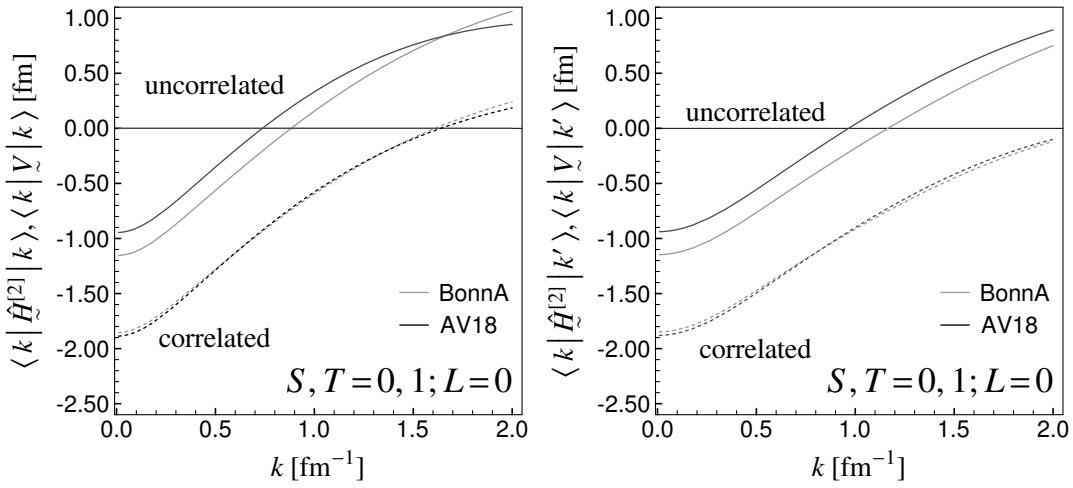

Figure 1.44: Correlated and uncorrelated Bonn-A and Argonne V18 interaction. Diagonal momentum space matrix elements in the $S, T = 0, 1$ channel (left) and off-diagonal matrix elements with $k' = 0.06\,\mathrm{fm}^{-1}$ (right). The correlated Bonn-A and Argonne V18 interactions are almost indistinguishable and more attractive than the uncorrelated interactions.

In Fig. 1.46 the diagonal matrix elements in the $S,T=1,0$ and $L=0$ channel are shown. As in the $S,T=0,1$ channel the matrix elements of the uncorrelated Bonn-A and Argonne V18 interaction are quite different. The application of the central correlation makes both interactions much more attractive but they still differ significantly. The additional application of tensor correlations leads to more attractive matrix elements. Here the stronger tensor correlations for the Argonne V18 interaction also give a much stronger effect in bringing the centrally correlated Argonne potential down to the fully correlated one. After full correlation the matrix elements of Bonn-A and Argonne V18 interaction are also in this channel almost identical. This is true for all three tensor correlators of different range.

In the $S,T=0,1$ channel the V_{lowk} potential is almost independent of the cutoff. In the $S,T=1,0$ channel this is no longer the case. In Fig. 1.47 the matrix element at $k=0$ is plotted as a function of the cutoff parameter Λ. In our correlator picture this cutoff dependence has to be translated into the dependence on the tensor correlator range.

Regarding the tensor correlations it is not possible to get a clear separation of scales between the tensor correlations and the medium to long range correlations in the many-body state. In the language of the V_{lowk} potential this problem is revealed by the fact that the potential is not independent of the cutoff Λ. In the UCOM approach we have to deal with the determination of the tensor correlation range that is not unique. Comparing the UCOM and V_{lowk} results, the tensor correlators α, β and γ correspond to cut-offs Λ of about $1.7\,\mathrm{fm}^{-1}$, $1.45\,\mathrm{fm}^{-1}$ and $1.2\,\mathrm{fm}^{-1}$.

The fact that the correlated interactions are almost identical in the low momentum regime shows that the detailed structure of the interaction at short distances is not important for the low energy region. With the unitary correlation operator we have a method at hand to extract the important low energy behavior. It is in this sense an alternative to the V_{lowk} approach which uses renormalization group techniques to derive the low-momentum potential.

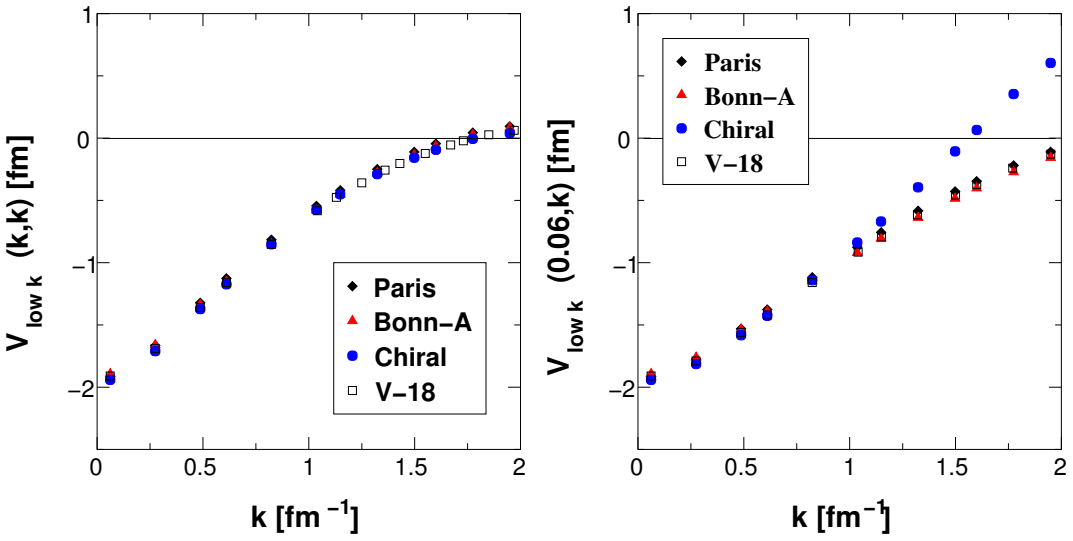

Figure 1.45: Diagonal elements of V_{lowk} in the $S,T=0,1$ channel for different potentials (left) and off-diagonal elements of V_{lowk} (right). Figure from [BKS+01].

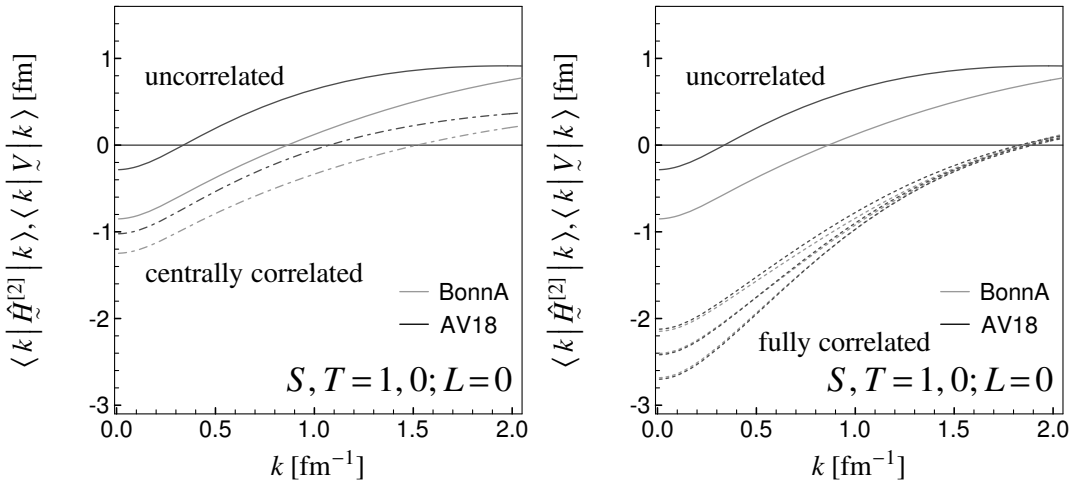

Figure 1.46: Correlated (dashed) and uncorrelated (solid) Bonn-A and Argonne V18 interaction diagonal momentum space matrix elements in the $S, T = 1, 0$ channel. On the left hand side only central correlations are used. On the right hand side the results using central and tensor correlations are displayed. The three dotted curves show the results with the three tensor correlators α, β and γ of differing range.

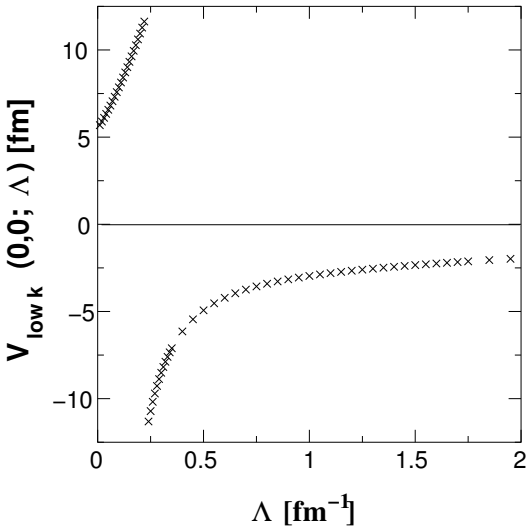

Figure 1.47: Zero momentum matrix element of the V_{lowk} potential in the $S, T = 1, 0$ channel as a function of the cutoff parameter Λ. The matrix element depends on the cutoff in a similar way as it depends in the UCOM approach on the range of the tensor correlator. Figure from [BKS+01].

Chapter 2

Fermionic Molecular Dynamics

Fermionic Molecular Dynamics (FMD) has been developed to describe heavy ion reactions in the low to medium energy regime (below the particle production threshold). As essential ingredient it uses antisymmetrized many-body states $\left| Q(t) \right\rangle$ to account for the fermionic nature of the nucleons. The single-particle states are of Gaussian shape in coordinate space. They are localized in phase space with a mean position, a mean momentum, and a complex width. The spin and isospin degrees of freedom are represented by two-component spinors. The equations of motion for the parameters of the single-particle states are derived from the time dependent variational principle [KS82]

$$\delta S = \delta \int_{t_1}^{t_2} dt \, \frac{\left\langle Q(t) \right| i\frac{d}{dt} - \underset{\sim}{H} \left| Q(t) \right\rangle}{\left\langle Q(t) \middle| Q(t) \right\rangle} = 0 \, . \tag{2.1}$$

The flexibility of the single-particle basis is not only essential for the description of dynamical situations like in heavy ion reactions but it also provides great advantages in nuclear structure studies where deformations or radial distributions quite different from those of harmonic oscillator states are important. Nonetheless harmonic oscillator eigenstates with good angular momentum quantum numbers can also be represented by linear combinations of Gaussians. It is easy to show that a linear superposition of Gaussians that are infinitesimally displaced in phase space are identical to eigenstates of the harmonic oscillator [Kra01]. For numerical purposes finite displacements that are still small compared to the widths work as well.

The ability of Gaussians to reproduce the harmonic oscillator wave functions is utilized in FMD calculations of doubly magic nuclei. Performing a variation of the parameters of all Gaussians the minimum of the energy is achieved for the harmonic oscillator shell model states in case of ^{4}He, ^{16}O and ^{40}Ca. These doubly magic nuclei therefore provide a link between the many-body calculations performed with the harmonic oscillator states in section 1.10 and the FMD calculations.

2.1 The FMD Model

We give here only a short summary of the FMD model. A detailed description is given in [FS97, FS00], technical details are given in [Nef98].

2.1.1 Single-Particle States

The single-particle states are described in coordinate space by a Gaussian. The Gaussians $\big|\, q \,\big\rangle = \big|\, a, \mathbf{b} \,\big\rangle$ are parameterized by the complex width a and the complex vector $\mathbf{b}$

$$\big\langle\, \mathbf{x} \,\big|\, a, \mathbf{b} \,\big\rangle = \exp\!\left\{-\frac{(\mathbf{x}-\mathbf{b})^2}{2a}\right\}, \tag{2.2}$$

where $\mathbf{b} = \mathbf{r} + ia\mathbf{p}$ is a combination of the real parameters for the mean position $\mathbf{r}$ and mean momentum $\mathbf{p}$

$$\mathbf{r} = \frac{\big\langle\, a, \mathbf{b} \,\big|\, \underset{\sim}{\mathbf{x}} \,\big|\, a, \mathbf{b} \,\big\rangle}{\big\langle\, a, \mathbf{b} \,\big|\, a, \mathbf{b} \,\big\rangle}, \qquad \mathbf{p} = \frac{\big\langle\, a, \mathbf{b} \,\big|\, \underset{\sim}{\mathbf{k}} \,\big|\, a, \mathbf{b} \,\big\rangle}{\big\langle\, a, \mathbf{b} \,\big|\, a, \mathbf{b} \,\big\rangle}\,. \tag{2.3}$$

The variances in coordinate and momentum space are determined by the real and imaginary parts of the width

$$\frac{3}{2}\frac{|a|^2}{\mathrm{Re}\{a\}} = \frac{\big\langle\, a, \mathbf{b} \,\big|\, (\underset{\sim}{\mathbf{x}}-\mathbf{r})^2 \,\big|\, a, \mathbf{b} \,\big\rangle}{\big\langle\, a, \mathbf{b} \,\big|\, a, \mathbf{b} \,\big\rangle}\,, \qquad \frac{3}{2}\frac{1}{\mathrm{Re}\{a\}} = \frac{\big\langle\, a, \mathbf{b} \,\big|\, (\underset{\sim}{\mathbf{k}}-\mathbf{p})^2 \,\big|\, a, \mathbf{b} \,\big\rangle}{\big\langle\, a, \mathbf{b} \,\big|\, a, \mathbf{b} \,\big\rangle} \tag{2.4}$$

The spin can be parametrized either by the three-component along the z-axis (sufficient for spin-saturated many-body states with $S = 0$) or by a full spinor for which the spin can posses arbitrary directions. The isospin is given by its three-component, fixing the nucleon to be either proton or neutron

$$\big|\, q_k \,\big\rangle = \big|\, a_k, \mathbf{b}_k \,\big\rangle \otimes \big|\, \chi_k \,\big\rangle \otimes \big|\, \xi_k \,\big\rangle\,, \tag{2.5}$$

$$\big|\, q_k \,\big\rangle = \big|\, a_k, \mathbf{b}_k \,\big\rangle \otimes \big|\, \chi_k^{\uparrow}, \chi_k^{\downarrow} \,\big\rangle \otimes \big|\, \xi_k \,\big\rangle\,. \tag{2.6}$$

For nuclear structure calculations we also use single-particle states that are superpositions of Gaussians

$$\big|\, q_k \,\big\rangle = \sum_j c_{k,j} \left(\big|\, a_{k,j}, \mathbf{b}_{k,j} \,\big\rangle \otimes \big|\, \chi_{k,j}^{\uparrow}, \chi_{k,j}^{\downarrow} \,\big\rangle \otimes \big|\, \xi_k \,\big\rangle \right). \tag{2.7}$$

This increased flexibility in the single-particle state leads to an improved description. This is particularly important for halo nuclei with their exponentially decreasing neutron density.

2.1.2 Many-Body States

An uncorrelated many-body state is given by a Slater determinant of single-particle states

$$\big|\, Q \,\big\rangle = \underset{\sim}{\mathcal{A}}\big(\big|\, q_1 \,\big\rangle \otimes \ldots \otimes \big|\, q_A \,\big\rangle\big)\,. \tag{2.8}$$

We can formally define correlated many-body states

$$\big|\, \hat{Q} \,\big\rangle = \underset{\sim}{C}_{\Omega}\underset{\sim}{C}_{r}\big|\, Q \,\big\rangle\,, \tag{2.9}$$

but technically we will always evaluate correlated operators (in two-body approximation) in uncorrelated many-body states

$$\frac{\big\langle\, \hat{Q} \,\big|\, \underset{\sim}{A} \,\big|\, \hat{Q} \,\big\rangle}{\big\langle\, \hat{Q} \,\big|\, \hat{Q} \,\big\rangle} \overset{C2}{=} \frac{\big\langle\, Q \,\big|\, [\underset{\sim}{C}_r^{\dagger}\underset{\sim}{C}_{\Omega}^{\dagger}\underset{\sim}{A}\underset{\sim}{C}_{\Omega}\underset{\sim}{C}_r]^{C2} \,\big|\, Q \,\big\rangle}{\big\langle\, Q \,\big|\, Q \,\big\rangle}\,. \tag{2.10}$$

2.1.3 Matrix Elements

As our single-particle states do not form an orthogonal basis the evaluation of matrix elements has to account for this non-orthogonality. We define the single-particle overlap matrix

$$\mathsf{n}_{kl} = \langle\, q_k \,|\, q_l \,\rangle \tag{2.11}$$

and its inverse

$$\mathsf{o} = \mathsf{n}^{-1} \,. \tag{2.12}$$

With the help of the inverse overlap matrix expectation values of one-body operators

$$\frac{\langle\, Q \,|\, \underset{\sim}{B}^{[1]} \,|\, Q \,\rangle}{\langle\, Q \,|\, Q \,\rangle} = \sum_{kl} \langle\, q_k \,|\, \underset{\sim}{b}^{[1]} \,|\, q_l \,\rangle \mathsf{o}_{lk} \,, \tag{2.13}$$

and two-body operators

$$\begin{aligned} \frac{\langle\, Q \,|\, \underset{\sim}{B}^{[2]} \,|\, Q \,\rangle}{\langle\, Q \,|\, Q \,\rangle} &= \frac{1}{2} \sum_{klmn} {}_a\langle\, q_k, q_l \,|\, \underset{\sim}{b}^{[2]} \,|\, q_m, q_n \,\rangle_a \, \mathsf{o}_{mk} \mathsf{o}_{nl} \\ &= \frac{1}{2} \sum_{klmn} \langle\, q_k, q_l \,|\, \underset{\sim}{b}^{[2]} \,|\, q_m, q_n \,\rangle (\mathsf{o}_{mk} \mathsf{o}_{nl} - \mathsf{o}_{nk} \mathsf{o}_{ml}) \end{aligned} \tag{2.14}$$

can be calculated. Because of the non-orthogonality the computational effort of FMD calculations scales with the number of Gaussians per single-particle state n_g and the particle number A as

$$\text{computational effort} \propto n_g^4 \times A^4 \,. \tag{2.15}$$

2.1.4 Interaction

The matrix elements of the single-particle overlap in coordinate space

$$R_{kl} = \langle\, a_k, \mathbf{b}_k \,|\, a_l, \mathbf{b}_l \,\rangle = (2\pi\alpha_{kl})^{3/2} \exp\!\left\{ \frac{\boldsymbol{\pi}_{kl}^2}{2\lambda_{kl}} \right\} , \tag{2.16}$$

and the one-body part of the correlated kinetic energy (the same as the uncorrelated kinetic energy) can be calculated analytically

$$\langle\, a_k, \mathbf{b}_k \,|\, \underset{\sim}{t} \,|\, a_l, \mathbf{b}_l \,\rangle = \frac{1}{2m} (3\lambda_{kl} + \boldsymbol{\pi}_{kl}^2) R_{kl} \,, \tag{2.17}$$

where we use the abbreviations

$$\lambda_{kl} = \frac{1}{a_k^\star + a_l} \,, \qquad \alpha_{kl} = \frac{a_k^\star a_l}{a_k^\star + a_l} = \lambda_{kl} \, a_k^\star a_l \,, \tag{2.18}$$

$$\boldsymbol{\pi}_{kl} = i \frac{\mathbf{b}_k{}^\star - \mathbf{b}_l}{a_k^\star + a_l} = i \, \lambda_{kl} (\mathbf{b}_k{}^\star - \mathbf{b}_l) \,, \tag{2.19}$$

$$\boldsymbol{\rho}_{kl} = \frac{a_l \mathbf{b}_k{}^\star + a_k^\star \mathbf{b}_l}{a_k^\star + a_l} = \lambda_{kl} (a_l \mathbf{b}_k{}^\star + a_k^\star \mathbf{b}_l) \,. \tag{2.20}$$

The radial dependencies of the correlated interaction are expressed to arbitrary accuracy by sums of Gaussians. In the case of a central potential we have

$$\underset{\sim}{v}^c \overset{\mathbf{r}}{\Rightarrow} \sum_i \gamma_i \exp\{-\frac{r^2}{2\kappa_i}\} \,. \tag{2.21}$$

This allows us to evaluate the matrix elements analytically. We obtain

$$\begin{aligned} v^c_{klmn} &= \langle\, a_k\mathbf{b}_k, a_l\mathbf{b}_l \,\big|\, \underset{\sim}{v}^c \,\big|\, a_m\mathbf{b}_m, a_n\mathbf{b}_n \,\rangle = \\ &= \sum_i \gamma_i (2\pi)^3 \,(\alpha_{km}\alpha_{ln})^{3/2} \Big(\frac{\kappa_i}{\alpha_{klmn}+\kappa_i}\Big)^{3/2} \exp\Big\{-\frac{\boldsymbol{\rho}^2_{klmn}}{2(\alpha_{klmn}+\kappa_i)} + \frac{1}{2}\Big(\frac{\boldsymbol{\pi}^2_{km}}{\lambda_{km}} + \frac{\boldsymbol{\pi}^2_{ln}}{\lambda_{ln}}\Big)\Big\} \\ &= \sum_i \gamma_i R_{km} R_{ln} \Big(\frac{\kappa_i}{\alpha_{klmn}+\kappa_i}\Big)^{3/2} \exp\Big\{-\frac{\boldsymbol{\rho}^2_{klmn}}{2(\alpha_{klmn}+\kappa_i)}\Big\} \end{aligned} \tag{2.22}$$

with

$$\alpha_{klmn} = \alpha_{km} + \alpha_{ln} \,, \qquad \boldsymbol{\rho}_{klmn} = \boldsymbol{\rho}_{km} - \boldsymbol{\rho}_{ln} \,, \qquad \boldsymbol{\pi}_{klmn} = \tfrac{1}{2}(\boldsymbol{\pi}_{km} - \boldsymbol{\pi}_{ln}) \,. \tag{2.23}$$

Here we can interpret $\boldsymbol{\rho}_{klmn}$ as the distance between the nucleons and $\boldsymbol{\pi}_{klmn}$ as the relative momentum of the nucleons (in the sense of a matrix element and not of an expectation value) and α_{klmn} can be interpreted as the width of the Gaussian in the relative coordinate.

As an illustration of a spin dependent interaction we show the spin-orbit interaction which is represented as

$$\underset{\sim}{v}^b \overset{\mathbf{r}}{\Rightarrow} \sum_i \gamma_i \exp\{-\frac{r^2}{2\kappa_i}\}(\mathbf{r}\times\mathbf{p})\cdot\mathbf{S} \,. \tag{2.24}$$

The matrix element then becomes

$$\begin{aligned} v^b_{klmn} &= \langle\, a_k\mathbf{b}_k\chi_k, a_l\mathbf{b}_l\chi_l \,\big|\, \underset{\sim}{v}^b \,\big|\, a_m\mathbf{b}_m\chi_m, a_n\mathbf{b}_n\chi_n \,\rangle \\ &= R_{km}R_{ln}(\boldsymbol{\rho}_{klmn}\times\boldsymbol{\pi}_{klmn})\cdot\mathbf{S}_{klmn} \sum_i \gamma_i \Big(\frac{\kappa_i}{\alpha_{klmn}+\kappa_i}\Big)^{5/2} \exp\Big\{-\frac{\boldsymbol{\rho}^2_{klmn}}{2(\alpha_{klmn}+\kappa_i)}\Big\} \end{aligned} \tag{2.25}$$

with the matrix element $\mathbf{S}_{klmn}$ of the spin operator.

The derivation of the above matrix elements and the matrix elements of the other interaction components are given in detail in [Nef98]. We only want to demonstrate that we express all matrix elements by analytical expressions and do not need to evaluate numerical integrals.

2.2 Nuclear Chart in FMD

The correlated Bonn-A interaction with the long ranged tensor correlator γ has been used within the FMD model to calculate ground state properties of nuclei up to ^{48}Ca. Here the following simplifications of the correlated interaction have been used:

- The interaction components $\mathbf{l}^2\mathbf{l}\cdot\mathbf{s}$ are projected onto the $\mathbf{l}\cdot\mathbf{s}$ components as follows

$$v^{l^2ls}(r)\,\mathbf{l}^2\mathbf{l}\cdot\mathbf{s} \longrightarrow \begin{cases} 6\,v^{l^2ls}(r)\,\mathbf{l}\cdot\mathbf{s} & S,T=1,0 \\ 2\,v^{l^2ls}(r)\,\mathbf{l}\cdot\mathbf{s} & S,T=1,1 \,, \end{cases} \tag{2.26}$$

  so that original and projected interaction are identical in the lowest contributing L channels.

- Interaction components which are of rank 2 are not taken into account. In the single Slater determinants of the FMD they give no contribution anyway.

In Fig. 2.1 the results of our FMD calculations are summarized. Shown is the deviation of the binding energy per nucleon from the experimental results. For the big chart the FMD code with a single Gaussian per single-particle state has been used. The lighter nuclei have been calculated also with two Gaussians per single-particle state.

The best agreement between FMD and experimental binding energies is achieved for the doubly magic nuclei ^{4}He, ^{16}O and ^{40}Ca. Here the FMD states are indeed identical to the harmonic oscillator shell model states. They are visualized in Fig. 2.2.

We can also observe that the FMD results underestimate the binding energies more and more with increasing distance from the shell closures. The deviations are larger and less systematic in case of the *p*-shell nuclei than in case of the *sd*-shell nuclei. Their description can be improved by using two Gaussians per single-particle state, whereas the doubly magic nuclei ^{4}He and ^{16}O show no change in binding energy by the extended single-particle basis.

The nuclei away from the shell closures exhibit intrinsically deformed ground states and often a pronounced cluster structure. Some examples are shown in Fig. 2.3. These nuclei do not have good angular momentum quantum numbers in the FMD description and should be projected to obtain the physical ground state. The energy of the intrinsically deformed states E_{deformed} is higher than the energy E_J of the angular momentum projected state. For this reason we cannot expect that we can describe the intrinsically deformed nuclei with a single Slater determinant as well as the spherical nuclei.

As discussed in section 1.10 the radii obtained with the correlated Bonn-A interaction are significantly smaller than the experimental results.

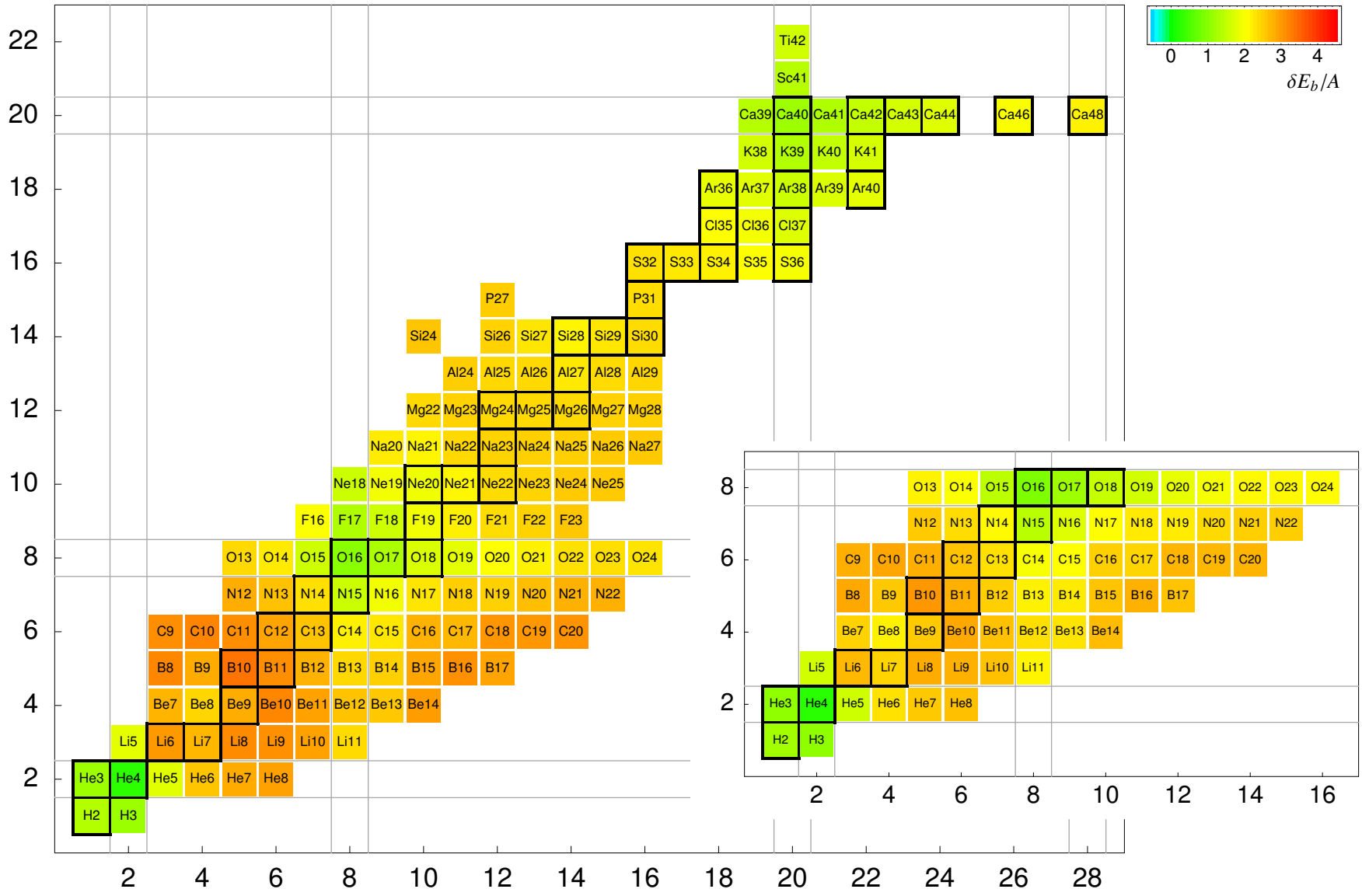

Figure 2.1: The nuclear chart calculated with the FMD model and the correlated Bonn-A interaction (using γ correlator). The color coding shows the deviation of the FMD binding energy from the experimental binding energy. The lighter nuclei calculated with the FMD model using two Gaussians per single-particle states give improved energies.

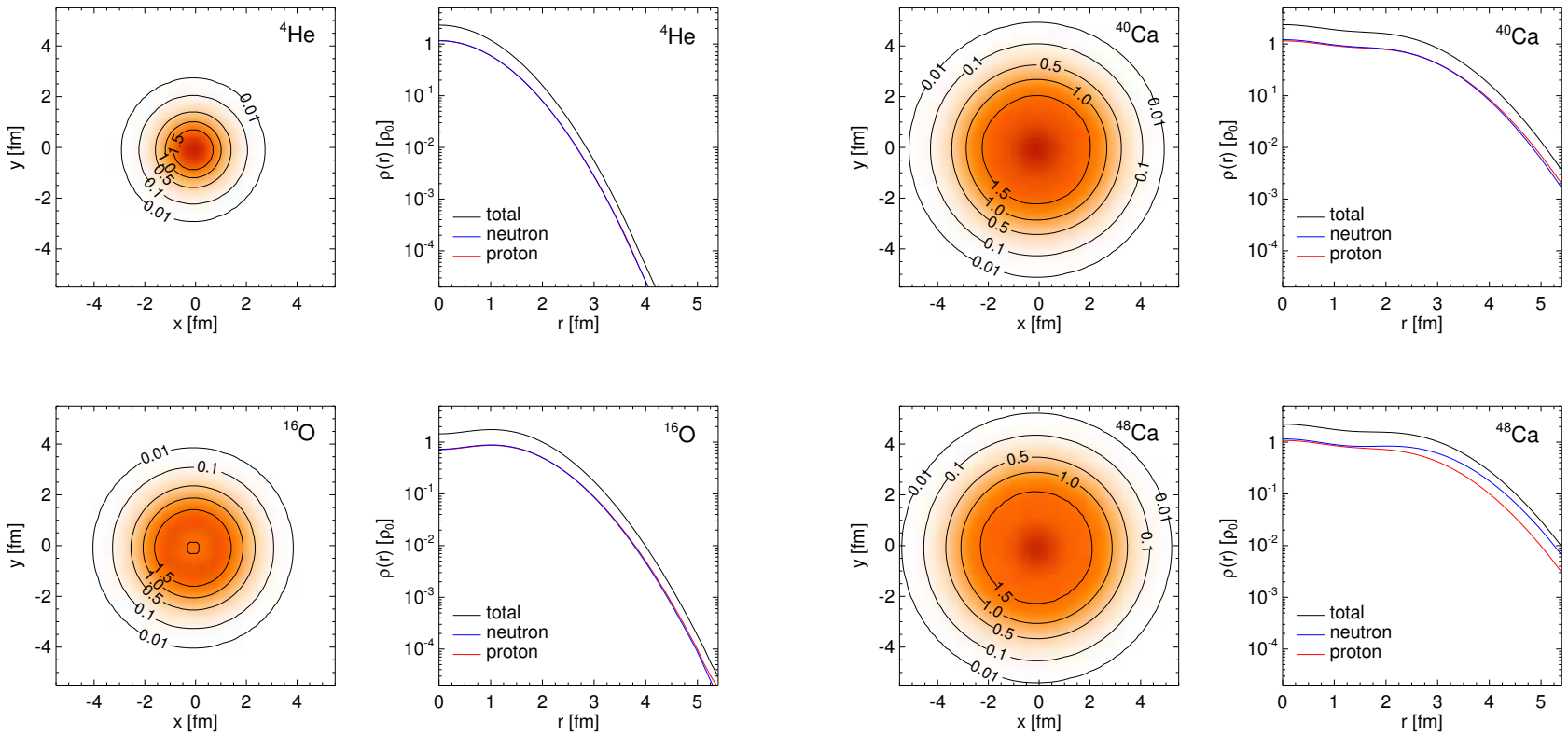

Figure 2.2: FMD ground states calculated with the correlated Bonn-A interaction. Shown are nucleon density cuts through the nuclei and radial density distributions in units of the nuclear matter density $\rho_0 = 0.17\,\mathrm{fm}^{-3}$.

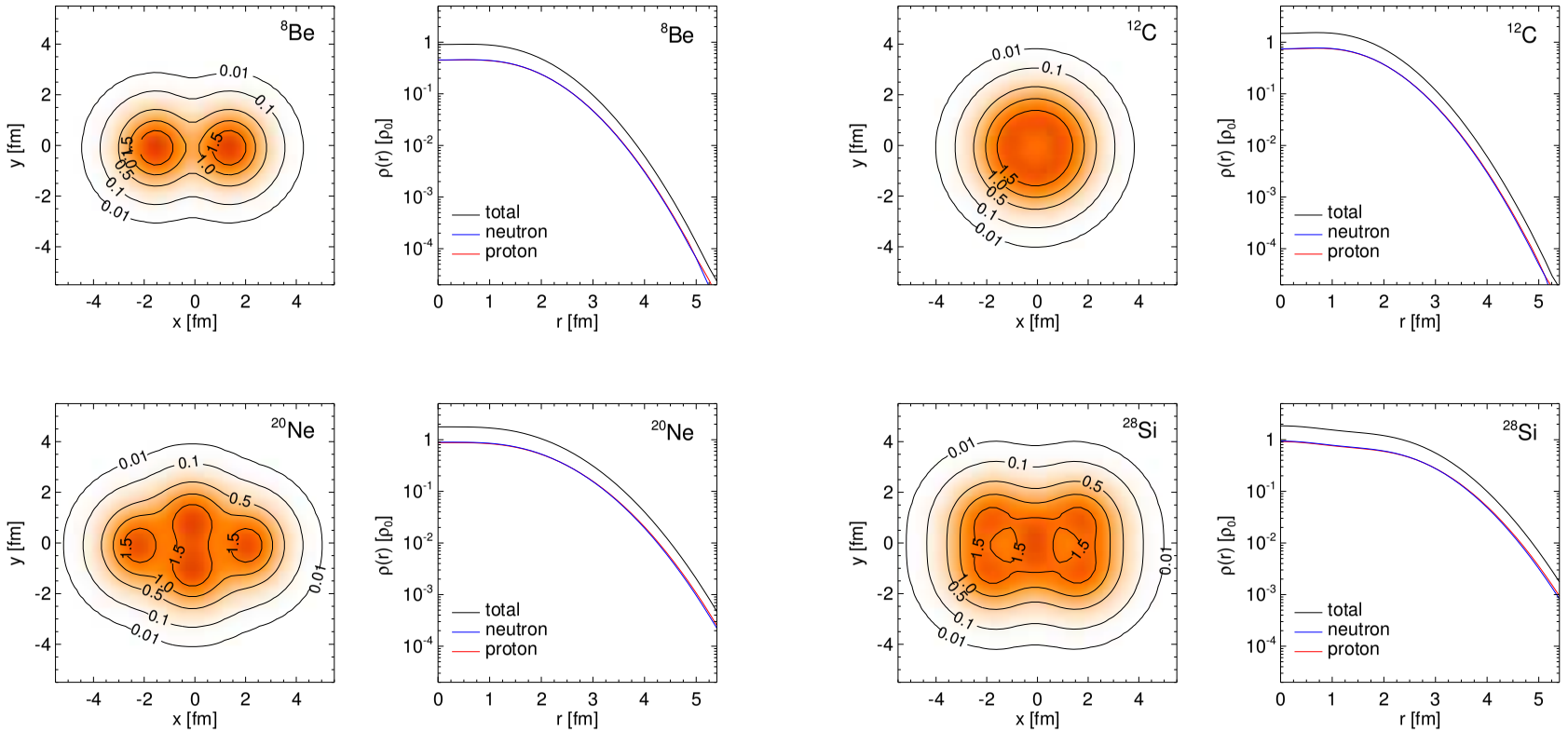

Figure 2.3: FMD ground states calculated with the correlated Bonn-A interaction. Shown are nucleon density cuts through the nuclei and radial density distributions in units of the nuclear matter density $\rho_0 = 0.17\,\mathrm{fm}^{-3}$.

	E_B^{FMD}	E_B^{Exp}	E_B^{FMD}/A	E_B^{Exp}/A	$\delta E_B/A$	r_{cms}^{FMD}	r_{cms}^{Exp}
H2	0.52	-2.23	0.26	-1.11	1.37	1.73	2.10
H3	-4.95	-8.48	-1.65	-2.83	1.18	1.66	1.68
He3	-4.14	-7.72	-1.38	-2.57	1.19	1.70	1.88
He4	-27.23	-28.30	-6.81	-7.07	0.27	1.60	1.68
Li6	-15.51	-32.00	-2.59	-5.33	2.75	1.98	2.57
Li7	-20.14	-39.24	-2.88	-5.61	2.73	2.10	2.41
Be9	-32.86	-58.16	-3.65	-6.46	2.81	2.24	2.51
B10	-34.72	-64.75	-3.47	-6.48	3.00	2.23	2.45
B11	-44.51	-76.20	-4.05	-6.93	2.88	2.20	2.42
C12	-59.42	-92.16	-4.95	-7.68	2.73	2.23	2.47
C13	-65.66	-97.11	-5.05	-7.47	2.42	2.22	2.44
C14	-78.02	-105.28	-5.57	-7.52	1.95	2.22	2.56
N14	-78.48	-104.66	-5.61	-7.48	1.87	2.26	2.54
N15	-94.32	-115.49	-6.29	-7.70	1.41	2.27	2.61
O16	-111.33	-127.62	-6.96	-7.98	1.02	2.31	2.73
O17	-109.71	-131.76	-6.45	-7.75	1.30	2.32	2.66
O18	-109.85	-139.81	-6.10	-7.77	1.66	2.33	2.73
F19	-108.78	-147.80	-5.73	-7.78	2.05	2.53	2.90
Ne20	-122.38	-160.65	-6.12	-8.03	1.91	2.57	3.01
Ne22	-127.96	-177.78	-5.82	-8.08	2.26	2.56	2.97
Na23	-132.83	-186.57	-5.78	-8.11	2.34	2.62	2.94
Mg24	-141.81	-198.26	-5.91	-8.26	2.35	2.69	3.08
Mg25	-147.36	-205.58	-5.89	-8.22	2.33	2.69	3.11
Mg26	-155.96	-216.68	-6.00	-8.33	2.34	2.70	3.06
Al27	-165.84	-224.95	-6.14	-8.33	2.19	2.78	3.04
Si28	-176.69	-236.54	-6.31	-8.45	2.14	2.85	3.09
Si29	-179.84	-245.02	-6.20	-8.45	2.25	2.83	3.08
Si30	-184.38	-255.63	-6.15	-8.52	2.37	2.83	3.18
P31	-186.95	-262.92	-6.03	-8.48	2.45	2.86	3.19
S32	-198.74	-271.78	-6.21	-8.49	2.28	2.84	3.24
S34	-220.10	-291.85	-6.47	-8.58	2.11	2.83	3.28
S36	-246.04	-308.72	-6.83	-8.58	1.74	2.84	3.28
Cl35	-229.65	-298.22	-6.56	-8.52	1.96	2.86	3.39
Cl37	-258.06	-317.11	-6.97	-8.57	1.60	2.86	3.38
Ar36	-238.64	-306.72	-6.63	-8.52	1.89	2.88	3.33
Ar40	-266.99	-343.82	-6.67	-8.60	1.92	2.92	3.43
K39	-282.20	-333.74	-7.24	-8.56	1.32	2.92	3.40
K41	-282.45	-351.62	-6.89	-8.58	1.69	2.95	3.42
Ca40	-294.73	-342.05	-7.37	-8.55	1.18	2.94	3.45
Ca48	-325.57	-416.00	-6.78	-8.67	1.88	3.03	3.45

Table 2.1: Groundstate binding energies and charge radii. FMD calculations and experimental values.

Appendix A

Notation

In this work we use the following notational conventions:

Vectors

Vectors in three-dimensional space are denoted in bold face, e.g. $\mathbf{r}$ and $\underset{\sim}{\mathbf{p}}_\Omega$ (a vector valued operator).

Labeling of one- and two-body states

A one-body state is usually labeled

$$\left| a; \chi\xi \right\rangle$$

with the wave function $\left\langle \mathbf{x} \middle| a \right\rangle$, the three-component of the spin χ and the isospin three-component ξ.

A two-body state can be labeled as

$$\left| \alpha; S\,M_S, T\,M_T \right\rangle$$

with the wave function $\left\langle \mathbf{r} \middle| \alpha \right\rangle$ in the relative coordinate $\mathbf{r}$ and total spin S, three-component of the spin M_S, total isospin T and isospin three-component M_T. For reasons of convenience the isospin part of the state may be omitted.

In many applications it is advantageous to use a two-body basis where orbital angular momentum L and total spin S of the nucleons are coupled to the total angular momentum J

$$\left| \alpha; (LS)JM, T M_T \right\rangle .$$

Operators

Operators in Hilbert space are denoted by an underlining wiggle. We conventionally use uppercase letters for operators in Fock space and lowercase letters for operators in one- or two-body space.

For example the Hamilton operator in Fock space is noted as $\underset{\sim}{H}$, the correlated Hamilton operator in Fock space as $\underset{\sim}{\hat{H}}$, the kinetic energy operator in one-body space $\underset{\sim}{t}$ and the potential energy operator in two-body space $\underset{\sim}{v}$.

In formal reasoning the particle-order of the operator is denoted explicitly, e.g. the irreducible three-body part of the correlated Hamilton operator is written as $\underset{\sim}{\hat{H}}^{[3]}$.

Coordinate Representation of Operators

Because of the radial dependence of the central and tensor correlation functions it is often more convenient to use the coordinate representation of operators. The fact that an operator is given in the coordinate space representation is denoted by the symbol $\overset{\mathbf{r}}{\Rightarrow}$, e.g.

$$\underset{\sim}{\mathbf{p}}_r \overset{\mathbf{r}}{\Rightarrow} \mathbf{p}_r \equiv \frac{\mathbf{r}}{r}\frac{1}{i}\left(\frac{1}{r}+\frac{\partial}{\partial r}\right)$$

and

$$\underset{\sim}{v}^{ls} \overset{\mathbf{r}}{\Rightarrow} v^{ls}(r)\,\mathbf{l}\cdot\mathbf{s}\ .$$

This has to be understood in the following sense

$$\langle\,\mathbf{r}\,|\,\underset{\sim}{\mathbf{p}}_r\,|\,\phi\,\rangle = \mathbf{p}_r\langle\,\mathbf{r}\,|\,\phi\,\rangle = \frac{\mathbf{r}}{r}\frac{1}{i}\left(\frac{1}{r}+\frac{\partial}{\partial r}\right)\phi(\mathbf{r})\ ,$$

and

$$\begin{aligned}\langle\,\mathbf{r}\chi\,|\,\underset{\sim}{v}^{ls}\,|\,\alpha;(ls)jm\,\rangle &= v^{ls}(r)\,\mathbf{l}\cdot\mathbf{s}\,\langle\,\mathbf{r}\chi\,|\,\alpha;(ls)jm\,\rangle \\ &= v^{ls}(r)\,R_\alpha(r)\sum_{m_l,m_s}\mathrm{C}\begin{pmatrix} l & s & j\\ m_l & m_s & m\end{pmatrix}\langle\,\hat{\mathbf{r}}\,|\,\underset{\sim}{\mathbf{l}}\,|\,l,m_l\,\rangle\cdot\langle\,\chi\,|\,\underset{\sim}{\mathbf{s}}\,|\,s,m_s\,\rangle\ ,\end{aligned}$$

where $R_\alpha(r)$ is the radial part of the single-particle wave function $\langle\,\mathbf{r}\chi\,|\,\alpha;(ls)jm\,\rangle$ and $\langle\,\hat{\mathbf{r}}\,|\,l,m_l\,\rangle$ the angular part.

Appendix B

UCOM formulas

In this appendix we summarize the properties and the algebra of the operators that appear in processing central and tensor correlations.

B.1 Radial Momentum

The central correlator shifts a pair of nucleons only radially in the relative coordinate and is constructed with the radial momentum operator $\underset{\sim}{p}_r$

$$\underset{\sim}{p}_r \overset{\mathbf{r}}{\Rightarrow} \frac{1}{2}\Big\{\mathbf{p}\cdot\frac{\mathbf{r}}{r}+\frac{\mathbf{r}}{r}\cdot\mathbf{p}\Big\} = \frac{1}{i}\Big(\frac{1}{r}+\frac{\partial}{\partial r}\Big)\,. \tag{B.1}$$

Useful representations of the radial momentum operator are

$$p_r = \frac{1}{i}\Big(\frac{1}{r}+\frac{\partial}{\partial r}\Big) = \frac{1}{i}\frac{1}{r}\frac{\partial}{\partial r}(r\circ)\,, \tag{B.2}$$

$$p_r^2 = -\frac{1}{r}\frac{\partial}{\partial r}\Big(r\frac{1}{r}\frac{\partial}{\partial r}r\circ\Big) = -\frac{1}{r}\frac{\partial^2}{\partial r^2}(r\circ)\,. \tag{B.3}$$

In this work the generator $\underset{\sim}{g}_r$ of the central correlations is written in terms of the radial momentum operator $\underset{\sim}{p}_r$. If one is not dealing with relative wave functions alternative representations can be used

$$\begin{aligned}\underset{\sim}{g}_r \overset{\mathbf{r}}{\Rightarrow} \frac{1}{2}\Big\{p_r s(r) + s(r)p_r\Big\} &= \frac{1}{2}\Big\{\mathbf{p}\cdot\frac{\mathbf{r}}{r}s(r) + s(r)\frac{\mathbf{r}}{r}\cdot\mathbf{p}\Big\}\\ &= \frac{i}{2}\Big\{\overleftarrow{\nabla}\cdot\frac{\mathbf{r}}{r}s(r) - s(r)\frac{\mathbf{r}}{r}\cdot\overrightarrow{\nabla}\Big\}\,.\end{aligned} \tag{B.4}$$

The momentum dependent interaction terms can also be expressed in different ways

$$\frac{1}{2}\Big(p_r^2 m(r) + m(r)p_r^2\Big) = p_r m(r) p_r - \frac{1}{2}m''(r) - \frac{m'(r)}{r} \tag{B.5}$$

$$= \Big(\mathbf{p}\cdot\frac{\mathbf{r}}{r}\Big)m(r)\Big(\frac{\mathbf{r}}{r}\cdot\mathbf{p}\Big) - \frac{1}{2}m''(r) \tag{B.6}$$

$$= \mathbf{p}\cdot m(r)\mathbf{p} - m(r)\frac{\mathbf{l}^2}{r^2} - \Big(\frac{m'(r)}{r}+\frac{1}{2}m''(r)\Big)\,. \tag{B.7}$$

B.2 Orbital Momentum Operator

The momentum operator $\underset{\sim}{\mathbf{p}}$ can be decomposed in the radial momentum $\underset{\sim}{\mathbf{p}}_r$ and the so called orbital momentum $\underset{\sim}{\mathbf{p}}_\Omega$

$$\underset{\sim}{\mathbf{p}} = \underset{\sim}{\mathbf{p}}_r + \underset{\sim}{\mathbf{p}}_\Omega \,, \tag{B.8}$$

that is not to be confused with the orbital angular momentum $\underset{\sim}{\mathbf{l}}$. The radial momentum operator $\underset{\sim}{\mathbf{p}}_r$ and the orbital momentum operator $\underset{\sim}{\mathbf{p}}_\Omega$

$$\underset{\sim}{\mathbf{p}}_r \overset{\mathbf{r}}{\Rightarrow} \frac{\mathbf{r}}{r} p_r = \frac{1}{2}\left[\frac{\mathbf{r}}{r}\left(\frac{\mathbf{r}}{r}\cdot\mathbf{p}\right) + \left(\mathbf{p}\cdot\frac{\mathbf{r}}{r}\right)\frac{\mathbf{r}}{r}\right], \qquad \underset{\sim}{\mathbf{p}}_\Omega \overset{\mathbf{r}}{\Rightarrow} \frac{1}{2r}\left(\mathbf{l}\times\frac{\mathbf{r}}{r} - \frac{\mathbf{r}}{r}\times\mathbf{l}\right) \tag{1.82}$$

do not commute. Using the elementary commutator relations of position and momentum we can verify

$$[p_r, \mathbf{p}_\Omega]_- = \frac{i}{r}\mathbf{p}_\Omega \tag{B.9}$$

and the scalar product commutator

$$[\mathbf{p}_r\cdot, \mathbf{p}_\Omega]_- = \mathbf{p}_r\cdot\mathbf{p}_\Omega - \mathbf{p}_\Omega\cdot\mathbf{p}_r = i\left(p_r\frac{1}{r} + \frac{1}{r}p_r\right) = -\frac{1}{r^2} + \frac{2i}{r}p_r \,. \tag{B.10}$$

From the definition it is obvious that $\mathbf{p}_\Omega$ commutes with functions which depend only on the relative distance r

$$[\mathbf{p}_\Omega, f(r)]_- = 0 \,. \tag{B.11}$$

We can further calculate the scalar product commutator with the position operator $\underset{\sim}{\mathbf{r}}$

$$[\mathbf{r}\cdot, \mathbf{p}_\Omega]_- = 2i \tag{B.12}$$

and using

$$\mathbf{p}^2 = \mathbf{p}_r^2 + \mathbf{p}_r\cdot\mathbf{p}_\Omega + \mathbf{p}_\Omega\cdot\mathbf{p}_r + \mathbf{p}_\Omega^2 \,, \tag{B.13}$$

we derive the properties

$$\mathbf{p}_r\cdot\mathbf{p}_\Omega + \mathbf{p}_\Omega\cdot\mathbf{p}_r = -\frac{1}{r^2} \,, \tag{B.14}$$

$$\mathbf{p}_\Omega^2 = \frac{1}{r^2}(\mathbf{l}^2 + 1) \,. \tag{B.15}$$

B.3 Algebra of Tensor Operators

We need the algebra of the scalar two-body operators (STB) for calculating correlated operators. The determination of the algebra is performed using the irreducible spherical tensor representation of the operators. We use the conventions of the Particle Data Book [Cea98].

B.3.1 Spherical Tensor Operators

An irreducible spherical tensor operators of rank k is noted as

$$\underset{\sim}{T}{}^{(k)}_q \tag{B.16}$$

The transformation from cartesian to spherical tensors of first rank is given by

$$\underset{\sim}{A}^{(1)}_{1} = -\frac{\underset{\sim}{A}_x + i\underset{\sim}{A}_y}{\sqrt{2}} \qquad \underset{\sim}{A}^{(1)}_{0} = \underset{\sim}{A}_z \qquad \underset{\sim}{A}^{(1)}_{-1} = \frac{\underset{\sim}{A}_x - i\underset{\sim}{A}_y}{\sqrt{2}} \,. \tag{B.17}$$

In general two tensor operators of rank j_1 and j_2 can be coupled to a tensor operator of rank j using the Clebsch-Gordan coefficients

$$\left\{\underset{\sim}{A}^{(j_1)}\,\underset{\sim}{B}^{(j_2)}\right\}^{(j)}_{q} \equiv \sum_{m_1,m_2} \mathrm{C}\left(\begin{matrix} j_1 & j_2 \\ m_1 & m_2 \end{matrix}\middle|\begin{matrix} j \\ q \end{matrix}\right) \underset{\sim}{A}^{(j_1)}_{m_1}\,\underset{\sim}{B}^{(j_2)}_{m_2} \,. \tag{B.18}$$

A shorthand notation is used for the coupled (and symmetrized) product of vector operators $\mathbf{a}$ and $\mathbf{b}$ in coordinate space

$$(\underset{\sim}{a}\,\underset{\sim}{b})^{(j)}_{q} = \frac{1}{2}\left(\left\{\underset{\sim}{a}^{(1)}\,\underset{\sim}{b}^{(1)}\right\}^{(j)}_{q} + \left\{\underset{\sim}{b}^{(1)}\,\underset{\sim}{a}^{(1)}\right\}^{(j)}_{q}\right) \,. \tag{B.19}$$

We also define coupled commutators and anti-commutators

$$[\underset{\sim}{A}^{(j_1)}, \underset{\sim}{B}^{(j_2)}]^{(j)}_{\pm q} \equiv \sum_{m_1,m_2} \mathrm{C}\left(\begin{matrix} j_1 & j_2 \\ m_1 & m_2 \end{matrix}\middle|\begin{matrix} j \\ q \end{matrix}\right) [\underset{\sim}{A}^{(j_1)}_{m_1}, \underset{\sim}{B}^{(j_2)}_{m_2}]_{\pm} \,. \tag{B.20}$$

The scalar product of spherical tensor operators (acting in different Hilbert spaces) of first rank is given by

$$\underset{\sim}{A}^{(1)} \cdot \underset{\sim}{T}^{(1)} = -\sqrt{3}\left\{\underset{\sim}{A}^{(1)} \otimes \underset{\sim}{T}^{(1)}\right\}^{(0)} \,,$$

and the scalar product of spherical tensor operators of second rank by

$$\underset{\sim}{A}^{(2)} \cdot \underset{\sim}{T}^{(2)} = \sqrt{5}\left\{\underset{\sim}{A}^{(2)} \otimes \underset{\sim}{T}^{(2)}\right\}^{(0)} \,.$$

Using the spherical tensors we can write for example the spin-orbit operator $\underset{\sim}{\mathbf{l}}\cdot\underset{\sim}{\mathbf{s}}$ as

$$\underset{\sim}{\mathbf{l}}\cdot\underset{\sim}{\mathbf{s}} = \underset{\sim}{l}^{(1)} \cdot \underset{\sim}{S}^{(1)} = -\sqrt{3}\left\{\underset{\sim}{l}^{(1)} \otimes \underset{\sim}{S}^{(1)}\right\}^{(0)} \tag{B.21}$$

and the tensor operator $\underset{\sim}{s}_{12}(\mathbf{a},\mathbf{b})$ can be expressed using the spherical tensors as

$$\underset{\sim}{s}_{12}(\mathbf{a},\mathbf{b}) = 3(\underset{\sim}{\boldsymbol{\sigma}}_1\cdot\underset{\sim}{\mathbf{a}})(\underset{\sim}{\boldsymbol{\sigma}}_2\cdot\underset{\sim}{\mathbf{b}}) - (\underset{\sim}{\boldsymbol{\sigma}}_1\cdot\underset{\sim}{\boldsymbol{\sigma}}_2)(\underset{\sim}{\mathbf{a}}\cdot\underset{\sim}{\mathbf{b}}) = 3\left\{\underset{\sim}{a}^{(1)}\,\underset{\sim}{b}^{(1)}\right\}^{(2)}\cdot\underset{\sim}{S}^{(2)} = 3\sqrt{5}\left\{(\underset{\sim}{a}\underset{\sim}{b})^{(2)}\otimes\underset{\sim}{S}^{(2)}\right\}^{(0)} \,,$$

with the operators $\underset{\sim}{S}^{(1)}$ and $\underset{\sim}{S}^{(2)}$ in the two-body spin space, see section B.3.5.

B.3.2 Calculating Commutators and Anticommutators

The calculation of correlated operators is based on the evaluation of the Baker-Campbell-Haussdorf formula Eq. (1.132). In this process we have to evaluate repeatedly the commutator of the generator $\underset{\sim}{g}_\Omega$ with scalar two-body operators (STB). These STBs can be of rank 0,1 or 2 in coordinate and spin space. The calculation of such a commutator is demonstrated on the example of the commutator

$$[\underset{\sim}{g}_\Omega, v^b(r)\,\underset{\sim}{\mathbf{l}}\cdot\underset{\sim}{\mathbf{s}}]_- = \vartheta(r)v^b(r)[\underset{\sim}{s}_{12}(\mathbf{r},\mathbf{p}_\Omega), \underset{\sim}{\mathbf{l}}\cdot\underset{\sim}{\mathbf{s}}]_- \,, \tag{B.22}$$

where the tensor correlation function $\vartheta(r)$ and the radial dependence $v^b(r)$ commute with the STBs and will not be considered in the following.

In the first step we rewrite the commutator using the spherical representation of the operators (see section B.3.1)

$$[\underset{\sim}{s}_{12}(\mathbf{r},\mathbf{p}_\Omega),\underset{\sim}{\mathbf{l}}\cdot\underset{\sim}{\mathbf{s}}]_- = \left[3\sqrt{5}\left\{(\underset{\sim}{r}\,\underset{\sim}{p}_\Omega)^{(2)}\otimes\underset{\sim}{S}^{(2)}\right\}^{(0)},-\sqrt{3}\left\{\underset{\sim}{l}^{(1)}\otimes\underset{\sim}{S}^{(1)}\right\}^{(0)}\right]_- . \tag{B.23}$$

In the next step we recouple the operators in coordinate and spin space using the formulas of section B.3.3. For our example we find

$$[\underset{\sim}{s}_{12}(\mathbf{r},\mathbf{p}_\Omega),\underset{\sim}{\mathbf{l}}\cdot\underset{\sim}{\mathbf{s}}]_- = 3\sqrt{5}\left\{[(\underset{\sim}{r}\,\underset{\sim}{p}_\Omega)^{(2)},\underset{\sim}{l}^{(1)}]^{(1)}_-\otimes\underset{\sim}{S}^{(1)}\right\}^{(0)} + 3\sqrt{\frac{15}{2}}\left\{[(\underset{\sim}{r}\,\underset{\sim}{p}_\Omega)^{(2)},\underset{\sim}{l}^{(1)}]^{(2)}_+\otimes\underset{\sim}{S}^{(2)}\right\}^{(0)} . \tag{B.24}$$

With the commutators and anticommutators of section B.3.4 the commutator can be simplified and rewritten in the cartesian tensor notation

$$\begin{aligned}[\underset{\sim}{s}_{12}(\mathbf{r},\mathbf{p}_\Omega),\underset{\sim}{\mathbf{l}}\cdot\underset{\sim}{\mathbf{s}}]_- &= -i3\sqrt{5}\left\{(\overline{\underset{\sim}{p}_\Omega\,\underset{\sim}{p}_\Omega})^{(2)}\otimes\underset{\sim}{S}^{(2)}\right\}^{(0)}\\ &= -i\bar{s}_{12}(\mathbf{p}_\Omega,\mathbf{p}_\Omega) .\end{aligned} \tag{B.25}$$

B.3.3 Products of STB operators

The products, commutators and anti-commutators of STB (scalar two-body) operators are calculated by performing a recoupling of the tensor operators with the help of 9j-symbols [VMK88]

$$\begin{aligned}&\left\{\underset{\sim}{A}^{(J_1)}\otimes\underset{\sim}{S}^{(J_1)}\right\}^{(0)}\left\{\underset{\sim}{B}^{(J_2)}\otimes\underset{\sim}{T}^{(J_2)}\right\}^{(0)} =\\ &\qquad\sum_{K=0}^{2}(2K+1)\begin{Bmatrix}J_1 & J_1 & 0\\ J_2 & J_2 & 0\\ K & K & 0\end{Bmatrix}\left\{\left\{\underset{\sim}{A}^{(J_1)}\,\underset{\sim}{B}^{(J_2)}\right\}^{(K)}\otimes\left\{\underset{\sim}{S}^{(J_1)}\,\underset{\sim}{T}^{(J_2)}\right\}^{(K)}\right\}^{(0)} .\end{aligned} \tag{B.26}$$

Here $\underset{\sim}{A}$ and $\underset{\sim}{B}$ are operators in the two-body coordinate space and $\underset{\sim}{S}$ and $\underset{\sim}{T}$ are operators in the two-body spin space. Because the two-body spin space is only four dimensional there is no tensor operator with a rank higher than two and the sum over K is restricted.

The following expansions for commutators and anticommutators make use of the fact that operators in coordinate and spin space commute

$$\begin{aligned}\underset{\sim}{A}\otimes\underset{\sim}{S}\cdot\underset{\sim}{B}\otimes\underset{\sim}{T} =&\frac{1}{4}[\underset{\sim}{A},\underset{\sim}{B}]_-\otimes[\underset{\sim}{S},\underset{\sim}{T}]_- + \frac{1}{4}[\underset{\sim}{A},\underset{\sim}{B}]_+\otimes[\underset{\sim}{S},\underset{\sim}{T}]_+ +\\ &\frac{1}{4}[\underset{\sim}{A},\underset{\sim}{B}]_-\otimes[\underset{\sim}{S},\underset{\sim}{T}]_+ + \frac{1}{4}[\underset{\sim}{A},\underset{\sim}{B}]_+\otimes[\underset{\sim}{S},\underset{\sim}{T}]_- ,\end{aligned} \tag{B.27}$$

and

$$[\underset{\sim}{A}\otimes\underset{\sim}{S},\underset{\sim}{B}\otimes\underset{\sim}{T}]_\pm = \frac{1}{2}[\underset{\sim}{A},\underset{\sim}{B}]_\pm\otimes[\underset{\sim}{S},\underset{\sim}{T}]_+ + \frac{1}{2}[\underset{\sim}{A},\underset{\sim}{B}]_\mp\otimes[\underset{\sim}{S},\underset{\sim}{T}]_- . \tag{B.28}$$

Using these expansions, Eq. (B.26) and the spin space relations from section B.3.5 the following expressions are obtained:

$$\begin{aligned}[\left\{\underset{\sim}{A}^{(1)}\otimes\underset{\sim}{S}^{(1)}\right\}^{(0)},\left\{\underset{\sim}{B}^{(1)}\otimes\underset{\sim}{S}^{(1)}\right\}^{(0)}]_\pm =& -\frac{2}{5\sqrt{3}}[\underset{\sim}{A}^{(1)},\underset{\sim}{B}^{(1)}]^{(0)}_\pm\otimes\Pi_1\\ &-\frac{1}{5}\sqrt{\frac{3}{2}}\left\{[\underset{\sim}{A}^{(1)},\underset{\sim}{B}^{(1)}]^{(1)}_\mp\otimes\underset{\sim}{S}^{(1)}\right\}^{(0)} + \frac{\sqrt{5}}{2}\left\{[\underset{\sim}{A}^{(1)},\underset{\sim}{B}^{(1)}]^{(2)}_\pm\otimes\underset{\sim}{S}^{(2)}\right\}^{(0)} ,\end{aligned} \tag{B.29}$$

$$[\{\underset{\sim}{A}^{(2)}\otimes\underset{\sim}{S}^{(2)}\}^{(0)},\{\underset{\sim}{B}^{(2)}\otimes\underset{\sim}{S}^{(2)}\}^{(0)}]_{\pm}=-\frac{4}{3\sqrt{5}}[\underset{\sim}{A}^{(2)},\underset{\sim}{B}^{(2)}]^{(0)}_{\pm}\otimes\Pi_1 + \sqrt{\frac{6}{5}}\{[\underset{\sim}{A}^{(2)},\underset{\sim}{B}^{(2)}]^{(1)}_{\mp}\otimes\underset{\sim}{S}^{(1)}\}^{(0)}+\sqrt{\frac{7}{15}}\{[\underset{\sim}{A}^{(2)},\underset{\sim}{B}^{(2)}]^{(2)}_{\pm}\otimes\underset{\sim}{S}^{(2)}\}^{(0)}\ , \quad \text{(B.30)}$$

$$[\{\underset{\sim}{A}^{(2)}\otimes\underset{\sim}{S}^{(2)}\}^{(0)},\{\underset{\sim}{B}^{(1)}\otimes\underset{\sim}{S}^{(1)}\}^{(0)}]_{\pm}= - \frac{1}{\sqrt{3}}\{[\underset{\sim}{A}^{(2)},\underset{\sim}{B}^{(1)}]^{(1)}_{\pm}\otimes\underset{\sim}{S}^{(1)}\}^{(0)}-\frac{1}{\sqrt{2}}\{[\underset{\sim}{A}^{(2)},\underset{\sim}{B}^{(1)}]^{(2)}_{\mp}\otimes\underset{\sim}{S}^{(2)}\}^{(0)}\ . \quad \text{(B.31)}$$

B.3.4 (Anti-)Commutator Relations for Coordinate Space Operators

The following relations have been verified with a Mathematica program using the elementary commutator relations of position and momentum operators

For the evaluation of the correlated radial part of the kinetic energy or a momentum dependent potential we need

$$[(\underset{\sim}{r}\,\underset{\sim}{p_\Omega})^{(2)},(\underset{\sim}{r}\,\underset{\sim}{p_\Omega})^{(2)}]^{(0)}_{-}=0\ , \qquad [(\underset{\sim}{r}\,\underset{\sim}{p_\Omega})^{(2)},(\underset{\sim}{r}\,\underset{\sim}{p_\Omega})^{(2)}]^{(0)}_{+}=\frac{1}{\sqrt{5}}(\underset{\sim}{\mathbf{l}}^2+3)\ , \quad \text{(B.32)}$$

$$[(\underset{\sim}{r}\,\underset{\sim}{p_\Omega})^{(2)},(\underset{\sim}{r}\,\underset{\sim}{p_\Omega})^{(2)}]^{(1)}_{-}=-\frac{5}{2}\underset{\sim}{l}^{(1)}\ , \qquad [(\underset{\sim}{r}\,\underset{\sim}{p_\Omega})^{(2)},(\underset{\sim}{r}\,\underset{\sim}{p_\Omega})^{(2)}]^{(1)}_{+}=0\ , \quad \text{(B.33)}$$

$$[(\underset{\sim}{r}\,\underset{\sim}{p_\Omega})^{(2)},(\underset{\sim}{r}\,\underset{\sim}{p_\Omega})^{(2)}]^{(2)}_{-}=0\ , \qquad [(\underset{\sim}{r}\,\underset{\sim}{p_\Omega})^{(2)},(\underset{\sim}{r}\,\underset{\sim}{p_\Omega})^{(2)}]^{(2)}_{+}=\sqrt{\frac{3}{7}}(\underset{\sim}{l}\,\underset{\sim}{l})^{(2)}\ . \quad \text{(B.34)}$$

In the evaluation of the correlated angular part of the kinetic energy the commutator

$$[(\underset{\sim}{r}\,\underset{\sim}{p_\Omega})^{(2)},\underset{\sim}{\mathbf{l}}^2]_{-}=2i(\overline{\underset{\sim}{p_\Omega}\,\underset{\sim}{p_\Omega}})^{(2)} \quad \text{(B.35)}$$

appears, where the short-hand notation

$$(\overline{\underset{\sim}{p_\Omega}\,\underset{\sim}{p_\Omega}})^{(2)}=2\underset{\sim}{r}^2(\underset{\sim}{p_\Omega}\,\underset{\sim}{p_\Omega})^{(2)}+(\underset{\sim}{l}\,\underset{\sim}{l})^{(2)}-\frac{1}{2}(\hat{\underset{\sim}{r}}\,\hat{\underset{\sim}{r}})^{(2)} \quad \text{(B.36)}$$

is used.

In calculating the tensor correlated spin-orbit interaction following commutators and anticommutators are needed:

$$[(\underset{\sim}{r}\,\underset{\sim}{p_\Omega})^{(2)},\underset{\sim}{l}^{(1)}]^{(1)}_{-}=0\ , \qquad [(\underset{\sim}{r}\,\underset{\sim}{p_\Omega})^{(2)},\underset{\sim}{l}^{(1)}]^{(1)}_{+}=0\ , \quad \text{(B.37)}$$

$$[(\underset{\sim}{r}\,\underset{\sim}{p_\Omega})^{(2)},\underset{\sim}{l}^{(1)}]^{(2)}_{-}=-\sqrt{6}(\underset{\sim}{r}\,\underset{\sim}{p_\Omega})^{(2)}\ , \qquad [(\underset{\sim}{r}\,\underset{\sim}{p_\Omega})^{(2)},\underset{\sim}{l}^{(1)}]^{(2)}_{+}=-i\sqrt{\frac{2}{3}}(\overline{\underset{\sim}{p_\Omega}\,\underset{\sim}{p_\Omega}})^{(2)}\ . \quad \text{(B.38)}$$

For correlating the tensor interaction we need

$$[(\underset{\sim}{r}\,\underset{\sim}{p_\Omega})^{(2)},(\hat{\underset{\sim}{r}}\,\hat{\underset{\sim}{r}})^{(2)}]^{(0)}_{-}=-\frac{2i}{\sqrt{5}}\ , \qquad [(\underset{\sim}{r}\,\underset{\sim}{p_\Omega})^{(2)},(\hat{\underset{\sim}{r}}\,\hat{\underset{\sim}{r}})^{(2)}]^{(0)}_{+}=0\ , \quad \text{(B.39)}$$

$$[(\underset{\sim}{r}\,\underset{\sim}{p_\Omega})^{(2)},(\hat{\underset{\sim}{r}}\,\hat{\underset{\sim}{r}})^{(2)}]^{(1)}_{-}=0\ , \qquad [(\underset{\sim}{r}\,\underset{\sim}{p_\Omega})^{(2)},(\hat{\underset{\sim}{r}}\,\hat{\underset{\sim}{r}})^{(2)}]^{(1)}_{+}=i\sqrt{\frac{2}{5}}\underset{\sim}{l}^{(1)}\ , \quad \text{(B.40)}$$

$$[(\underset{\sim}{r}\,\underset{\sim}{p_\Omega})^{(2)},(\hat{\underset{\sim}{r}}\,\hat{\underset{\sim}{r}})^{(2)}]^{(2)}_{-}=i\sqrt{\frac{3}{7}}(\hat{\underset{\sim}{r}}\,\hat{\underset{\sim}{r}})^{(2)}\ , \qquad [(\underset{\sim}{r}\,\underset{\sim}{p_\Omega})^{(2)},(\hat{\underset{\sim}{r}}\,\hat{\underset{\sim}{r}})^{(2)}]^{(2)}_{+}=0\ . \quad \text{(B.41)}$$

In higher orders of the Baker-Campbell-Hausdorff expansion the following commutators and anti-commutators have to be used

$$[(\underset{\sim}{r}\,\underset{\sim}{p_\Omega})^{(2)},(\underset{\sim}{l}\,\underset{\sim}{l})^{(2)}]_-^{(0)}=0\,,\qquad [(\underset{\sim}{r}\,\underset{\sim}{p_\Omega})^{(2)},(\underset{\sim}{l}\,\underset{\sim}{l})^{(2)}]_+^{(0)}=0\,, \tag{B.42}$$

$$[(\underset{\sim}{r}\,\underset{\sim}{p_\Omega})^{(2)},(\underset{\sim}{l}\,\underset{\sim}{l})^{(2)}]_-^{(1)}=0\,,\qquad [(\underset{\sim}{r}\,\underset{\sim}{p_\Omega})^{(2)},(\underset{\sim}{l}\,\underset{\sim}{l})^{(2)}]_+^{(1)}=0\,, \tag{B.43}$$

$$[(\underset{\sim}{r}\,\underset{\sim}{p_\Omega})^{(2)},(\underset{\sim}{l}\,\underset{\sim}{l})^{(2)}]_-^{(2)}=i\sqrt{\frac{7}{3}}(\overline{\underset{\sim}{p_\Omega}\,\underset{\sim}{p_\Omega}})^{(2)}\,,\qquad [(\underset{\sim}{r}\,\underset{\sim}{p_\Omega})^{(2)},(\underset{\sim}{l}\,\underset{\sim}{l})^{(2)}]_+^{(2)}=0\,, \tag{B.44}$$

and

$$[(\underset{\sim}{r}\,\underset{\sim}{p_\Omega})^{(2)},(\overline{\underset{\sim}{p_\Omega}\,\underset{\sim}{p_\Omega}})^{(2)}]_-^{(0)}=\frac{i}{\sqrt{5}}(8\underset{\sim}{\mathbf{l}}^2+9)\,,\quad [(\underset{\sim}{r}\,\underset{\sim}{p_\Omega})^{(2)},(\overline{\underset{\sim}{p_\Omega}\,\underset{\sim}{p_\Omega}})^{(2)}]_+^{(0)}=0\,, \tag{B.45}$$

$$[(\underset{\sim}{r}\,\underset{\sim}{p_\Omega})^{(2)},(\overline{\underset{\sim}{p_\Omega}\,\underset{\sim}{p_\Omega}})^{(2)}]_-^{(1)}=0\,,\qquad [(\underset{\sim}{r}\,\underset{\sim}{p_\Omega})^{(2)},(\overline{\underset{\sim}{p_\Omega}\,\underset{\sim}{p_\Omega}})^{(2)}]_+^{(1)}=-i\sqrt{\frac{2}{5}}(2\underset{\sim}{\mathbf{l}}^2+\frac{17}{2})\underset{\sim}{l}^{(1)}\,, \tag{B.46}$$

$$[(\underset{\sim}{r}\,\underset{\sim}{p_\Omega})^{(2)},(\overline{\underset{\sim}{p_\Omega}\,\underset{\sim}{p_\Omega}})^{(2)}]_-^{(2)}=5i\sqrt{\frac{3}{7}}(\underset{\sim}{l}\,\underset{\sim}{l})^{(2)}\,, \tag{B.47}$$

$$[\underset{\sim}{l}^{(1)},\underset{\sim}{l}^{(1)}]_-^{(0)}=0\,,\qquad [\underset{\sim}{l}^{(1)},\underset{\sim}{l}^{(1)}]_+^{(0)}=-\frac{2}{\sqrt{3}}\underset{\sim}{\mathbf{l}}^2\,, \tag{B.48}$$

$$[\underset{\sim}{l}^{(1)},\underset{\sim}{l}^{(1)}]_-^{(1)}=-\sqrt{2}\underset{\sim}{l}^{(1)}\,,\qquad [\underset{\sim}{l}^{(1)},\underset{\sim}{l}^{(1)}]_+^{(1)}=0\,, \tag{B.49}$$

$$[\underset{\sim}{l}^{(1)},\underset{\sim}{l}^{(1)}]_-^{(2)}=0\,,\qquad [\underset{\sim}{l}^{(1)},\underset{\sim}{l}^{(1)}]_+^{(2)}=-(\underset{\sim}{l}\,\underset{\sim}{l})^{(2)}\,, \tag{B.50}$$

$$[(\underset{\sim}{\hat{r}}\,\underset{\sim}{\hat{r}})^{(2)},\underset{\sim}{l}^{(1)}]_-^{(2)}=-\sqrt{6}(\underset{\sim}{\hat{r}}\,\underset{\sim}{\hat{r}})^{(2)}\,,\qquad [(\underset{\sim}{\hat{r}}\,\underset{\sim}{\hat{r}})^{(2)},\underset{\sim}{l}^{(1)}]_+^{(2)}=-i\sqrt{\frac{8}{3}}(\underset{\sim}{r}\,\underset{\sim}{p_\Omega})^{(2)}\,, \tag{B.51}$$

$$[(\underset{\sim}{l}\,\underset{\sim}{l})^{(2)},\underset{\sim}{l}^{(1)}]_-^{(2)}=-\sqrt{6}(\underset{\sim}{l}\,\underset{\sim}{l})^{(2)}\,,\qquad [(\underset{\sim}{l}\,\underset{\sim}{l})^{(2)},\underset{\sim}{l}^{(1)}]_+^{(2)}=0\,, \tag{B.52}$$

$$[(\overline{\underset{\sim}{p_\Omega}\,\underset{\sim}{p_\Omega}})^{(2)},\underset{\sim}{l}^{(1)}]_-^{(2)}=-\sqrt{6}(\overline{\underset{\sim}{p_\Omega}\,\underset{\sim}{p_\Omega}})^{(2)}\,,\qquad [(\overline{\underset{\sim}{p_\Omega}\,\underset{\sim}{p_\Omega}})^{(2)},\underset{\sim}{l}^{(1)}]_+^{(2)}=-\frac{8}{3}(\overline{\underset{\sim}{p_\Omega}\,\underset{\sim}{p_\Omega}})^{(2)}\,, \tag{B.53}$$

$$[(\underset{\sim}{\hat{r}}\,\underset{\sim}{\hat{r}})^{(2)},(\underset{\sim}{\hat{r}}\,\underset{\sim}{\hat{r}})^{(2)}]_-^{(0)}=0\,,\qquad [(\underset{\sim}{\hat{r}}\,\underset{\sim}{\hat{r}})^{(2)},(\underset{\sim}{\hat{r}}\,\underset{\sim}{\hat{r}})^{(2)}]_+^{(0)}=-\frac{4}{3\sqrt{5}}\,, \tag{B.54}$$

$$[(\underset{\sim}{\hat{r}}\,\underset{\sim}{\hat{r}})^{(2)},(\underset{\sim}{\hat{r}}\,\underset{\sim}{\hat{r}})^{(2)}]_-^{(1)}=0\,,\qquad [(\underset{\sim}{\hat{r}}\,\underset{\sim}{\hat{r}})^{(2)},(\underset{\sim}{\hat{r}}\,\underset{\sim}{\hat{r}})^{(2)}]_+^{(1)}=0\,, \tag{B.55}$$

$$[(\underset{\sim}{\hat{r}}\,\underset{\sim}{\hat{r}})^{(2)},(\underset{\sim}{\hat{r}}\,\underset{\sim}{\hat{r}})^{(2)}]_-^{(2)}=0\,,\qquad [(\underset{\sim}{\hat{r}}\,\underset{\sim}{\hat{r}})^{(2)},(\underset{\sim}{\hat{r}}\,\underset{\sim}{\hat{r}})^{(2)}]_+^{(2)}=-\frac{4}{\sqrt{21}}(\underset{\sim}{\hat{r}}\,\underset{\sim}{\hat{r}})^{(2)}\,. \tag{B.56}$$

B.3.5 (Anti-)Commutator Relations for Spin Operators

In the two-body spin space we have the projectors $\underset{\sim}{\Pi}_0$ to total spin 0 and $\underset{\sim}{\Pi}_1$ to total spin 1,

$$\underset{\sim}{\Pi}_0=\frac{1}{4}(1-\underset{\sim}{\boldsymbol{\sigma}}\otimes\underset{\sim}{\boldsymbol{\sigma}})\,,\qquad \underset{\sim}{\Pi}_1=\frac{1}{4}(3+\underset{\sim}{\boldsymbol{\sigma}}\otimes\underset{\sim}{\boldsymbol{\sigma}})\,, \tag{B.57}$$

the total spin operator $\underset{\sim}{S}^{(1)}$ which is a tensor operator of rank 1

$$\underset{\sim}{S}^{(1)} = \frac{1}{2}(\underset{\sim}{\sigma}^{(1)} \otimes \underset{\sim}{1} + \underset{\sim}{1} \otimes \underset{\sim}{\sigma}^{(1)}) \tag{B.58}$$

and the tensor operator $\underset{\sim}{S}^{(2)}$ of rank 2

$$\underset{\sim}{S}^{(2)} = \left\{\underset{\sim}{S}^{(1)}\,\underset{\sim}{S}^{(1)}\right\}^{(2)} . \tag{B.59}$$

Using the properties of the Pauli matrices the following commutators and anticommutators can be verified

$$[\underset{\sim}{S}^{(1)}, \underset{\sim}{S}^{(1)}]_{-}^{(0)} = 0 , \qquad [\underset{\sim}{S}^{(1)}, \underset{\sim}{S}^{(1)}]_{+}^{(0)} = -\frac{4}{\sqrt{3}}\underset{\sim}{\Pi}_1 , \tag{B.60}$$

$$[\underset{\sim}{S}^{(1)}, \underset{\sim}{S}^{(1)}]_{-}^{(1)} = -\sqrt{2}\underset{\sim}{S}^{(1)} , \qquad [\underset{\sim}{S}^{(1)}, \underset{\sim}{S}^{(1)}]_{+}^{(1)} = 0 \tag{B.61}$$

$$[\underset{\sim}{S}^{(1)}, \underset{\sim}{S}^{(1)}]_{-}^{(2)} = 0 , \qquad [\underset{\sim}{S}^{(1)}, \underset{\sim}{S}^{(1)}]_{+}^{(2)} = \underset{\sim}{S}^{(2)} , \tag{B.62}$$

$$[\underset{\sim}{S}^{(2)}, \underset{\sim}{S}^{(1)}]_{-}^{(1)} = 0 , \qquad [\underset{\sim}{S}^{(2)}, \underset{\sim}{S}^{(1)}]_{+}^{(1)} = -2\sqrt{\frac{5}{3}}\underset{\sim}{S}^{(1)} , \tag{B.63}$$

$$[\underset{\sim}{S}^{(2)}, \underset{\sim}{S}^{(1)}]_{-}^{(2)} = \sqrt{6}\underset{\sim}{S}^{(2)} , \qquad [\underset{\sim}{S}^{(2)}, \underset{\sim}{S}^{(1)}]_{+}^{(2)} = 0 , \tag{B.64}$$

$$[\underset{\sim}{S}^{(2)}, \underset{\sim}{S}^{(2)}]_{-}^{(0)} = 0 , \qquad [\underset{\sim}{S}^{(2)}, \underset{\sim}{S}^{(2)}]_{+}^{(0)} = \frac{8}{3}\sqrt{5}\Pi_1 , \tag{B.65}$$

$$[\underset{\sim}{S}^{(2)}, \underset{\sim}{S}^{(2)}]_{-}^{(1)} = 2\sqrt{10}\underset{\sim}{S}^{(1)} , \qquad [\underset{\sim}{S}^{(2)}, \underset{\sim}{S}^{(2)}]_{+}^{(1)} = 0 , \tag{B.66}$$

$$[\underset{\sim}{S}^{(2)}, \underset{\sim}{S}^{(2)}]_{-}^{(2)} = 0 , \qquad [\underset{\sim}{S}^{(2)}, \underset{\sim}{S}^{(2)}]_{+}^{(2)} = 2\sqrt{\frac{7}{3}}\underset{\sim}{S}^{(2)} . \tag{B.67}$$

B.3.6 Cartesian Tensor Operator Relations

Summarizing the efforts we get the following important relations expressed in the cartesian tensor operators

$$\underset{\sim}{\bar{s}}_{12}(\mathbf{p}_\Omega, \mathbf{p}_\Omega) = 2r^2\underset{\sim}{s}_{12}(\mathbf{p}_\Omega, \mathbf{p}_\Omega) + \underset{\sim}{s}_{12}(\mathbf{l}, \mathbf{l}) - \frac{1}{2}\underset{\sim}{s}_{12}(\hat{\mathbf{r}}, \hat{\mathbf{r}}) , \tag{B.68}$$

$$(\underset{\sim}{\mathbf{l}}\cdot\underset{\sim}{\mathbf{s}})^2 = \frac{2}{3}\underset{\sim}{\mathbf{l}}^2\underset{\sim}{\Pi}_1 - \frac{1}{2}\underset{\sim}{\mathbf{l}}\cdot\underset{\sim}{\mathbf{s}} + \frac{1}{6}\underset{\sim}{s}_{12}(\mathbf{l}, \mathbf{l}) , \tag{B.69}$$

$$\underset{\sim}{s}_{12}(\mathbf{r}, \mathbf{p}_\Omega)^2 = 6(\underset{\sim}{\mathbf{l}}^2 + 3)\underset{\sim}{\Pi}_1 + \frac{45}{2}\underset{\sim}{\mathbf{l}}\cdot\underset{\sim}{\mathbf{s}} + \frac{3}{2}\underset{\sim}{s}_{12}(\mathbf{l}, \mathbf{l}) . \tag{B.70}$$

The commutators needed for the calculation of the correlated interaction are

$$[\underset{\sim}{s}_{12}(\mathbf{r},\mathbf{p}_\Omega),\underset{\sim}{s}_{12}(\hat{\mathbf{r}},\hat{\mathbf{r}})]_- = -24i\underset{\sim}{\Pi}_1 - 18i\underset{\sim}{\mathbf{l}}\cdot\underset{\sim}{\mathbf{s}} + 3i\underset{\sim}{s}_{12}(\hat{\mathbf{r}},\hat{\mathbf{r}}) \tag{B.71}$$

$$[\underset{\sim}{s}_{12}(\mathbf{r},\mathbf{p}_\Omega),\underset{\sim}{\mathbf{l}}\cdot\underset{\sim}{\mathbf{s}}]_- = -i\bar{\underset{\sim}{s}}_{12}(\mathbf{p}_\Omega,\mathbf{p}_\Omega) \tag{B.72}$$

$$[\underset{\sim}{s}_{12}(\mathbf{r},\mathbf{p}_\Omega),\underset{\sim}{\mathbf{l}}^2]_- = 2i\bar{\underset{\sim}{s}}_{12}(\mathbf{p}_\Omega,\mathbf{p}_\Omega) \tag{B.73}$$

$$[\underset{\sim}{s}_{12}(\mathbf{r},\mathbf{p}_\Omega),\underset{\sim}{s}_{12}(\mathbf{l},\mathbf{l})]_- = 7i\bar{\underset{\sim}{s}}_{12}(\mathbf{p}_\Omega,\mathbf{p}_\Omega) \tag{B.74}$$

$$[\underset{\sim}{s}_{12}(\mathbf{r},\mathbf{p}_\Omega),\bar{\underset{\sim}{s}}_{12}(\mathbf{p}_\Omega,\mathbf{p}_\Omega)]_- = i(96\underset{\sim}{\mathbf{l}}^2+108)\underset{\sim}{\Pi}_1 + i(36\underset{\sim}{\mathbf{l}}^2+153)\underset{\sim}{\mathbf{l}}\cdot\underset{\sim}{\mathbf{s}} + 15i\underset{\sim}{s}_{12}(\mathbf{l},\mathbf{l}) \tag{B.75}$$

$$[\underset{\sim}{s}_{12}(\mathbf{r},\mathbf{p}_\Omega),\underset{\sim}{\mathbf{l}}^2\underset{\sim}{\mathbf{l}}\cdot\underset{\sim}{\mathbf{s}}]_- = -i(\underset{\sim}{\mathbf{l}}^2+3)\bar{\underset{\sim}{s}}_{12}(\mathbf{p}_\Omega,\mathbf{p}_\Omega) \tag{B.76}$$

$$\begin{aligned}[\underset{\sim}{s}_{12}(\mathbf{r},\mathbf{p}_\Omega),\underset{\sim}{\mathbf{l}}^2\bar{\underset{\sim}{s}}_{12}(\mathbf{p}_\Omega,\mathbf{p}_\Omega)]_- &= i(144\underset{\sim}{\mathbf{l}}^4+600\mathbf{l}^2+324)\underset{\sim}{\Pi}_1 \\ &\quad + i(36\underset{\sim}{\mathbf{l}}^4+477\underset{\sim}{\mathbf{l}}^2+477)\underset{\sim}{\mathbf{l}}\cdot\underset{\sim}{\mathbf{s}} + i(27\underset{\sim}{\mathbf{l}}^2+51)\underset{\sim}{s}_{12}(\mathbf{l},\mathbf{l})\,.\end{aligned} \tag{B.77}$$

B.4 Matrix Elements in Angular Momentum Eigenstates

The matrix elements of tensor operators in angular momentum eigenstates $\big|(ls)j\big\rangle$ have to be calculated using the matrix elements of the basic operators given in section B.4.1 and the corresponding angular momentum couplings. For convenience we list the evaluated matrix elements in the lowest angular momentum states.

The $\underset{\sim}{\mathbf{l}}^2$, $\underset{\sim}{\mathbf{l}}\cdot\underset{\sim}{\mathbf{s}}$ and $\underset{\sim}{s}_{12}(\mathbf{l},\mathbf{l})$ operators have only diagonal matrix elements. The $\underset{\sim}{s}_{12}(\hat{\mathbf{r}},\hat{\mathbf{r}})$ operator has diagonal and off-diagonal matrix elements.

	$\underset{\sim}{\mathbf{l}}^2$	$\underset{\sim}{\mathbf{l}}\cdot\underset{\sim}{\mathbf{s}}$	$\underset{\sim}{s}_{12}(\hat{\mathbf{r}},\hat{\mathbf{r}})$	$\underset{\sim}{s}_{12}(\mathbf{l},\mathbf{l})$
$\langle(11)0\big\vert\circ\big\vert(11)0\rangle$	2	-2	-4	10
$\langle(01)1\big\vert\circ\big\vert(01)1\rangle$	0	0	0	0
$\langle(11)1\big\vert\circ\big\vert(11)1\rangle$	2	-1	-2	-5
$\langle(21)1\big\vert\circ\big\vert(21)1\rangle$	6	-3	0	21
$\langle(11)2\big\vert\circ\big\vert(11)2\rangle$	2	1	2	1
$\langle(21)2\big\vert\circ\big\vert(21)2\rangle$	6	-1	$-\frac{8}{5}$	-21
$\langle(31)2\big\vert\circ\big\vert(31)2\rangle$	12	-4	$-\frac{2}{5}$	36
$\langle(21)3\big\vert\circ\big\vert(21)3\rangle$	6	2	2	6
$\langle(31)3\big\vert\circ\big\vert(31)3\rangle$	12	-1	$-\frac{10}{7}$	-45
$\langle(41)3\big\vert\circ\big\vert(41)3\rangle$	20	-5	$-\frac{4}{7}$	55
$\langle(31)4\big\vert\circ\big\vert(31)4\rangle$	12	3	2	15
$\langle(41)4\big\vert\circ\big\vert(41)4\rangle$	20	-1	$-\frac{4}{3}$	-77
$\langle(51)4\big\vert\circ\big\vert(51)4\rangle$	30	-6	$-\frac{2}{3}$	78
$\langle(41)5\big\vert\circ\big\vert(41)5\rangle$	20	4	2	28
$\langle(51)5\big\vert\circ\big\vert(51)5\rangle$	30	-1	$-\frac{14}{11}$	-117
$\langle(61)5\big\vert\circ\big\vert(61)5\rangle$	42	-7	$-\frac{8}{11}$	105

The $\underset{\sim}{s}_{12}(\mathbf{r}, \mathbf{p}_\Omega)$ and $\underset{\sim}{\bar{s}}_{12}(\mathbf{p}_\Omega, \mathbf{p}_\Omega)$ operators have only off-diagonal matrix elements.

	$\underset{\sim}{s}_{12}(\hat{\mathbf{r}}, \hat{\mathbf{r}})$	$\underset{\sim}{\bar{s}}_{12}(\mathbf{p}_\Omega, \mathbf{p}_\Omega)$	$\underset{\sim}{s}_{12}(\mathbf{r}, \mathbf{p}_\Omega)$
$\langle (01)1 \,\vert\circ\vert\, (21)1 \rangle$	$2\sqrt{2}$	$-9\sqrt{2}$	$-3i\sqrt{2}$
$\langle (11)2 \,\vert\circ\vert\, (31)2 \rangle$	$\frac{6\sqrt{6}}{5}$	$-15\sqrt{6}$	$-3i\sqrt{6}$
$\langle (21)3 \,\vert\circ\vert\, (41)3 \rangle$	$\frac{12\sqrt{3}}{7}$	$-42\sqrt{3}$	$-6i\sqrt{3}$
$\langle (31)4 \,\vert\circ\vert\, (51)4 \rangle$	$\frac{4\sqrt{5}}{3}$	$-54\sqrt{5}$	$-6i\sqrt{5}$
$\langle (41)5 \,\vert\circ\vert\, (61)5 \rangle$	$\frac{6\sqrt{30}}{11}$	$-33\sqrt{30}$	$-3i\sqrt{30}$

All not explicitly listed matrix elements are zero.

B.4.1 Matrix Elements of Basic Operators

For the evaluation of STB matrix elements in an angular momentum basis we need the matrix elements for the basic operators $\underset{\sim}{\mathbf{r}}$, $\underset{\sim}{\mathbf{p}}$, $\underset{\sim}{\mathbf{p}}_\Omega$ and $\underset{\sim}{\mathbf{l}}$. All STB matrix elements can then be calculated with the help of the Clebsch-Gordan coefficients.

Vector operators can only connect states with $|l - l'| \leq 1$.

$$\langle r; l+1, m' \,\vert\, \underset{\sim}{r}^{(1)}_q \,\vert\, r; l, m \rangle = \mathrm{C}\begin{pmatrix} l & 1 & | & l+1 \\ m & q & | & m' \end{pmatrix} \sqrt{\frac{l+1}{2l+3}} r \,, \tag{B.78}$$

$$\langle r; l-1, m' \,\vert\, \underset{\sim}{r}^{(1)}_q \,\vert\, r; l, m \rangle = -\mathrm{C}\begin{pmatrix} l & 1 & | & l-1 \\ m & q & | & m' \end{pmatrix} \sqrt{\frac{l}{2l-1}} r \,. \tag{B.79}$$

The matrix elements of the full momentum operator

$$\langle r; l+1, m' \,\vert\, \underset{\sim}{p}^{(1)}_q \,\vert\, r; l, m \rangle = \frac{1}{i}\mathrm{C}\begin{pmatrix} l & 1 & | & l+1 \\ m & q & | & m' \end{pmatrix} \sqrt{\frac{l+1}{2l+3}} \left[\left(\frac{1}{r} + \frac{\partial}{\partial r} \right) - (l+1)\frac{1}{r} \right] , \tag{B.80}$$

$$\langle r; l-1, m' \,\vert\, \underset{\sim}{p}^{(1)}_q \,\vert\, r; l, m \rangle = -\frac{1}{i}\mathrm{C}\begin{pmatrix} l & 1 & | & l-1 \\ m & q & | & m' \end{pmatrix} \sqrt{\frac{l}{2l-1}} \left[\left(\frac{1}{r} + \frac{\partial}{\partial r} \right) + l\frac{1}{r} \right] . \tag{B.81}$$

and the orbital momentum operator differ by the radial momentum matrix elements (by construction)

$$\langle r; l+1, m' \,\vert\, \underset{\sim}{p}^{(1)}_{\Omega,q} \,\vert\, r; l, m \rangle = -\frac{1}{i}\mathrm{C}\begin{pmatrix} l & 1 & | & l+1 \\ m & q & | & m' \end{pmatrix} \sqrt{\frac{l+1}{2l+3}} (l+1)\frac{1}{r} \,, \tag{B.82}$$

$$\langle r; l-1, m' \,\vert\, \underset{\sim}{p}^{(1)}_{\Omega,q} \,\vert\, r; l, m \rangle = -\frac{1}{i}\mathrm{C}\begin{pmatrix} l & 1 & | & l-1 \\ m & q & | & m' \end{pmatrix} \sqrt{\frac{l}{2l-1}} l\frac{1}{r} \,. \tag{B.83}$$

The orbital angular momentum operator has only diagonal matrix elements

$$\langle l', m' \,\vert\, \underset{\sim}{l}^{(1)}_q \,\vert\, l, m \rangle = \mathrm{C}\begin{pmatrix} l & 1 & | & l' \\ m & q & | & m' \end{pmatrix} \sqrt{l(l+1)}\delta_{l,l'} \,. \tag{B.84}$$

In the spin space we have

$$\langle\, 1m' \,\big|\, \underset{\sim}{S}{}^{(1)}_q \,\big|\, 1m \,\rangle = \mathrm{C}\begin{pmatrix} 1 & 1 & \Big| & 1 \\ m & q & \Big| & m' \end{pmatrix} \sqrt{2} \tag{B.85}$$

$$\langle\, 1m' \,\big|\, \underset{\sim}{S}{}^{(2)}_q \,\big|\, 1m \,\rangle = \mathrm{C}\begin{pmatrix} 1 & 2 & \Big| & 1 \\ m & q & \Big| & m' \end{pmatrix} 2\sqrt{\frac{5}{3}} \tag{B.86}$$

Appendix C

Harmonic Oscillator Shell Model States and the Talmi Transformation

The shell model using harmonic oscillator states is a often used model for nuclear structure studies. The harmonic oscillator states [ST75]

$$\begin{aligned}\phi^a_{nlm}(\mathbf{r}) &= \frac{R_{nl}(a)(r)}{r} Y^l_m(\hat{\mathbf{r}}) \\ &= \frac{1}{\Gamma(l+\frac{3}{2})} \frac{\sqrt{2\Gamma(l+n+\frac{1}{2})}}{\sqrt{\Gamma(n)}} \frac{1}{\sqrt{a}^{l+\frac{3}{2}}} e^{-\frac{r^2}{2a}} r^l F\Big(1-n, l+\frac{3}{2}; \frac{r^2}{a}\Big) Y^l_m(\hat{\mathbf{r}})\end{aligned} \tag{C.1}$$

have the unique feature of allowing the separation of center-of-mass and internal motion in a two-body product state. This property can be used in the calculation of interaction matrix elements with the help of the Talmi transformation.

C.1 Talmi Coefficients

The Talmi coefficients [ST75, Irv72] provide the transformation of a product of two single-particle oscillator wave functions to the product of a function of the center-of-mass motion $\mathbf{R} = \frac{1}{2}(\mathbf{r}_1 + \mathbf{r}_2)$ and a function of the relative motion depending on the relative position vector $\mathbf{r} = \mathbf{r}_1 - \mathbf{r}_2$

$$\phi^a_{n_1 l_1 m_1}(\mathbf{r}_1)\phi^a_{n_2 l_2 m_2}(\mathbf{r}_2) = \sum_{NLMnlm} \left\langle \begin{matrix} n_1 l_1 m_1 \\ n_2 l_2 m_2 \end{matrix} \middle| \begin{matrix} NLM \\ nlm \end{matrix} \right\rangle \phi^{a/2}_{NLM}(\mathbf{R})\, \phi^{2a}_{nlm}(\mathbf{r}) \,. \tag{C.2}$$

We calculate the Talmi coefficient by explicitly performing the integrals over the oscillator wave functions.

With the help of the Talmi transformation matrix elements of operators depending only on the relative motion can be calculated as

$$\begin{aligned}\langle\, n_1 l_1 m_1; n_2 l_2 m_2 \,\big|\, \underset{\sim}{v} \,\big|\, n'_1 l'_1 m'_1; n'_2 l'_2 m'_2 \,\rangle = \\ \sum_{\substack{NLM \\ nlmn'l'm'}} \left\langle \begin{matrix} n_1 l_1 m_1 \\ n_2 l_2 m_2 \end{matrix} \middle| \begin{matrix} NLM \\ nlm \end{matrix} \right\rangle \left\langle \begin{matrix} n'_1 l'_1 m'_1 \\ n'_2 l'_2 m'_2 \end{matrix} \middle| \begin{matrix} NLM \\ n'l'm' \end{matrix} \right\rangle \langle\, nlm \,\big|\, \underset{\sim}{v} \,\big|\, n'l'm' \,\rangle \,,\end{aligned} \tag{C.3}$$

with the relative wave functions

$$\langle\, \mathbf{r} \,|\, nlm \,\rangle = \phi^{2a}_{nlm}(\mathbf{r}) \,. \tag{C.4}$$

Including the spin χ and isospin ξ degrees of freedom we get for scalar and isoscalar operators the following result

$$\begin{aligned}
&\langle\, n_1 l_1 m_1 \chi_1 \xi_1 ; n_2 l_2 m_2 \chi_2 \xi_2 \,|\, \underset{\sim}{v} \,|\, n'_1 l'_1 m'_1 \chi'_1 \xi'_1 ; n'_2 l'_2 m'_2 \chi'_2 \xi'_2 \,\rangle = \\
&\sum_{\substack{nn' \\ jmll's \\ tm_t}} \sum_{\substack{m_l m'_l \\ m_s m'_s}} \sum_{NLM} \left\langle \begin{matrix} n_1 l_1 m_1 \\ n_2 l_2 m_2 \end{matrix} \middle| \begin{matrix} NLM \\ nlm_l \end{matrix} \right\rangle \left\langle \begin{matrix} n'_1 l'_1 m'_1 \\ n'_2 l'_2 m'_2 \end{matrix} \middle| \begin{matrix} NLM \\ n' l' m'_l \end{matrix} \right\rangle \mathrm{C}\left(\begin{matrix} \frac{1}{2} & \frac{1}{2} \\ \xi_1 & \xi_2 \end{matrix} \middle| \begin{matrix} t \\ m_t \end{matrix} \right) \mathrm{C}\left(\begin{matrix} \frac{1}{2} & \frac{1}{2} \\ \xi'_1 & \xi'_2 \end{matrix} \middle| \begin{matrix} t \\ m_t \end{matrix} \right) \\
&\times \mathrm{C}\left(\begin{matrix} \frac{1}{2} & \frac{1}{2} \\ \chi_1 & \chi_2 \end{matrix} \middle| \begin{matrix} s \\ m_s \end{matrix} \right) \mathrm{C}\left(\begin{matrix} \frac{1}{2} & \frac{1}{2} \\ \chi'_1 & \chi'_2 \end{matrix} \middle| \begin{matrix} s \\ m'_s \end{matrix} \right) \mathrm{C}\left(\begin{matrix} l & s \\ m_l & m_s \end{matrix} \middle| \begin{matrix} j \\ m \end{matrix} \right) \mathrm{C}\left(\begin{matrix} l' & s \\ m'_l & m'_s \end{matrix} \middle| \begin{matrix} j \\ m \end{matrix} \right) \langle\, n(ls)j, t \,|\, \underset{\sim}{v} \,|\, n'(l's)j, t \,\rangle \,.
\end{aligned} \tag{C.5}$$

Using this formula the matrix elements of arbitrary shell model configurations can be calculated.

C.2 Doubly-Magic Nuclei

For closed shell nuclei whose ground state is described in the shell model by completely occupied shells we get the following results.

Given are the expectation values for a two-body operator $\underset{\sim}{A}$ that is defined in the four spin-isospin channels

$$\underset{\sim}{a} = \sum_{ST} \underset{\sim}{a}_{ST} \, \underset{\sim}{\Pi}_{ST} \,. \tag{C.6}$$

In the case of ^{4}He all nucleons are in the $1s$ one-particle state. There are only contributions from the even channels in the ^{4}He expectation value (the isospin labels have been omitted in the two-body states $|\, n(LS)J \,\rangle$ for brevity)

$$\langle\, {}^4\mathrm{He} \,|\, \underset{\sim}{A} \,|\, {}^4\mathrm{He} \,\rangle = 3\langle\, 1(00)0 \,|\, \underset{\sim}{a}_{01} \,|\, 1(00)0 \,\rangle + 3\langle\, 1(01)1 \,|\, \underset{\sim}{a}_{10} \,|\, 1(01)1 \,\rangle \,. \tag{C.7}$$

In ^{16}O the $1s$ and $1p$ shells are fully occupied. We have contributions from the odd channels and contributions with higher relative angular momentum in the even channels

$$\begin{aligned}
&\langle\, {}^{16}\mathrm{O} \,|\, \underset{\sim}{A} \,|\, {}^{16}\mathrm{O} \,\rangle = \\
&\quad 6\langle\, 1(10)1 \,|\, \underset{\sim}{a}_{00} \,|\, 1(10)1 \,\rangle \\
&\quad + 21\langle\, 1(00)0 \,|\, \underset{\sim}{a}_{01} \,|\, 1(00)0 \,\rangle + \frac{3}{2}\langle\, 2(00)0 \,|\, \underset{\sim}{a}_{01} \,|\, 2(00)2 \,\rangle + \frac{15}{2}\langle\, 1(20)2 \,|\, \underset{\sim}{a}_{01} \,|\, 1(20)2 \,\rangle \\
&\quad + 21\langle\, 1(01)1 \,|\, \underset{\sim}{a}_{10} \,|\, 1(01)1 \,\rangle + \frac{3}{2}\langle\, 2(01)1 \,|\, \underset{\sim}{a}_{10} \,|\, 2(01)1 \,\rangle \\
&\quad + \frac{3}{2}\langle\, 1(21)1 \,|\, \underset{\sim}{a}_{10} \,|\, 1(21)1 \,\rangle + \frac{5}{2}\langle\, 1(21)2 \,|\, \underset{\sim}{a}_{10} \,|\, 1(21)2 \,\rangle + \frac{7}{2}\langle\, 1(21)3 \,|\, \underset{\sim}{a}_{10} \,|\, 1(21)3 \,\rangle \\
&\quad + 6\langle\, 1(11)0 \,|\, \underset{\sim}{a}_{11} \,|\, 1(11)0 \,\rangle + 18\langle\, 1(11)1 \,|\, \underset{\sim}{a}_{11} \,|\, 1(11)1 \,\rangle + 30\langle\, 1(11)2 \,|\, \underset{\sim}{a}_{11} \,|\, 1(11)2 \,\rangle \,.
\end{aligned} \tag{C.8}$$

In ^{40}Ca the $1s$, $1p$, $2s$ and $1d$ shells are fully fully occupied and we obtain

$$
\begin{aligned}
&\langle\, {}^{40}\mathrm{Ca} \,|\, \underset{\sim}{A} \,|\, {}^{40}\mathrm{Ca} \,\rangle = \\
&\quad 30\langle\, 1(10)1 \,|\, \underset{\sim}{a}_{00} \,|\, 1(10)1 \,\rangle + \frac{9}{2}\langle\, 2(10)1 \,|\, \underset{\sim}{a}_{00} \,|\, 2(10)1 \,\rangle + \frac{21}{2}\langle\, 1(30)3 \,|\, \underset{\sim}{a}_{00} \,|\, 1(30)3 \,\rangle \\
&\quad + \frac{555}{8}\langle\, 1(00)0 \,|\, \underset{\sim}{a}_{01} \,|\, 1(00)0 \,\rangle + \frac{105}{8}\langle\, 2(00)0 \,|\, \underset{\sim}{a}_{01} \,|\, 2(00)0 \,\rangle + \frac{9}{8}\langle\, 3(00) \,|\, \underset{\sim}{a}_{01} \,|\, 3(00)0 \,\rangle \\
&\quad + \frac{525}{8}\langle\, 1(20)2 \,|\, \underset{\sim}{a}_{01} \,|\, 1(20)2 \,\rangle + \frac{45}{8}\langle\, 2(20)2 \,|\, \underset{\sim}{a}_{01} \,|\, 2(20)2 \,\rangle + \frac{81}{8}\langle\, 1(40)4 \,|\, \underset{\sim}{a}_{01} \,|\, 1(40)4 \,\rangle + \\
&\quad + \frac{555}{8}\langle\, 1(01)1 \,|\, \underset{\sim}{a}_{10} \,|\, 1(01)1 \,\rangle + \frac{105}{8}\langle\, 2(01)1 \,|\, \underset{\sim}{a}_{10} \,|\, 2(01)1 \,\rangle + \frac{9}{8}\langle\, 3(01)1 \,|\, \underset{\sim}{a}_{10} \,|\, 3(01)1 \,\rangle \\
&\quad + \frac{105}{8}\langle\, 1(21)1 \,|\, \underset{\sim}{a}_{10} \,|\, 1(21)1 \,\rangle + \frac{175}{8}\langle\, 1(21)2 \,|\, \underset{\sim}{a}_{10} \,|\, 1(21)2 \,\rangle + \frac{245}{8}\langle\, 1(21)3 \,|\, \underset{\sim}{a}_{10} \,|\, 1(21)3 \,\rangle \\
&\quad + \frac{9}{8}\langle\, 2(21)1 \,|\, \underset{\sim}{a}_{10} \,|\, 2(21)1 \,\rangle + \frac{15}{8}\langle\, 2(21)2 \,|\, \underset{\sim}{a}_{10} \,|\, 2(21)2 \,\rangle + \frac{21}{8}\langle\, 2(21)3 \,|\, \underset{\sim}{a}_{10} \,|\, 2(21)3 \,\rangle \\
&\quad + \frac{21}{8}\langle\, 1(41)3 \,|\, \underset{\sim}{a}_{10} \,|\, 1(41)3 \,\rangle + \frac{27}{8}\langle\, 1(41)4 \,|\, \underset{\sim}{a}_{10} \,|\, 1(41)4 \,\rangle + \frac{33}{8}\langle\, 1(41)5 \,|\, \underset{\sim}{a}_{10} \,|\, 1(41)5 \,\rangle \\
&\quad + 30\langle\, 1(11)0 \,|\, \underset{\sim}{a}_{11} \,|\, 1(11)0 \,\rangle + 90\langle\, 1(11)1 \,|\, \underset{\sim}{a}_{11} \,|\, 1(11)1 \,\rangle + 150\langle\, 1(11)2 \,|\, \underset{\sim}{a}_{11} \,|\, 1(11)2 \,\rangle \\
&\quad + \frac{9}{2}\langle\, 2(11)0 \,|\, \underset{\sim}{a}_{11} \,|\, 2(11)0 \,\rangle + \frac{27}{2}\langle\, 2(11)1 \,|\, \underset{\sim}{a}_{11} \,|\, 2(11)1 \,\rangle + \frac{45}{2}\langle\, 2(11)2 \,|\, \underset{\sim}{a}_{11} \,|\, 2(11)2 \,\rangle \\
&\quad + \frac{49}{2}\langle\, 1(31)2 \,|\, \underset{\sim}{a}_{11} \,|\, 1(31)2 \,\rangle + \frac{63}{2}\langle\, 1(31)3 \,|\, \underset{\sim}{a}_{11} \,|\, 1(31)3 \,\rangle + \frac{77}{2}\langle\, 1(31)4 \,|\, \underset{\sim}{a}_{11} \,|\, 1(31)4 \,\rangle \,.
\end{aligned}
\tag{C.9}
$$

C.3 Explicit Operator Expectation Values

For some operators the matrix elements in the harmonic oscillator basis can be calculated analytically.

Intrinsic Kinetic Energy (uncorrelated)

The expectation value of the uncorrelated intrinsic kinetic energy $\langle\, \underset{\sim}{T} - \underset{\sim}{T}_{cm} \,\rangle$ is given by

$$
{}^{4}\mathrm{He}: \ \frac{1}{m}\frac{9}{4a} \qquad {}^{16}\mathrm{O}: \ \frac{1}{m}\frac{69}{4a} \qquad {}^{40}\mathrm{Ca}: \ \frac{1}{m}\frac{237}{4a} \,. \tag{C.10}
$$

Coulomb Interaction (uncorrelated)

If we neglect the effect of the central correlations on the expectation values of the Coulomb interaction we obtain

$$
{}^{4}\mathrm{He}: \ 2\frac{e^2}{\sqrt{2\pi a}} \qquad {}^{16}\mathrm{O}: \ \frac{83}{2}\frac{e^2}{\sqrt{2\pi a}} \qquad {}^{40}\mathrm{Ca}: \ \frac{7905}{32}\frac{e^2}{\sqrt{2\pi a}} \,. \tag{C.11}
$$

Radius r_{rms} (uncorrelated)

The uncorrelated r_{rms} radius of the doubly-magic nuclei (or the one-body contribution of the correlated radius) is given by

$$
{}^{4}\mathrm{He}: \ \frac{3}{2\sqrt{2}}\sqrt{a} \qquad {}^{16}\mathrm{O}: \ \frac{\sqrt{69}}{4\sqrt{2}}\sqrt{a} \qquad {}^{40}\mathrm{Ca}: \ \frac{\sqrt{237}}{4\sqrt{5}}\sqrt{a} \,. \tag{C.12}
$$

Appendix D

Correlator Parameters

D.1 Correlator Parameterizations

The correlation functions $R_+(r)$ and $\vartheta(r)$ are used in parameterized form. For the correlators determined from the zero-energy scattering solutions a fit to a suitable parameterization is performed.

In this work we use the following parameterizations for the central correlation functions

$$R_+(r) = r + \alpha \left(\frac{r}{\beta}\right)^{\eta} \exp\left\{-\exp\left\{\frac{r}{\beta}\right\}\right\}, \tag{D.1}$$

$$R_+(r) = r + \alpha\gamma^{\eta}\left(1 - \exp\left\{-\left(\frac{r}{\gamma}\right)^{\eta}\right\}\right)\exp\left\{-\frac{r}{\beta}\right\} \tag{D.2}$$

and

$$R_+(r) = r + \alpha\gamma^{\eta}\left(1 - \exp\left\{-\left(\frac{r}{\gamma}\right)^{\eta}\right\}\right)\exp\left\{\exp -\left\{\frac{r}{\beta}\right\}\right\}. \tag{D.3}$$

For the tensor correlation functions $\vartheta(r)$ the parameterizations

$$\vartheta(r) = \alpha\gamma^{\eta}\left(1 - \exp\left\{-\left(\frac{r}{\gamma}\right)^{\eta}\right\}\right)\exp\left\{-\frac{r}{\beta}\right\} \tag{D.4}$$

and

$$\vartheta(r) = \alpha\gamma^{\eta}\left(1 - \exp\left\{-\left(\frac{r}{\gamma}\right)^{\eta}\right\}\right)\exp\left\{-\exp\left\{\frac{r}{\beta}\right\}\right\} \tag{D.5}$$

are used.

D.2 Malfliet-Tjon V Potential

correlator	channel	type	α	β	γ	η
zero	all	(D.1)	0.947	0.937		0.410
min	all	(D.1)	0.917	0.902		0.413

D.3 Modified Afnan-Tang S3 Potential

correlator	channel	type	α	β	γ	η
zero	01	(D.1)	1.754	1.109		0.643
zero	10	(D.1)	1.422	0.951		0.783
zero	odd	(D.2)	0.785	1.052	0.432	1
min	01	(D.1)	1.587	1.074		0.597
min	10	(D.1)	1.265	0.852		0.817
min^{α}	odd	(D.3)	1.066	0.994	1.545	1
min^{β}	odd	(D.3)	1.642	1.282	0.464	1
min^{γ}	odd	(D.3)	2.253	1.666	0.277	1

D.4 Bonn-A Potential

Central Correlators

correlator	channel	type	α	β	γ	η
zero	00	(D.2)	0.341	8.696	0.891	2
zero	01	(D.1)	1.280	0.840		0.702
zero	10	(D.1)	1.263	0.891		0.750
zero	11	(D.1)	0.714	1.292		0.836
min^{α}	00	(D.3)	0.250	1.406	1000.0	2
min^{β}	00	(D.3)	0.348	1.797	1.449	2
min	01	(D.1)	1.199	0.808		0.734
min	10	(D.1)	1.132	0.779		0.848
min	11	(D.1)	0.658	1.198		0.798
min – ^{4}He	01	(D.1)	1.344	0.899		0.699
min – ^{4}He	10	(D.1)	1.256	0.853		0.811

Tensor Correlators

correlator	channel	type	α	β	γ	η
zero	10	(D.4)	0.410	6.898	0.761	2
zero	11	(D.4)	-0.013	1.697	1.240	3
min^{α}	10	(D.5)	0.412	1.287	4.994	2
min^{β}	10	(D.5)	0.408	1.834	1.215	2
min^{γ}	10	(D.5)	0.420	2.745	0.925	2
min	10	(D.4)	0.170	2.372	0.863	2
min^{α}	11	(D.5)	-0.032	3.353	1.106	3
min	11	(D.4)	-0.014	1.699	1.197	3
$min^{\alpha} - {}^4\mathrm{He}$	10	(D.5)	0.468	1.241	100.0	2
$min^{\beta} - {}^4\mathrm{He}$	10	(D.5)	0.398	1.472	100.0	2
$min^{\gamma} - {}^4\mathrm{He}$	10	(D.5)	0.383	2.551	1.109	2
$min - {}^4\mathrm{He}$	10	(D.4)	0.152	7.201	0.741	2

D.5 Argonne V8' and Argonne V18 Potential

Central Correlators

correlator	channel	type	α	β	γ	η
zero	00	(D.2)	1.201	4.453	0.237	1
zero	01	(D.1)	1.484	0.873		0.422
zero	10	(D.1)	1.426	0.917		0.446
zero	11	(D.2)	0.978	0.570	0.550	1
min^{α}	00	(D.3)	1.804	1.272	0.424	1
min^{β}	00	(D.3)	2.306	1.603	0.307	1
min	01	(D.1)	1.379	0.885		0.372
min	10	(D.1)	1.296	0.849		0.419
min	11	(D.3)	3.102	1.374	0.187	1
$min - {}^4\mathrm{He}$	01	(D.1)	1.380	0.981		0.336
$min - {}^4\mathrm{He}$	10	(D.1)	1.372	0.907		0.419

Tensor Correlators

correlator	channel	type	α	β	γ	η
zero	10	(D.4)	0.288	3.247	0.435	1
zero	11	(D.4)	-0.025	1.573	1.203	1
min^{α}	10	(D.5)	0.530	1.298	1000.0	1
min^{β}	10	(D.5)	0.579	1.717	1.590	1
min^{γ}	10	(D.5)	0.786	2.665	0.488	1
min	10	(D.4)	0.341	2.153	0.407	1
min^{α}	11	(D.5)	-0.081	3.477	0.420	1
min	11	(D.4)	-0.027	1,685	0.864	1
$min^{\alpha} - {}^4\mathrm{He}$	10	(D.5)	0.590	1.266	100.0	1
$min^{\beta} - {}^4\mathrm{He}$	10	(D.5)	0.520	1.554	100.0	1
$min^{\gamma} - {}^4\mathrm{He}$	10	(D.5)	0.621	2.446	0.883	1
$min - {}^4\mathrm{He}$	10	(D.4)	0.361	4.017	0.303	1

Bibliography

[BKS+01] S. Bogner, T. Kuo, A. Schwenk, D. Entem and R. Machleidt, *Towards a Unique Low Momentum Nucleon-Nucleon Interaction*, (2001), nucl-th/0108041.

[Bro71] G. Brown, *Unified Theory of Nuclear Models and Forces*, North-Holland, third edition, 1971.

[Cea98] C. Caso and et al, *Review of Particle Physics*, The European Physical Journal **C3**, 1 (1998).

[CFFdS96] G. Có, A. Fabrocini, S. Fantoni and F. de Saavedra, *Model calculations of doubly closed shell nuclei in CBF theory*, Nucl. Phys. **A605**, 359 (1996).

[CK93] S. Chin and E. Krotscheck, *Collective excited states of a model* ^{16}O *nucleus*, Nuc. Phys. **A560**, 151 (1993).

[EM01] D. Entem and R. Machleidt, *Accurate nucleon nucleon potential based upon chiral perturbation theory*, (2001), nucl-th/0108057.

[FdSC00] A. Fabrocini, F. A. de Saavedra and G. Co', *Ground state correlations in* ^{16}O *and* ^{40}Ca, Phys. Rev. **C61**, 044302 (2000).

[FdSCF98] A. Fabrocini, F. de Saavedra, G. Co' and P. Folgarait, *Ground state of* $N = Z$ *doubly closed shell nuclei in correlated basis function theory*, Phys. Rev. **C57**, 1668 (1998).

[FNRS98] H. Feldmeier, T. Neff, R. Roth and J. Schnack, *A Unitary Correlation Operator Method*, Nucl. Phys. **A632**, 61 (1998).

[FS97] H. Feldmeier and J. Schnack, *Fermionic Molecular Dynamics*, Prog. Part. Nucl. Phys. **39**, 393 (1997).

[FS00] H. Feldmeier and J. Schnack, *Molecular dynamics for fermions*, Rev. Mod. Phys. **72**, 655 (2000).

[GFMP81] R. Guardiola, A. Faessler, H. Müther and A. Polls, *Brueckner Theory and Jastrow Approach for Finite Nuclei*, Nucl. Phys. **A371**, 79 (1981).

[GMN+96] R. Guardiola, P. Moliner, J. Navarro, R. Bishop, A. Puente and N. Walet, *Translationally invariant treatment of pair correlations in nuclei: I. Spin and isospin dependent correlations*, Nuc. Phys. **A609**, 218 (1996).

[GP98] R. Guardiola and M. Portesi, *State-dependent Jastrow correlation functions for 4He nuclei*, J. Phys. **G24**, L37 (1998).

[HM99] J. H. Heisenberg and B. Mihaila, *Ground state correlations and mean-field in* ^{16}O, Phys. Rev. **C59**, 1440 (1999).

[HZ85] U. Helmbrecht and J. Zabolitzky, *Stochastic Solution of the Schrödinger Equation for Finite Fermi Systems*, Nuc. Phys. **A442**, 109 (1985).

[Irv72] J. Irvine, *Nuclear Structure Theory*, Pergamon Press, first edition, 1972.

[KNG+01] H. Kamada, A. Nogga, W. Glöckle, E. Hiyama, M. Kamimura, K. Varga, Y. Suzuki, M. Viviani, A. Kievsky, S. Rosati, J. Carlson, S. Pieper, R. Wiringa, P. Navratil, B. Barrett, N. Barnea, W. Leidemann and G. Orlandini, *Benchmark Test Calculation of a Four-Nucleon Bound State*, Phys. Rev. **C64**, 044001 (2001).

[Kra01] P. Krafft, Fermionische Molekulardynamik mit Konfigurationsmischung, Master's thesis, TU Darmstadt, 2001.

[KS82] P. Kramer and M. Saraceno, *Geometry of the Time-Dependent Variational Principle in Quantum Mechanics*, Number 140 in Lecture Notes in Physics, Springer, 1982.

[Mac89] R. Machleidt, *The Meson Theory of Nuclear Forces and Nuclear Structure*, Adv. Nucl. Phys. **19**, 189 (1989).

[Mac01] R. Machleidt, *High-precision, charge-dependent Bonn nucleon-nucleon potential*, Phys. Rev. **C63**, 024001 (2001).

[MP00] H. Müther and A. Polls, *Two-Body Correlations in Nuclear Systems*, Prog. Part. Nucl. Phys **45**, 243 (2000).

[MT69] R. Malfliet and J. Tjon, *Solution of the Faddeev equations for the triton problem using local two particle interactions*, Nucl. Phys. **A127**, 161 (1969).

[Nef98] T. Neff, Fermionische Molekulardynamik mit Konfigurationsmischungen und realistischen Wechselwirkungen, Master's thesis, TU Darmstadt, 1998.

[NVB00] P. Navrátil, J. Vary and B. Barrett, *Large-basis* ab inito *no-core shell model and its application to* ^{12}C, Phys. Rev **C62**, 054311 (2000).

[PPC+97] B. Pudliner, V. Pandharipande, J. Carlson, S. Pieper and R. Wiringa, *Quantum Monte Carlo calculations of nuclei with* $A \leq 7$, Phys. Rev. **C56**, 1720 (1997).

[PPWC01] S. Pieper, V. Pandharipande, R. Wiringa and J. Carlson, *Realistic models of pion-exchange three-nucleon interactions*, Phys. Rev. **C64**, 014001 (2001).

[PW01] S. Pieper and R. Wiringa, *Quantum Monte Carlo Calculations of Light Nuclei*, (2001), nucl-th/0103005.

[Ric99] D. Richards, *Lattice gauge theory: QCD from quarks to hadrons*, (1999), nucl-th/0006020.

[Rot00] R. Roth, *Effektive Wechselwirkungen für Quantenflüssigkeiten und Quantengase: Kernmaterie, flüssiges Helium und ultrakalte atomare Fermigase*, PhD thesis, TU Darmstadt, 2000.

[ST75] A. Sitenko and V. Tartakovskii, *Lectures on the Theory of the Nucleus*, Pergamon Press, 1975.

[VMK88] D. A. Varshalovich, A. N. Moskalev and V. K. Khersonskii, *Quantum Theory of Angular Momentum*, World Scientific, 1988.

[VS95] K. Varga and Y. Suzuki, *Precise solution of few-body problems with stochastic variational method on correlated Gaussian basis*, Phys. Rev. **C52**, 2885 (1995).

[Wei90] S. Weinberg, *Nuclear forces from chiral Lagrangians*, Phys. Lett. **B251**, 288 (1990).

[Wei91] S. Weinberg, *Effective chiral Lagrangians for nucleon - pion interactions and nuclear forces*, Nuc. Phys. **B363**, 3 (1991).

[Wir92] R. Wiringa, *Monte Carlo calculations of few body and light nuclei*, Nucl. Phys. **A543**, 199 (1992).

[WPCP00] R. B. Wiringa, S. C. Pieper, J. Carlson and V. R. Pandharipande, *Quantum Monte Carlo calculations of A=8 nuclei*, Phys. Rev. **C62**, 014001 (2000).

[WSA84] R. Wiringa, R. Smith and T. Ainsworth, *Nucleon Nucleon Potentials with and without delta (1232) Degrees of Freedom*, Phys. Rev. **C29**, 1207 (1984).

[WSS95] R. Wiringa, V. Stoks and R. Schiavilla, *Accurate nucleon-nucleon potential with charge-independence breaking*, Phys. Rev. **C51**, 38 (1995).

Lebenslauf

Zur Person

Geburtsdatum:	24. November 1971
Geburtsort:	Bensheim
Eltern:	Ludwig und Katharina Neff geb. Becker
Familienstand:	ledig

Bildungsweg

07/1978 – 05/1982	Besuch der Felsenmeerschule Reichenbach (Grundschule)
07/1982 – 06/1991	Besuch des Alten Kurfürstlichen Gymnasiums in Bensheim
06/1991	Abitur
09/1991 – 09/1993	Grundstudium an der Technischen Hochschule Darmstadt
09/1993	Physik Vordiplom
09/1993 – 07/1998	Hauptstudium an der Technischen Hochschule Darmstadt
11/1995 – 07/1998	Diplomarbeit bei der Gesellschaft für Schwerionenforschung mit dem Thema „*Fermionische Molekulardynamik mit Konfigurationsmischungen und realistischen Wechselwirkungen*"
07/1998	Physik Diplom (mit Auszeichnung bestanden)
08/1998 – 04/1999	Wissenschaftliche Hilfskraft bei der Gesellschaft für Schwerionenforschung und Anfertigung der Disseration
05/1999 – 06/2000	Zivildienst bei den Städtischen Kindergärten in Heppenheim
07/2000 – 12/2001	Wissenschaftliche Hilfskraft bei der Gesellschaft für Schwerionenforschung und Anfertigung der Disseration

Danksagung

An erster Stelle möchte ich bei meinem Doktorvater Prof. Dr. Hans Feldmeier für die intensive und engagierte Betreuung während der gesamten Promotionszeit bedanken. Bei allen fachlichen und auch sonstigen Problemen war er immer ein offener und hilfreicher Ansprechpartner. Sein Anspruch, physikalische Fragestellungen nicht nur formal abzuhandeln sondern auch anschaulich zu beleuchten, lieferte insbesondere bei der schwierigen Suche nach dem Tensorkorrelator immer wieder neue Ansatzpunkte.

Desweiteren möchte ich der gesamten Theoriegruppe der GSI und hier insbeondere Herrn Prof. Dr. Wolfgang Nörenberg für die hervorragenden Arbeitsbedingungen danken. So konnte ich u.a. am Hirschegg Workshop teilnehmen und auch während meiner Zeit als Zivildienstleistender im Kindergarten blieb der Kontakt zur Arbeitsgruppe bestehen.

Zu dem hervorragenden Klima in der Arbeitsgruppe trugen auch die anderen Mitglieder der Arbeitsgruppe nicht unwesentlich bei, nennen möchte ich hier zuvorderst meine Komilitonen Hendrik van Hees und Robert Roth. Ihnen gilt auch mein Dank für ihr Engagement beim Korrekturlesen dieser Arbeit. Auch Jürgen Schnack, der meine ersten Erfahrungen mit der Fermionischen Molekulardynamik begleitete und Peter Krafft bin ich dankbar für die fruchtbare Zusammenarbeit. Nicht zu vergessen sind natürlich die oftmals tiefschürfenden Diskussionen am Mittags- oder Kaffeetisch.

Danken möchte ich auch der Studienstiftung des deutschen Volkes, die mir während des Studiums finanziell und ideell zur Seite stand. Nicht zuletzt möchte ich bei meiner Mutter bedanken, die mir immer mit Geduld und Verständnis zur Seite stand